Study on multi-period fringe projection interferometry for shape measurements

March, 2008

Graduate School of Science and Technology
Niigata University

Hai Huan

CONTENTS

Chapter 1

Introduction

1.1 Historical review for surface profile measurement

There are many kinds of methods for measuring surface profiles of objects which are continual surface or step surface. Single-wavelength interferometry is used to measure a surface which the change of the optical path difference between two measuring points is smaller than a half-wavelength. Fringe projection interferometry uses the fringe patterns to measure objects with large change of surface profile. Multi-period fringe projection Interferometry uses multiple period fringe patterns to measure object surfaces with discontinuities. First, we do a review to past works.

1.1.1 Single-Wavelength Interferometry

Single-wavelength interferometry is used to measure a smooth and continuous surface on which the change of the optical path difference between two measuring points is smaller than a half-wavelength.[1] Figure 1-1 shows a schematic of the basic configuration of representative Single-Wavelength Interferometry (Twyman-Green Interferometer) for measurement of the surface profile of object. In this method interference pattern is produced by the optical path difference (OPD) between the object wave and reference wave on the image plane of the object surface. The intensity distribution of the interference pattern is expressed as

$$S = A + B\cos[\alpha(x, y)], \tag{1-1}$$

$$\alpha(x, y) = \frac{2\pi}{\lambda} 2r(x, y) \tag{1-2}$$

where λ is wavelength of the light source, $r(x)$ is surface profile of the object, A and B are constants relating to the intensity of light source. Phase $\alpha(x)$ can be obtained from several methods, such as phase-shifting method[2], fast Fourier transform method[3], and sinusoidal phase modulating method[4]. Since the calculated phase lies in the range from $-\pi$ to π, spatial phase unwrapping must be carried out to recover the surface profile, which is shown in Fig. 1-2.

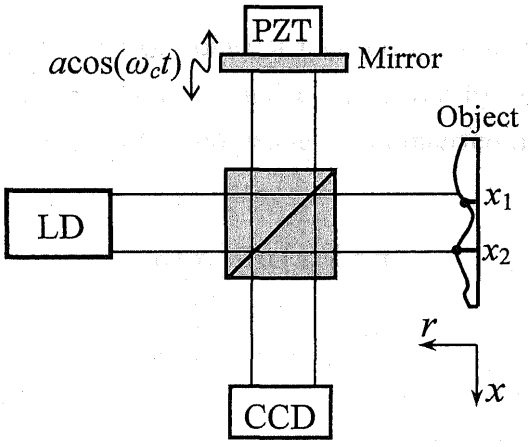

Fig. 1-1 Twyman-Green Interferometer for measurement of surface profile of object.

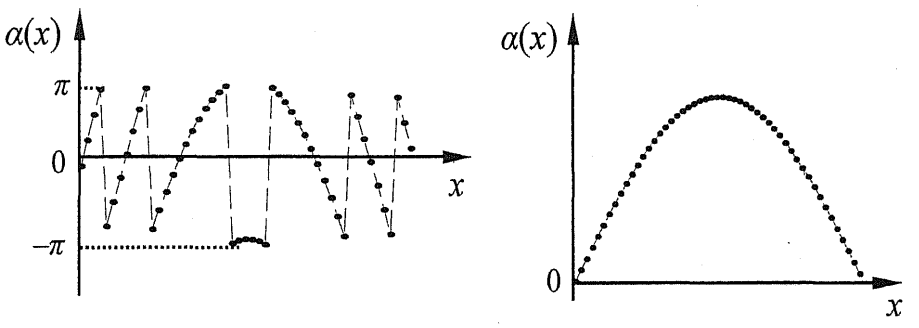

Fig. 1-2 Spatial phase unwrapping process of single-wavelength interferometry

In Fig. 1-1, x_1 and x_2 are two adjacent measuring points. When phase values and surface profiles on the points x_1 and x_2 are given by $\alpha(x_1)$, $\alpha(x_2)$, $r(x_1)$ and $r(x_2)$, the measurement range of single-wavelength interferometry is given by

$$\left|\alpha(x_1)-\alpha(x_2)\right|<\pi \tag{1-3}$$

$$\left|r(x_1)-r(x_2)\right|<\frac{\lambda}{4} \tag{1-4}$$

Surface profile $r(x)$ can be calculated by Eq. (1-2). Equation (1-4) indicates that the surface profile difference between two adjacent measuring points is limited smaller than a fourth-wavelength. It is difficult for single-wavelength interferometry to measure objects with large change of surface profile. The fringe projection method is proposed to solve this problem.

1.1.2 Fringe Projection Method

Fringe projection method uses the fringe patterns projected onto the object surfaces which are generated with either a grating or two laser beams[5]. Figure 1-3 shows the optical setup for this measurement.

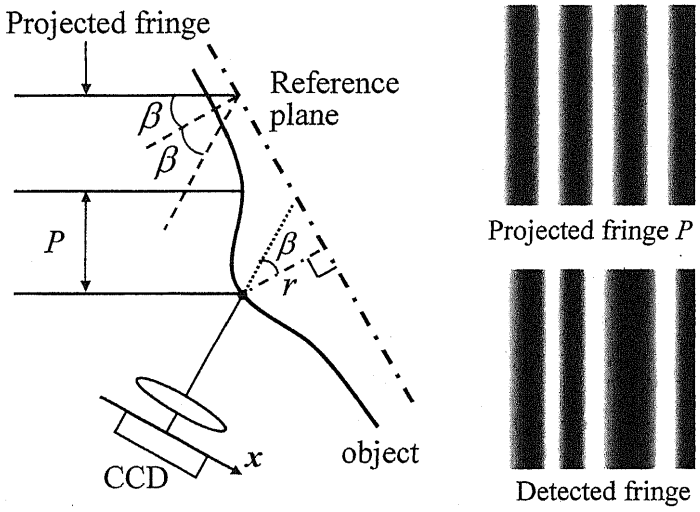

Fig. 1-3 Fringe projection method for measurement of surface profile of object.

When the period of the project fringe is denoted by P, the interference signal detected at the detection plane is given by

$$S = A + B\cos[\frac{2\pi x}{P} + \alpha(x)] \tag{1-5}$$

$$\alpha(x) = 2\pi\frac{2\sin\beta}{P}r(x) = 2\pi\frac{S}{P}2r(x) \tag{1-6}$$

where $S = \sin\beta$. Equations (1-5) and (1-6) indicate that the measurement range of fringe projection method is much larger than the single-wavelength interferometry. The measurement precision of fringe projection method is related to the period of fringe pattern. Fringe pattern with small period is required to increase measurement precision. When the period of fringes presented on the CCD image sensor is less than the size of CCD pixel, measurement can not be performed.

The surface profile of the object is obtained from a phase distribution of the fringe patterns which is calculated by the phase- shifting method[2] or by the Fourier transform method.[3] Since the calculated phase distribution of the fringe

pattern lies in the range from $-\pi$ to π, spatial phase unwrapping must be carried out to recover the surface profile. Figure 1-4 shows the spatial phase unwrapping result of on line of the detected fringe shown in Fig. 1-2.

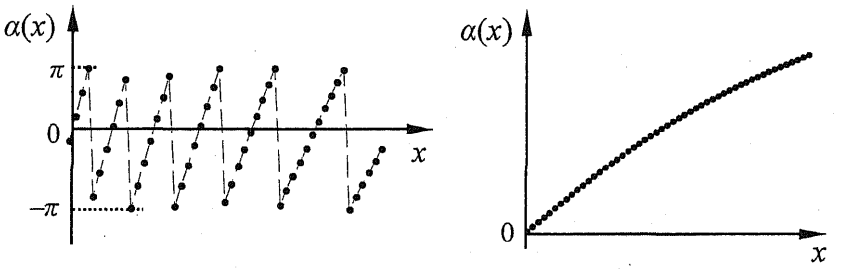

Wrapped Phase Distribution Unwrapped Phase Distribution

Fig. 1-4 Spatial phase unwrapping process of fringe projection method.

However, since the phases of two adjacent measurement points are compared and connected in spatial phase unwrapping, it is impossible to recover the surface profile with discontinuities such as height steps or spatially isolated surfaces which cause phase jumps larger than 2π. The fringe projection techniques using only one-period fringe projection are difficult to measure object surfaces with the discontinuities.

1.1.3 Multi-period Fringe Projection Method

Recently multi-period fringe projection method has been used to measure object surfaces with the discontinuities. Multi-period fringe projection method has some analogy with multi-wavelength interferometer techniques[6-8]. The optical setup for this measurement is shown in Fig. 1-5. The optical configuration for projecting fringe pattern is the same as that in Fig. 1-2. The difference between the two methods is that a series of period P_1, P_2, ..., P_M is projected on the surface of the object in the multi-period fringe projection method.

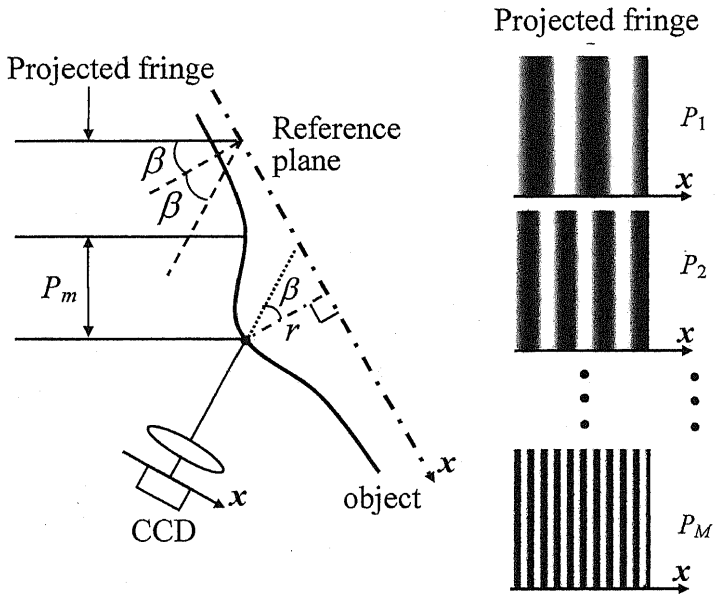

Fig. 1-5 Multi-period fringe projection method for measurement of surface profile of object.

1.1.3.A: Spatiotemporal Phase Unwrapping Method

One basic idea of multi-period fringe projection method is to use a fringe pattern with a large period which makes the phase jump smaller than 2π for the spatial phase unwrapping. And it gives the phase distribution $\alpha_1(x)<\pi$ in the measurement which is shown in Fig.1-6 (a). $\alpha_0(x)$ is the phase distribution of lower surface of the step profile. Since $\alpha_1(x)<\pi$, the spatial phase unwrapping can be used to get the surface profile. The measurement accuracy is not high for a large period of $P_1=P_{\max}$, a fringe pattern of a small periods is used to improve the accuracy, which gives the phase distribution $\alpha_2(x)>2\pi$ as shown in Fig. 1-6 (b). If the measurement error of $\alpha_1(x)$ is smaller than P_2, The measurement result is given by

$$\begin{aligned} \alpha_{21}(x) &= 2m\pi + \alpha_2(x) \\ m &= [m_c]_R \end{aligned} \tag{1-7}$$

where m_c is given by

$$m_C = \frac{1}{2\pi}\frac{[\alpha_1(x)P_1 - \alpha_2(x)P_2]}{P_2} \tag{1-8}$$

and $[y]_R$ means the round off value of y. This process is repeated until the smallest period P_M=$P_{\min}$ is used, which is shown in Fig. 1-6 (c). This method is called spatiotemporal phase unwrapping method (SP method)[9-10]. The measurement range of this method is determined by the fringe pattern with largest period P_{max}. The precision of this method is equal to the measurement precision obtained when the fringe pattern with smallest period P_{min} is used.

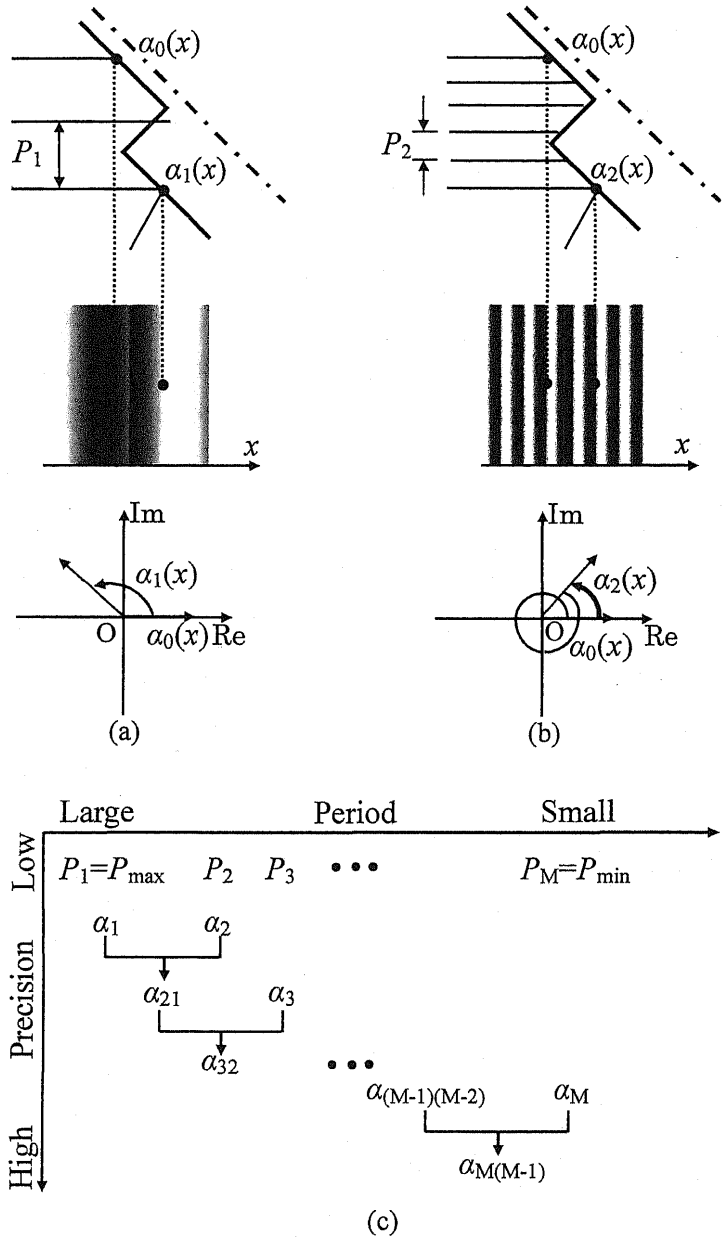

Fig. 1-6 Process of SP Method

1.1.3.B: Temporal Phase-unwrapping Method

Another basic idea of multi-period fringe projection method is to use the phase change of the projected fringe pattern on each measurement point of the object surface when the fringe period is scanned, which is called temporal

phase-unwrapping method (TP method) [11-14]. The principle of TP method is shown in Fig. 1-7, where $k_m=2\pi/P_m$ is the wave number of fringe patterns. The wrapped phase values α_m are measured during the scanning of the fringe period, which is shown in Fig. 1-7 (b). The wrapped phase values α_{Um} are unwrapped along the time direction. These unwrapped phase values on each measurement point are used to estimate the gradient of the phase change which provids the height of the object surface, which is shown in Fig. 1-7 (c). The measurement range of TP method is inversely proportional to the scanning interval Δk of k_m, and the phase difference between two adjacent point should be satisfied the condition that

$$0 < | \alpha_{i+1}(x) - \alpha_i(x) | < \pi \tag{1-9}$$

The measurement precision is several tens of microns.

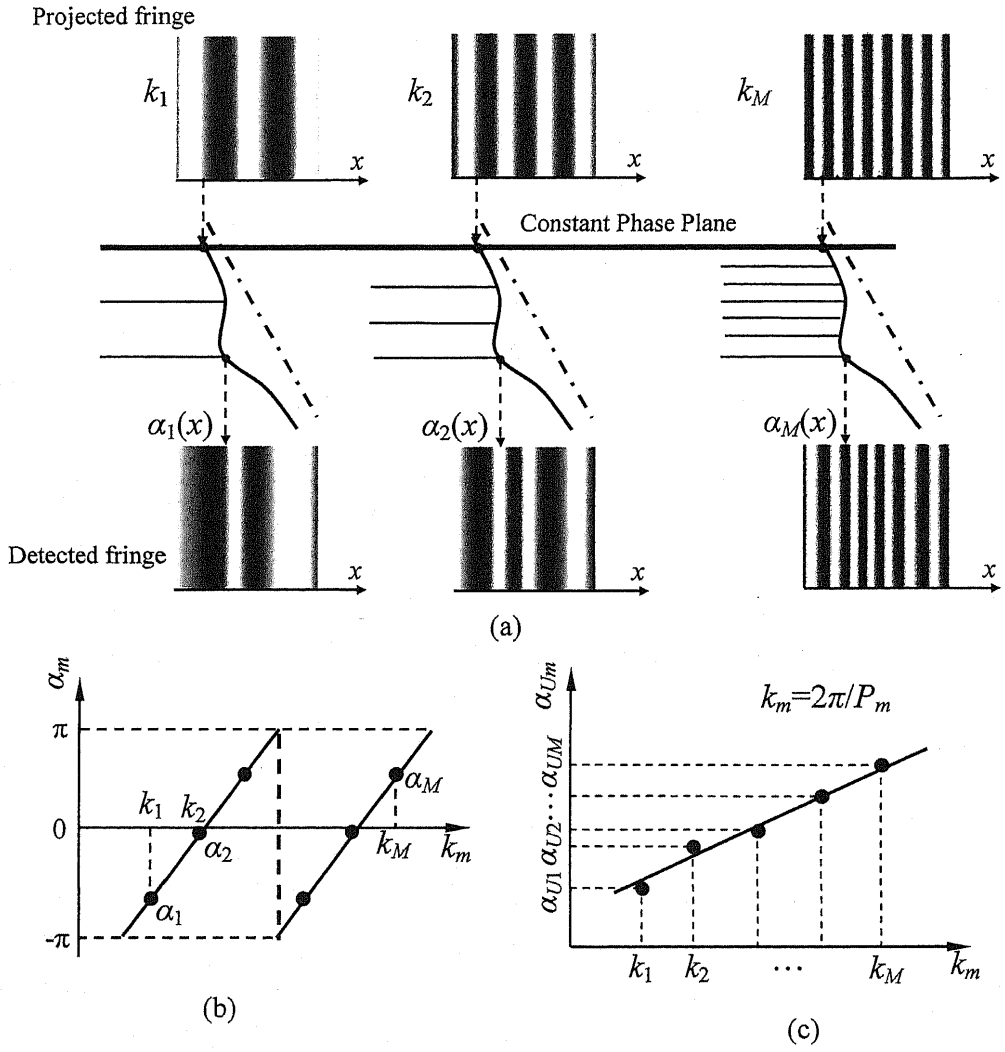

Fig. 1-7 Principle of TP method.

An important thing in the temporal phase-unwrapping method is how to realize a constant plane where the phase of the fringe pattern does not change while the period of the fringe pattern is scanned. For an example, in Ref. 12 the rotation axis of the mirror was used as the constant phase plane, which is not exact because of mechanical technique. The exactness of the constant phase plane directly affects the measurement accuracy.

Table 1-1 Comparison of three measurement methods

Method	Standard of measurement	Position difference between two adjacent point	Measurement precision*
Single-wavelength interferometry	Optical wavelength λ	Smaller than $\lambda/4$	$\lambda/100$
Fringe projection method	Period of fringe P	Smaller than $P/2$	$P/100$
Multi-period fringe projection method	Multi-period fringes $P_1, P_2 \ldots P_M$	Larger than fringe projection method	Dependent on the unwrapping algorithms

* It is assumed that the precision of the phase measurement is $2\pi/100$.

Comparison between the single-wavelength interfermetry, fringe projection method and multi-period projection method is shown in Tab. 1-1. From Tab. 1-1, high precision can be obtained by using the single-wavelength method, but the measurement range of this method is very small. The fringe projection method cannot be used to measure objects with discontinuities. The multi-period fringe projection method is suitable for measuring objects with large change of surface profile or surface profiles with discontinuities.

1.2 New Method Propose in This Thesis

A back-propagation method (BP method) [15-17] is incorporated into the multi-period fringe projection.

1.2.1 Sinusoidal Phase modulating interferometry for BP method

The sinusoidal phase modulating interferometry is used in the thesis, which is shown in Fig. 1-8. The multi-period fringe patterns are produced by a Twyman-Green interferometer. Piezoelectric transducer 1 (PZT1) changes the

angle θ of mirror 1, which changes the periods P_m of the interference fringe. The piezoelectric transducer 2 (PZT2) vibrates sinusoidally to produce the sinusoidal phase modulation in the interference fringe. The fringe pattern is projected on the surface of object and is detected by CCD camera.

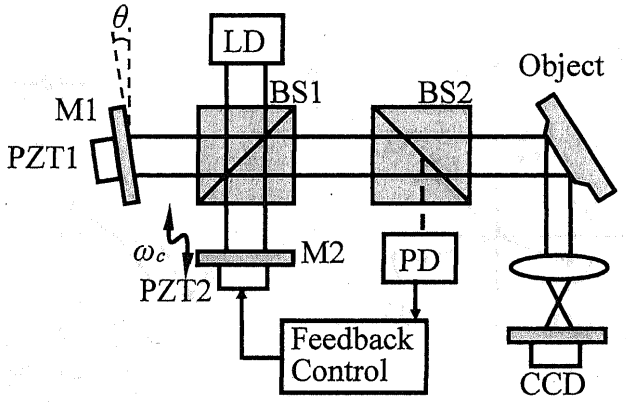

Fig. 1-8 SPM interferometry for the BP method

It is also important for this method to realize a constant phase plane where the phase of the fringe pattern does not change while the period of the fringe pattern is scanned. In our experiment an electrical feedback control system is used to realize a constant phase plane which is more accuracy than TP method.

1.2.2 Back-propagation method

Amplitudes and phases of the fringe patterns with different periods on the object surface are detected by using sinusoidal phase-modulating interferometry[4]. Optical fields $D_m(z)$ of the different fringe periods on the object surface are made from the detected amplitudes and phases, which is shown in Fig. 1-9 (a). Since the optical fields $D_O(0)$ on the constant phase point are not changed during the scanning of the fringe period, the optical fields $D_m(z)$ on each point of the object surface are back-propagated to the constant phase point along z axis direction, which is shown in Fig. 1-9 (b) and (c).

When the back-propagated fields reach to the constant phase point, the amplitude of the sum of the back-propagated fields with the different fringe periods becomes maximum and its phase becomes zero, which is shown in Fig.1-9(d). The back-propagation distance z from the each point of the object to the constant phase point provides the position of the object surface.

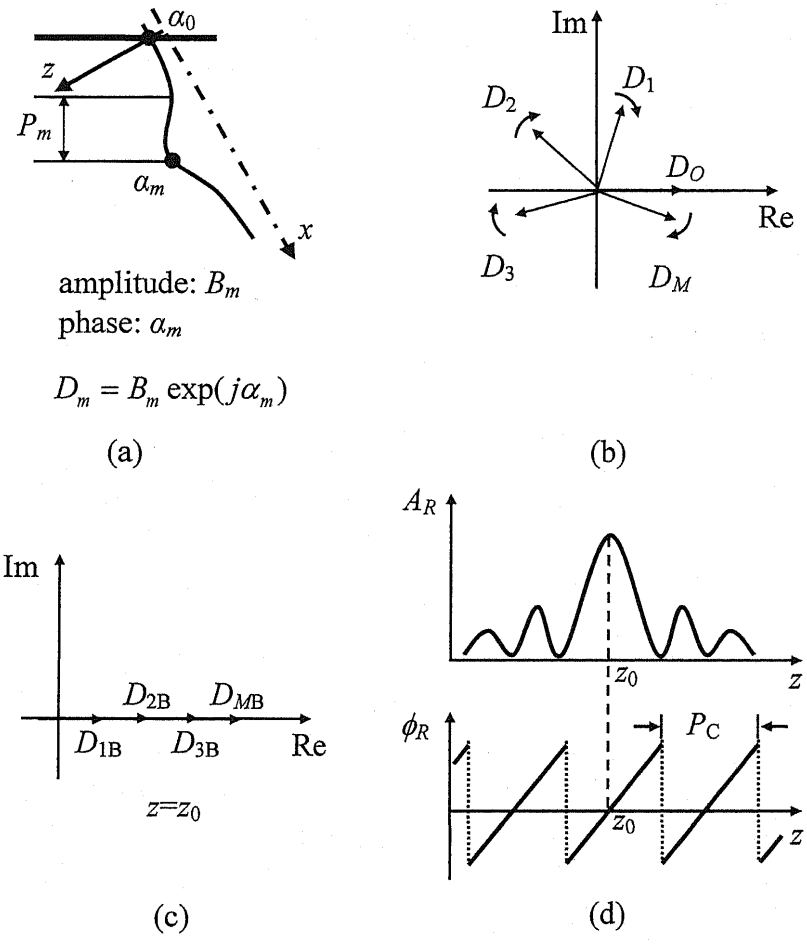

Fig. 1-9 Principle of BP method.

The measurement range of BP method is inversely proportional to the scanning interval Δk of k_m, and the measurement precision is better than TP method.

1.2.3 Comparison between three methods of multi-period fringe projection

Table 1-2 Comparison between three methods using the multi-period fringe projection

Unwrapping methods	Measurement range	Constant point in measurement	Measurement precision*
SP method	Smaller than maximum period P_{max}	not necessary	about $P_{min}/50$
TP method	Inversely proportional to the scanning interval Δk	necessary	$P_C/25$
BP method	Inversely proportional to the scanning interval Δk	necessary	$P_C/100$

* It is assumed that the precision of the phase measurement is $2\pi/50$.

Comparison between three unwrapping methods using in the multi-period fringe projection is shown in Tab. 1-2. Both TP method and BP method need a constant point in the measurement. The measurement precision of the BP method is higher than the TP method if the precision of the phase measurement is $2\pi/50$. The constant point in the measurement is not necessary for the spatiotemporal phase unwrapping method, but the measurement range is lower than the back-propagation method. Furthermore, the measurement accuracy of SP method is not so high because the phase value obtained from the smallest fringe period is used and the intermediate phase values are discarded.

1.3 Dissertation structure

The dissertation is structured as shown in Fig. 1-10.

In Chapter 1, single-wavelength interferometry, fringe projection method and multi-period fringe projection method are introduced and compared. The advantages of the multi-period fringe projection using back-propagation method are presented.

In Chapter 2, the principle of the sinusoidal phase modulating method and the detection of time-varying phase in SPM are described. The fundamental characteristics of two-dimensional Charge Couple Device (CCD), and the phase-lock control system producing constant phase point in the fringe patterns are introduced.

In Chapter 3, the multi-period fringe projection interferometry and the back-propagation method are presented. Characteristics of the back-propagation method are discussed, and the numerical analysis on back-propagation method has been done. The back-propagation method is compared with the phase gradient method which was used in other multi-period fringe projection methods. It is confirmed that the back-propagation method has a higher accuracy than the other methods. In experiments, a step profile made by gauge blocks and a step profile made by aluminum plates are measured. It is confirmed in the experiments that a distance of several millimeters can be measured with a high accuracy of several micros by using the back-propagation method in the multi-period fringe projection.

In Chapter 4, the back-propagation method is used to measure the object with two surfaces. First, it has been described that how the interference signal reflected from the two surfaces of the object. Then, how to detect the position of the two surfaces of the object by using back-propagation method is described. In experiments, a glass plate and an acrylic plate are measured. It is confirmed in the experiments that the shapes of two surfaces with thickness of several millimeters can be measured with a high accuracy of several micros by using the back-propagation method in the multi-period fringe projection.

Since the fringe period scanning is discrete, the measurement speed of the back-propagation method described in Chapters 3 and 4 is slow. In order to

increase the measurement speed, the continuous period-scanning for back-propagation method is proposed in Chapter 5. The triangular-wave vibration signal was applied to one mirror of the interferometer. The period of fringe pattern is changed continuously. The time-varying phase distribution is detected in SPM at one time. The positions of two surfaces are obtained from the back-propagation method. In experiments, an acrylic plate is measured. The measurement precision is the same as the method introduced in Chapter 4, and measurement speed is faster than that in Chapter 4.

In Chapter 6, the properties and results of this dissertation are presented.

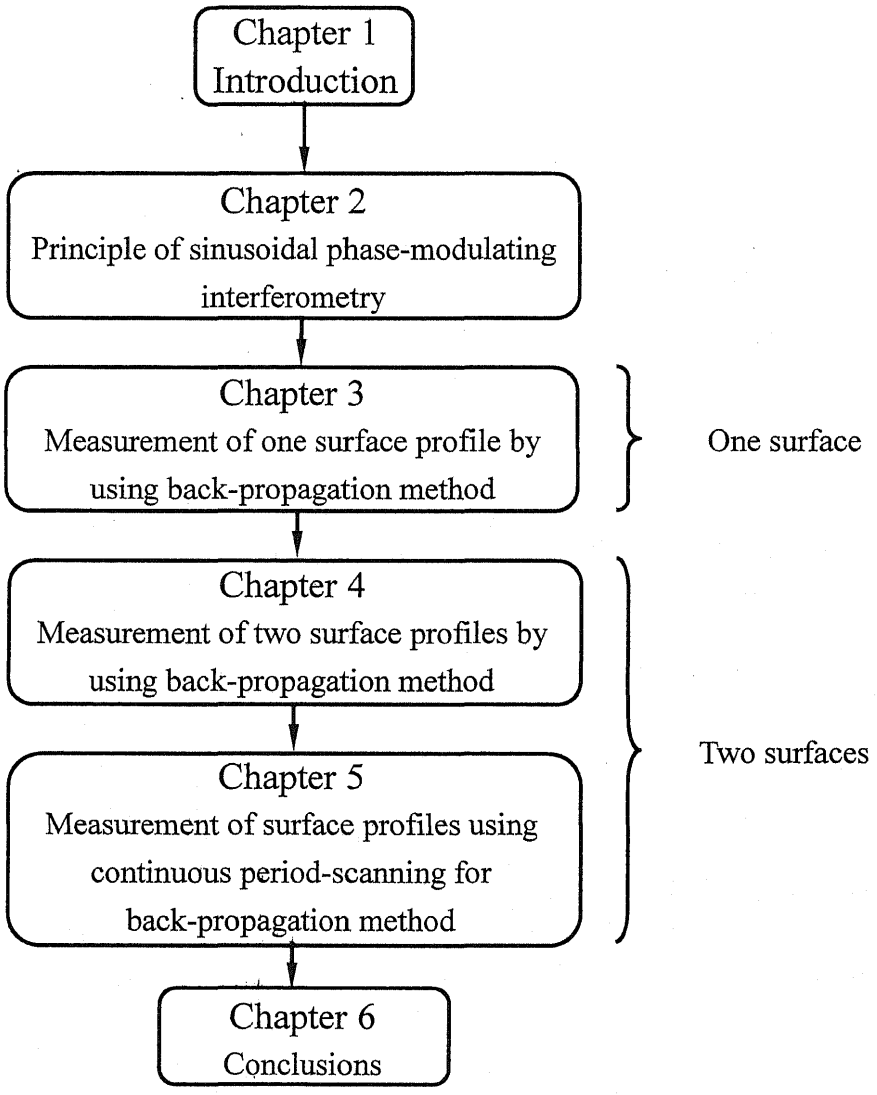

Fig. 1-10 Organization of this dissertation.

Chapter 2

Principle of sinusoidal phase-modulating interferometry

Sinusoidal phase-modulation interferometry used in the experiment is introduced in this chapter. First, in section 2.1, the sinusoidal phase-modulation interferometer is introduced. In the SPM interferometer, the reference mirror is vibrated sinusoidally in order to incorporate the sinusoidal phase modulation. The amplitude and the phase of the interference signal are calculated with the sinusoidal phase modulation method. Next the continuous period scanning SPM interferometer is introduced in section 2.2. In continuous period scanning SPM interferometer, the frequency components of the interference signal are calculated by using Fourier transformation. A change of the phase distribution is reflected into the frequency components of the interference signal.

A phase-lock system for reducing the effects of vibrations is installed in a SPM interferometer using a laser diode (LD), which is introduced in section 2.3. The phase fluctuation caused by the vibration is reduced by changing the applied voltage of the PZT with the phase-lock control system.

2.1 Sinusoidal phase-modulation interferometry

Figure 2-1 shows an interferometer where the sinusoidal phase-modulation is performed by vibrating the mirror M1 with a piezoelectric transducer (PZT). The vibration of the mirror is given by

$$A(t) = a\cos(\omega_c t + \theta) \tag{2-1}$$

where $a\cos(\omega_c t)$ is a sinusoidal phase modulating term, θ is the initial phase, $\omega_C/2\pi$ is the modulation frequency.

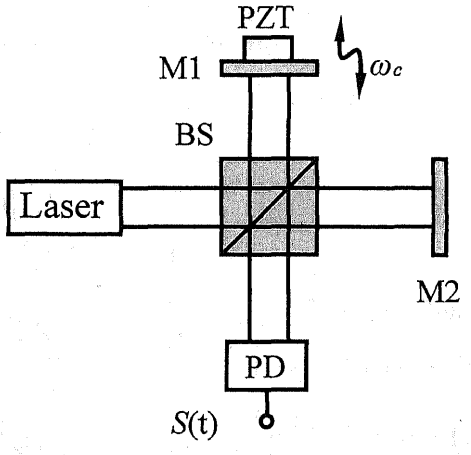

Fig 2-1 Sinusoidal phase-modulation interferometer

The intensity distribution of the sinusoidally vibrating interference pattern (SVIP) is express by

$$S(t) = A + B\cos[Z_c\cos(\omega_c t + \theta) + \alpha] \tag{2-2}$$

where A is a constant, B is amplitude of the time-varying component. When the period of the interference pattern is P, The modulation amplitude is $Z_c=2\pi a/P$, and the phase is $\alpha=2\pi x/P$.

The ac component of Eq. (2-2) is written as

$$S(t) = B\cos[Z_c\cos(\omega_c t + \theta) + \alpha] \tag{2-3}$$

The Bessel function expansion of Eq. (2.3) is given by

$$
\begin{aligned}
S(t) &= \cos\left[Z_c \cos(\omega_c t + \theta) + \alpha \right] \\
&= \cos\alpha \cos\left[Z_c \cos(\omega_c t + \theta) \right] - \sin\alpha \sin\left[Z_c \cos(\omega_c t + \theta) \right] \\
&= \cos\alpha \{ J_0(Z_c) + 2\sum_{m=1}^{\infty} J_{2m}(Z_c)(-1)^m \cos[2m(\omega_c t + \theta)] \} \\
&\quad -\sin\alpha \{ 2\sum_{m=1}^{\infty} J_{2m-1}(Z_c)(-1)^{m-1} \cos[(2m-1)(\omega_c t + \theta)] \}
\end{aligned}
\tag{2-4}
$$

where $J_n(Z_c)$ is the *n-th* order Bessel function.

The fast Fourier transform of Eq. (2-4) is given by

$$
\begin{aligned}
F(\omega) &= \Im\{S(t)\} \\
&= \cos\alpha \left\{ \begin{array}{l} J_0(Z_c)\delta(\omega) \\ +\sum_{m=1}^{\infty} J_{2m}(Z_c)(-1)^m \left[\begin{array}{l} e^{j2m\theta}\delta(\omega - 2m\omega_c) \\ +e^{-j2m\theta}\delta(\omega + 2m\omega_c) \end{array} \right] \end{array} \right\} \\
&\quad +\sin\alpha \left\{ \sum_{m=1}^{\infty} J_{2m-1}(Z_c)(-1)^m \left[\begin{array}{l} e^{j(2m-1)\theta}\delta\left[\omega - (2m-1)\omega_c\right] \\ +e^{-j(2m-1)\theta}\delta\left[\omega + (2m-1)\omega_c\right] \end{array} \right] \right\}
\end{aligned}
\tag{2-5}
$$

The spectrum of the Eq. (2-5) is shown in Fig. 2-2. The distribution of Bessel function is shown in Fig.2-3. From the spectrum, Z_c, α, θ are calculated.

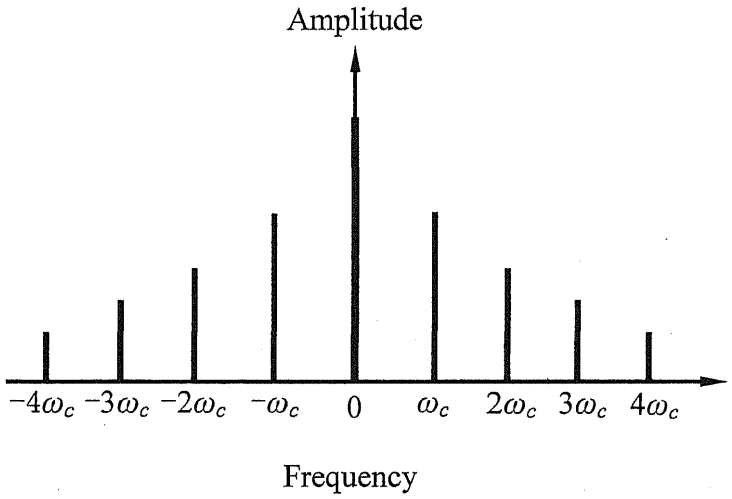

Fig. 2-2 Spectrum distribution of $F(\omega)$

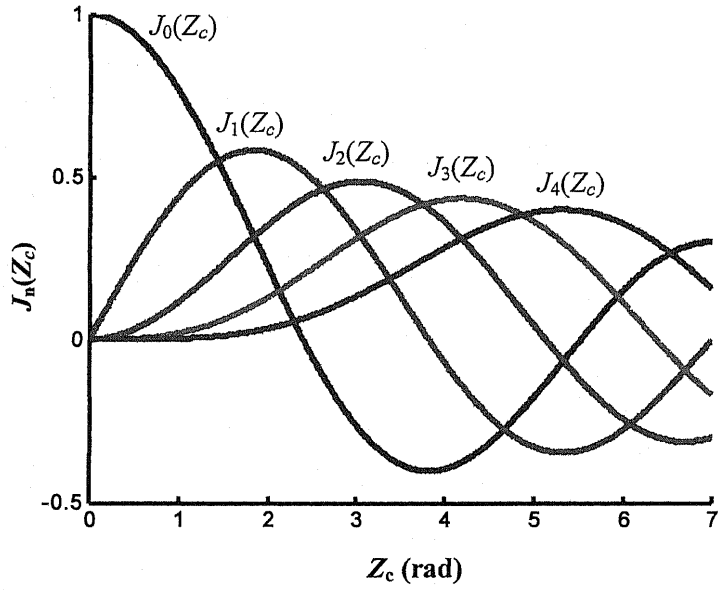

Fig. 2-3 Distribution of the *n-th* order Bessel function

The expressions for each frequency component are

$$F(\omega_c) = -\sin\alpha J_1(Z_c)e^{j\theta}, \tag{2-6}$$

$$F(2\omega_c) = -\cos\alpha J_2(Z_c)e^{j2\theta}, \tag{2-7}$$

$$F(3\omega_c) = \sin\alpha J_3(Z_c)e^{j3\theta}, \tag{2-8}$$

$$F(4\omega_c) = \cos\alpha J_4(Z_c)e^{j4\theta}. \tag{2-9}$$

2.1.1 *Z* calculation

Denoting Fourier transform of $S(t)$ by $F(\omega)$, the modulation amplitude Z_c is obtained from Eq. (2-6) and Eq. (2-8), and Z is calculated by

$$\left|\frac{F(3\omega_c)}{F(\omega_c)}\right| = \left|\frac{\sin\alpha J_3(Z_c)e^{j3\theta}}{-\sin\alpha J_1(Z_c)e^{j\theta}}\right| = \left|\frac{J_3(Z_c)}{J_1(Z_c)}\right| = r_{31} \tag{2-10}$$

By using the relation of z and r_{31} as shown in Fig. 2-4, the value of Z_c can be obtained.

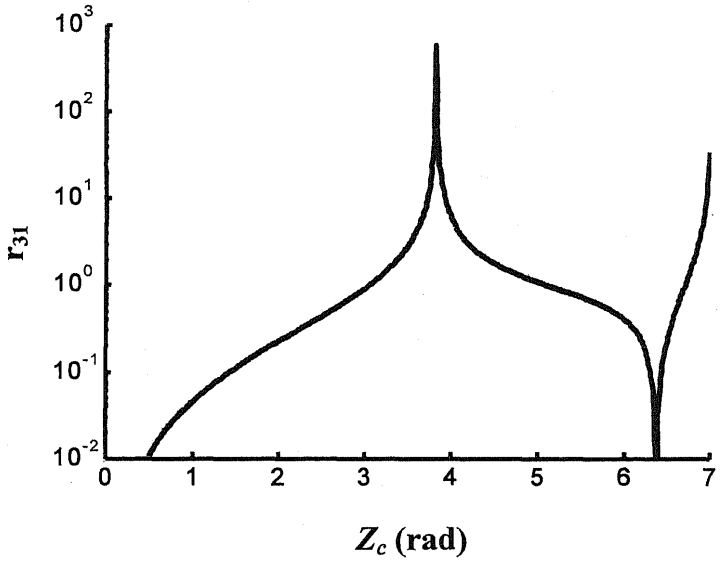

Fig. 2-4 The relationship between the ratio r_{31} and the modulating depth Z_c

2.1.2 θ calculation

From the calculated value of Z_c and Eq. (2-10), the initial modulation phase θ can be given by the argument of the complex number $F(\omega_c)$ as follow:

$$\begin{aligned} Arg\{-F(\omega_c)\} &= Arg\{\sin\alpha J_1(Z_c)e^{j\theta}\} \\ &= \begin{cases} \theta & (\alpha \geq 0) \\ \theta+\pi & (\alpha < 0) \end{cases} \end{aligned} \tag{2-11}$$

where, $J_1(Z_c)>0$, $-\pi \leq \alpha \leq \pi$, $-\pi \leq \theta \leq \pi$

2.1.3 α calculation

when Z and θ are determined, phase α can be calculated from Eqs. (2-6) and (2-7) as

$$\frac{F(\omega_c)/J_1(Z_c)}{F(2\omega_c)/J_2(Z_c)} = \frac{\sin\alpha}{\cos\alpha} = \tan\alpha \tag{2-12}$$

since from the Eq. (2-12), sign of phase α can not clear. For the sake of clarity, the calculated initial phase θ is used to determine the sign of α as follows:

a) sign of $\sin\alpha$

$$-\frac{\mathrm{Re}\{F(\omega_c)\}}{\cos\theta} = -\frac{-\sin\alpha\cos\theta J_1(Z_c)}{\cos\theta} = \sin\alpha J_1(Z_c) \tag{2-13}$$

b) sign of $\cos\alpha$

$$-\frac{\mathrm{Re}\{F(2\omega_c)\}}{\cos 2\theta} = -\frac{-\cos\alpha\cos 2\theta J_2(Z_c)}{\cos 2\theta} = \cos\alpha J_2(Z_c) \tag{2-14}$$

From a) and b), phase α can be given exactly by

$$\tan\alpha = \frac{|F(\omega_c)/J_1(Z_c)| \times \mathrm{sgn}[-\mathrm{Re}\{F(\omega_c)\}/\cos\theta]}{|F(2\omega_c)/J_2(Z_c)| \times \mathrm{sgn}[-\mathrm{Re}\{F(2\omega_c)\}/\cos 2\theta]} \tag{2-15}$$

where, sign function is

$$\begin{aligned} \mathrm{sgn}[x] &= +1 \quad (x \geq 0) \\ &= -1 \quad (x \leq 0) \end{aligned} \tag{2-16}$$

2.2 Detection of time-varying phase in SPM

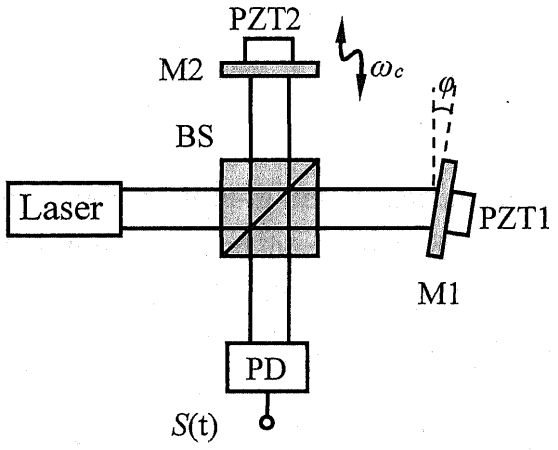

Fig. 2-5 Continuous period scanning SPM interferometry

Fig. 2-5 shows a configuration of continuous period scanning SPM interferometer which produces the time-varying phase signal. The beams reflected from mirror M1 and mirror M2 produce the interference fringe. Piezoelectric transducer 1 (PZT1) changes the angle φ of mirror 1 continuously, which changes the periods P of the interference fringe. The piezoelectric transducer 2 (PZT2) vibrates sinusoidally to produce the sinusoidal phase modulation in the interference fringe. The interference signal detected on the PD is given by

$$S(t) = A + B\cos[Z_c \cos(\omega_c t + \theta) + \Phi(t)]. \tag{2-17}$$

where

$$\Phi(t) = k(t)x + \alpha \tag{2-18}$$

where $k=2\pi/P$, and it is called wave number of the fringe pattern. As we have explained in section 2.1, $S(t)$ is expanded in Bessel functions. The fast Fourier

transform of $S(t)$ is given by

$$F(\omega)=\delta(\omega)+\Im\{B\cos[\Phi(t)]\}\otimes[\sum_{m=-\infty}^{\infty}(-1)^m A_{2m}\delta(\omega-2m\omega_c)] \\ +\Im\{B\sin[\Phi(t)]\}\otimes\{\sum_{m=-\infty}^{\infty}(-1)^m A_{2m-1}\delta[\omega-(2m-1)\omega_c]\} \tag{2-19}$$

where $A_m=J_{|m|}(Z_c)\exp(jm\theta)$, $J_{|m|}$ is *m-th* Bessel function, $\delta(\omega)$ is the delta function, $\Im\{y\}$ is a Fourier transform of y, and the symbol $\otimes$ represents convolution. The spectrum distribution of Eq. (2-19) is shown in Fig. 2-6

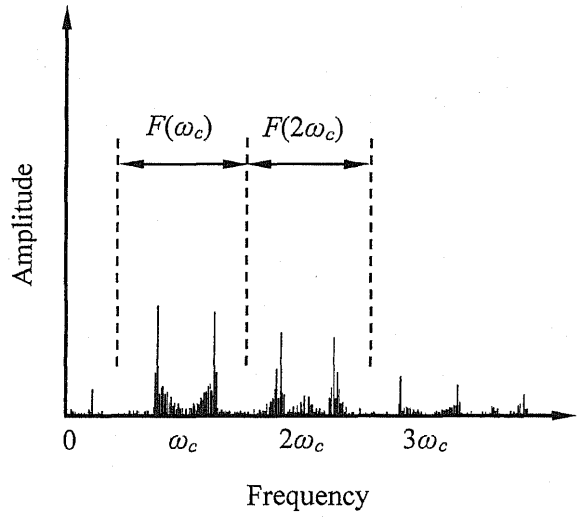

Fig. 2-6 Spectrum distribution of $F(\omega)$

- In the conditions

$$\Im\{B\cos[\Phi(t)]\}=0 \quad |\omega|\geq\omega_c/2 \tag{2-20}$$

$$\Im\{B\sin[\Phi(t)]\}=0 \quad |\omega|\geq\omega_c/2 \tag{2-21}$$

we designate the frequency components existing in the ranges of $\omega_c/2<\omega<3\omega_c/2$ and $3\omega_c/2<\omega<5\omega_c/2$ by $F_1(\omega)$ and $F_2(\omega)$, respectively. Then we have

$$F_1(\omega-\omega_c)=-2BJ_1(Z_c)\exp(j\theta)\Im\{\sin[\Phi(t)]\},\quad |\omega|<\omega_c/2 \tag{2-22}$$

$$F_2(\omega-2\omega_c)=-2BJ_2(Z_c)\exp(j2\theta)\Im\{\cos[\Phi(t)]\}\quad |\omega|<\omega_c/2 \tag{2-23}$$

By taking the inverse Fourier transform of Eqs. (2-22) and (2-23), we can obtain the functions of $\sin[\Phi(t)]$ and $\cos[\Phi(t)]$, which is given by

$$2B\sin[\Phi(t)]=\Im^{-1}\left[\frac{F_1(\omega-\omega_c)}{-J_1(Z_c)\exp(j\theta)}\right], \tag{2-24}$$

$$2B\cos[\Phi(t)]=\Im^{-1}\left[\frac{F_2(\omega-2\omega_c)}{-J_2(Z_c)\exp(j2\theta)}\right]. \tag{2-25}$$

where $\Im^{1}\{y\}$ is a inverse Fourier transform of y. The phase distribution of $\Phi(t)$ is given by

$$\begin{aligned}\Phi(t)&=\tan^{-1}\left[\frac{2B\sin[\Phi(t)]}{2B\cos[\Phi(t)]}\right]\\&=\tan^{-1}\left[\frac{\Im^{-1}[F_1(\omega-\omega_c)/J_1(Z_c)\exp(j\theta)]}{\Im^{-1}[F_2(\omega-2\omega_c)/J_2(Z_c)\exp(j2\theta)]}\right]\end{aligned} \tag{2-26}$$

2.3 Signal detection with a CCD image sensor

When a two-dimensional CCD image sensor (hereafter it is called CCD, the CCD here used is PHOTRON FASTCAM-PCI 2K) is used as a photodetector, the output of the CCD is an integration of the time-varying signal $S(t)$ over the storage period T_A of the CCD. T_A must be equal to the sampling interval $\Delta t=(1/p)(1/f_C)$), where p=8 or 16 and $f_C=\omega_C/2\pi$. The output $g(m\Delta t)$ of the CCD is represented by

$$g(m\Delta t) = \int_{-T_A/2}^{T_A/2} S(t + m\Delta t)dt \qquad m = 0,1,2,\cdots,M-1 \tag{2-27}$$

Fourier transform $F(m\Delta f)$ is obtained from Fourier transform $G(m\Delta f)$ of $g(m\Delta t)$ which is given by

$$G(m\Delta f) = F(m\Delta f)[\sin(\pi m / M)/(\pi m / M)], \tag{2-28}$$

where $\Delta f = 1/M\Delta t$, $T_A = T_C/16$ is the charge storage period. T_A is set to a 1/8 period of the modulating signal in our system as shown in Fig. 2-7.

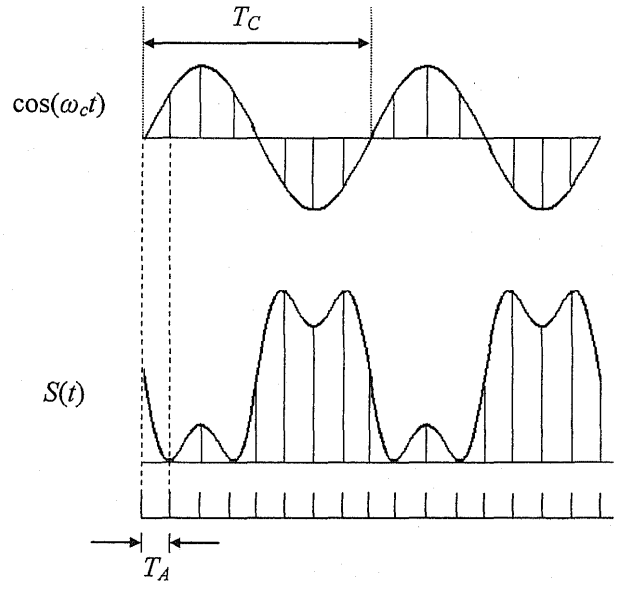

Fig. 2-7 Modulating signal and interference signal

2.4 Phase-lock control in SPM interferometry

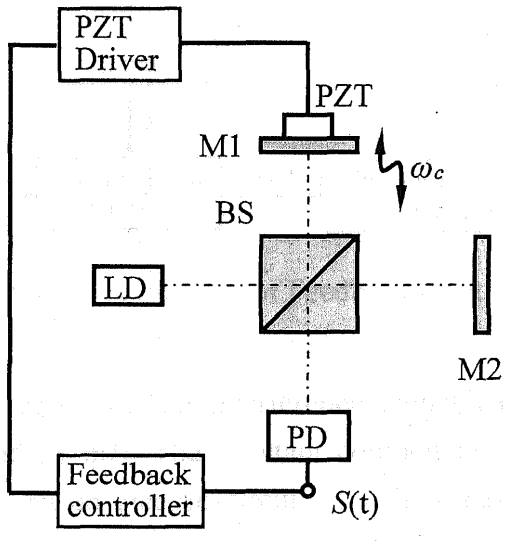

Fig. 2-8 Phase-lock control system in SPM interferometer

A phase-lock system for reducing the effects of vibrations and producing exactly the constant phase point of the fringe pattern is installed in a SPM interferometer as shown in Fig. 2-8. The phase fluctuation caused by the vibration is reduced by changing the applied voltage of the PZT with the feedback controller.

The intensity distribution of the sinusoidally vibrating interference pattern (SVIP) is expressed by

$$S(t) = A + B\cos[Z_c \cos(\omega_c t + \theta) + \alpha] \tag{2-29}$$

where A is a constant, B is amplitude of the time-varying component.

The block diagram of feedback controller is shown in Fig. 2-9. It is consists of a high-pass filter, a sampling pulse generator, a sample-and-hold circuit, and a proportional-integral controller.

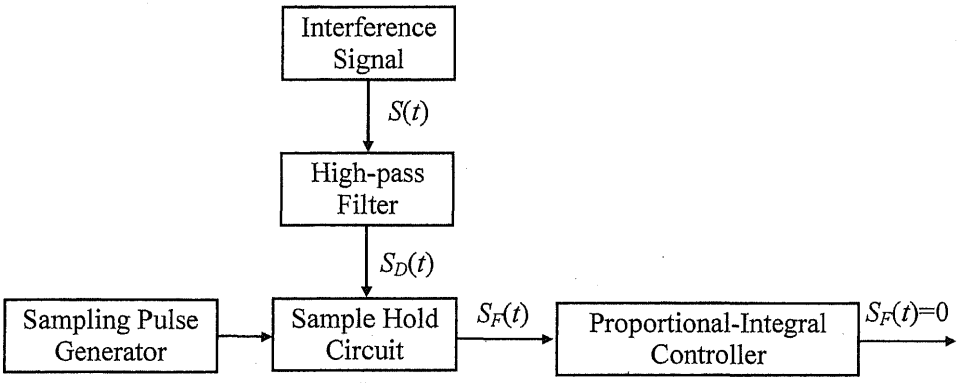

Fig. 2-9 Block diagram of Feedback Controller

The fluctuation in phase of the interference signal caused by mechanical vibrations is expressed by $\eta(t)$. The constant component A in the interference signal is eliminated with an electric circuit of a high-pass filter, and the DC component of the signal is given by

$$S_D(t) = B\cos[Z_c\cos(\omega_c t + \theta) + \alpha + \eta(t)] \tag{2-30}$$

The feedback signal is generated from $S_D(t)$ by use of a sampling technique. Figure 2-10 illustrates a series of waveforms in the signal processing.
The sinusoidal signal is fed into the sampling pulse generator. The sampling pulse is shown in Fig. 2-10(b). $S_D(t)$ is sampled and held by using the sample-and-hold circuit, when $\cos(\omega_c t + \theta)$ is equal to zero, a phase-detected signal is given by

$$S_F(t) = B_F\cos[\alpha(t) + \eta(t)] \tag{2-31}$$

This signal is used as a feedback signal with which the applied voltage of the PZT is controlled. The effect of the mechanical vibrations is eliminated by controlling the applied voltage so that $S_F(t)$ becomes to zero with proportional and integral feedback controller. Then the phase of $\alpha + \eta(t)$ becomes to a constant of $\pi/2$, and the signal at the phase of $\pi/2$ is shown as in Fig .2-10(c).

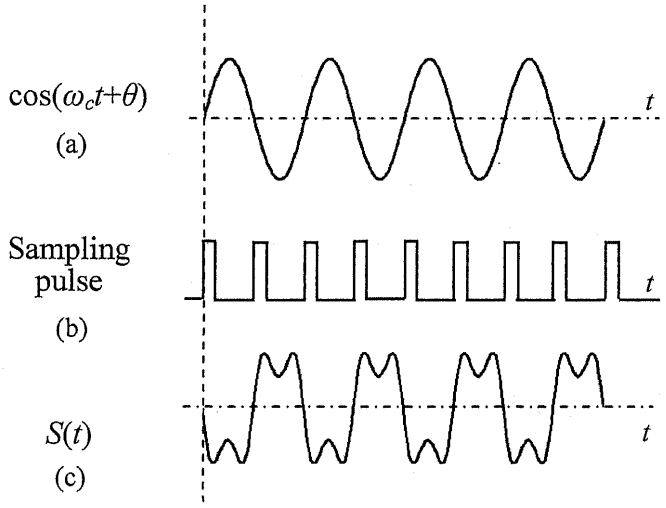

Fig. 2-10 Schematic of the feedback control: (a) sinusoidal signal for the phase modulation, (b) sampling pulse, (c) interference signal.

Chapter 3

Measurement of one surface profile by using back-propagation method

3.1 Introduction

Moiré and fringe projection techniques are noncontact optical techniques that have been widely applied in industry for measuring 3-D profile of object surfaces[5]. These two techniques use the fringe patterns projected onto the object surfaces which are generated with either a grating or two laser beams. The surface profile of the object is obtained from a phase distribution of the fringe pattern which is calculated by the phase-shifting method[2] or by the Fourier transform method[3]. Since the phase distribution of the fringe pattern lies in the range from $-\pi$ to π, spatial phase unwrapping must be carried out to recover the surface profile. However, since the phases of two adjacent measurement points are compared and connected in spatial phase unwrapping, it is impossible to recover the surface profile with discontinuities such as height steps or spatially isolated surfaces which cause phase jumps larger than 2π. The moiré and fringe projection techniques using only one-period fringe projection are difficult to measure object surfaces with the discontinuities.

Recently some methods using multi-period fringe projection have been proposed to measure object surfaces with the discontinuities. These methods have some analogy with multi-wavelength interferometer techniques[6-8]. One basic idea of multi-period fringe projection technique is to use a fringe pattern with a large period which makes the phase jump smaller than 2π for the spatial phase unwrapping. Since the measurement accuracy is not high when the period of the fringe is large, fringe patterns of small periods are used to improve the accuracy.

A simple method based on this idea has been reported in Ref. 9 in which just two different periods were used. This idea was developed by using fringe patterns of several periods for measuring discontinuous objects with a higher accuracy as described in Ref. 10. Another basic idea of multi-period fringe projection technique is to use the intensity or phase change of the projected fringe pattern on each measurement point of the object surface when the fringe period is scanned. A method using the intensity change in a shadow moiré profilometry was reported in Ref. 18. The intensity change with time was a sinusoidal waveform on each point of the object surface, and the height distribution on the object was proportional to the frequency of the intensity change. Since the Fourier-transform was used to obtain the frequency of the intensity change, the wave number or the reciprocal of the fringe period must be increased exactly at the same interval. Also in multi-period fringe projection, a similar method using the intensity change and its frequency was reported in Ref.13. A method using the phase change on each measurement point was reported in Ref. 11 which is called temporal phase-unwrapping method. Interference fringes with different periods were projected on the object surface at different times. The wrapped phase values measured during the scanning of the fringe period were unwrapped along the time axis on each measurement point. The height of the object surface on each point was obtained from the total value[12] of the phase change occurred during the scanning of the fringe period. The measurement accuracy of this method using the total value is not so high because only the two phase values at the largest and the smallest fringe periods are used and the intermediate phase values are discarded. In Ref. 13 these intermediate phase values were used to estimate the gradient of the phase change which provided the height of the object surface in the same way as that in multi-wavelength interferometers. Several methods using multi-period fringe projection were compared through numerical simulations and very simple experiments in Refs. 13 and 14. It is important for achieving a higher measurement accuracy to use effectively all phase values obtained during the scanning of the fringe period. Another important thing in the temporal phase-unwrapping method is how to realize a constant phase point where the phase of the fringe pattern does not change while the period of the fringe pattern is scanned. For an example, in Ref. 12 the rotation axis of the mirror was used as

the constant phase point. The exactness of the constant phase point directly affects the measurement accuracy.

In this chapter a multi-period fringe-projection is executed with an interferometer in a similar way to Ref. 12. However using sinusoidal phase-modulating interferometry enables us to produce exactly the constant phase point of the fringe pattern by a phase-lock technique[19]. The constant phase point produced electrically in this paper has higher accuracy than that produced mechanically in Ref. 12. Amplitudes and phases of the fringe patterns with different periods on the object surface are detected by using sinusoidal phase-modulating interferometry[4]. Optical fields of the different fringe periods on the object surface are made from the detected amplitudes and phases. Since the optical fields on the constant phase point are not changed during the scanning of the fringe period, the optical fields on each point of the object surface are back-propagated to the constant phase point. When the back-propagated fields reach to the constant phase point, the amplitude of the sum of the back-propagated fields with the different fringe periods becomes maximum and its phase becomes zero. The back-propagation distance from the each point of the object to the constant phase point provides the position of the object surface. This method is hereafter called back-propagation method. Simulations make it clear that measurement results by the back-propagation method are not sensitive to noises contained in the measured phase. Although the back-propagation method needs a long computation time, it achieves a measurement accuracy higher than the other methods in the multi-period fringe projection. In experiments, a step profile made by gauge blocks and a step profile made by aluminum plates are measured. It is confirmed in the experiments that a distance of several millimeters can be measured with a high accuracy of several micros by using the back-propagation method in the multi-period fringe projection.

3.2 Interferometer and back-propagation method

A schematic configuration for the multi-period fringe projection interferometry is shown in Fig.3-1. Two plane waves of wavelength λ propagating in different directions produce a parallel interference fringe in the space. The coordinate

system (x_p, y_p, z_p) is involved with the fringe pattern as shown in Fig. 1. The intersecting angles between the two waves and the z_p axis are $\pm\theta_m$, respectively. The period of the fringe pattern is expressed by $P_m=\lambda/2\theta_m$ since $\sin\theta_m\approx\theta_m$ when θ_m is small. Changing the intersecting angles θ_m as θ_0, θ_1..., and θ_{M-1}, the periods of the fringe pattern P_m are scanned as P_0, P_1..., and P_{M-1} accordingly. The phase of the interference fringe at $x_p=0$ is kept at $\pi/2$ during the period scanning by using a feedback control system. The phase distribution in the coordinate system (x_p, y_p, z_p) is written as

$$\alpha_m(z_p, x_p) = k_m x_p + \frac{\pi}{2}, \tag{3-1}$$

where $k_m = \frac{2\pi}{P_m}$, and it is called wave number of the fringe pattern.

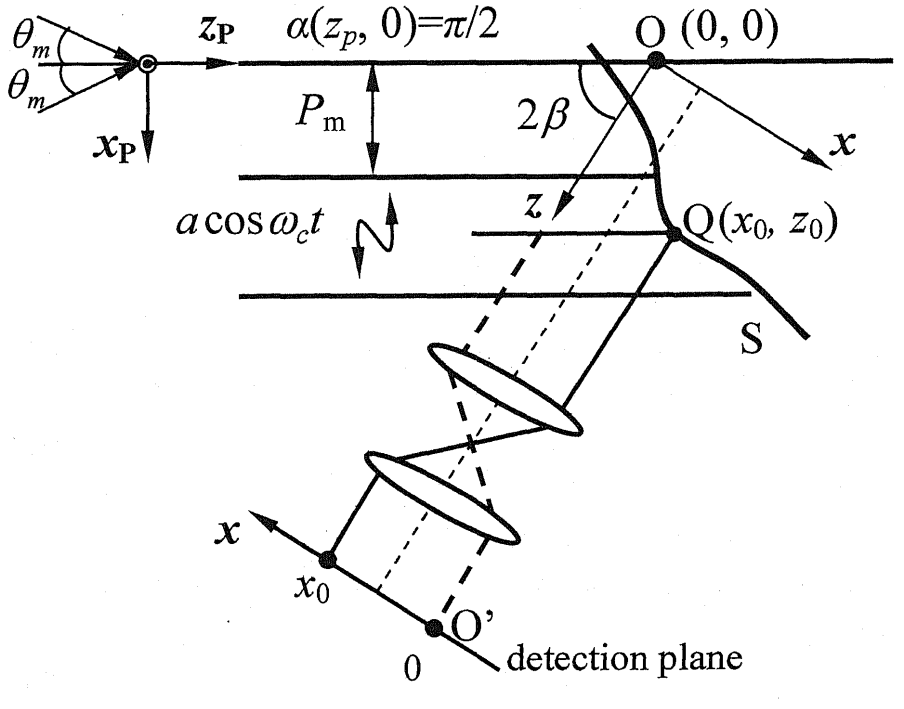

Fig 3-1 Schematic configuration for multi-period fringe projection and detection of the fringe patterns by sinusoidal phase-modulating interferometry.

It is assumed that there is a point object Q on the surface of the object. An image of the point is formed on a detection plane with an afocal imaging system. Another coordinate system (x, y, z) involved with the imaging system is defined. The original O of the coordinate system (x, y, z) is the same as that of the coordinate system (x_p, y_p, z_p). The z axis is parallel to the optical axis of the imaging system. The intersection angle of the axis z_p and the axis z is 2β. The phase distribution in the coordinate system (x, y, z) is written as

$$\alpha_m(x,z) = k_m(x\cos 2\beta + z\sin 2\beta) + \frac{\pi}{2}. \tag{3-2}$$

The position of the point object Q is expressed by $x=x_0$ and $z=z_0$. The magnification of the imaging system is assumed to be unit for the sake of simplicity. The size of an object is limited to less than the aperture of the afocal imaging system. The position of $x=0$ on the detection plane corresponds to the original O and the image of the point object Q is formed at $x=x_0$ on the detection plane. The interference fringe intensity oscillates sinusoidally in the direction of the x_p axis with the form of $a\cos\omega_c t$ in order to incorporate the sinusoidal phase-modulating interferometry. Then the following interference signal produced by the point object Q is detected on the detection plane:

$$I_m(x_0,t) = A_m + B_m\cos[a\cos\omega_c t + \alpha_m(x_0,z_0)], \quad m = 0,\cdots,M-1. \tag{3-3}$$

The amplitude B_m and the phase α_m of the interference signal are calculated with the sinusoidal phase modulation method. The calculated value of $\alpha_m(z_0)$ is wrapped in the range between $-\pi$ and π. Since the original point of the coordinate x on the detection plane is decided by finding a position where the phase α_m is a constant value of $\pi/2$ during the scanning of the fringe period, the coordinate x_0 of the object is provided by the position of the detection plane. The following phase α_{mz} is extracted from the phase $\alpha_m(x_0, z_0)$ by subtracting the value of $k_m x_0\cos 2\beta+\pi/2$ from the calculated value of $\alpha_m(z_0)$:

$$\alpha_{mz}(z_0) = k_m z_0 \sin 2\beta. \tag{3-4}$$

The range of $\alpha_{mz}(z_0)$ is between $2n\pi$-π and $2n\pi$+π, where n is an integer value and the component of $2n\pi$ is removed from the $\alpha_{mz}(z_0)$. Since the coordinate x_0 of the object is known, a method which is called the back-propagation method is used to get the coordinate z_0 of the point object.

In the back-propagation method, the detected field of the point object Q is made as

$$D_m(x_0, z_0) = B_m \exp[j\alpha_{mz}(z_0)]. \tag{3-5}$$

When the detected field D_m is back-propagated to a position z, the back-propagated field of $U_m(x_0, z)$ is given by

$$U_m(x_0, z) = D_m \exp[-j\alpha_{mz}(z)], \quad m = 0, \cdots, M-1. \tag{3-6}$$

The sum of the back-propagated fields over all of k_m produces the following reconstruction field as a function of back-propagation position z:

$$U_R(z) = \sum_{m=0}^{M-1} U_m(z) = \sum_{m=0}^{M-1} B_m \exp[-jSk_m(z - z_0)], \tag{3-7}$$

where S is the incline coefficient which is written as S=sin2β and k_m is the wave number of the fringe pattern. k_m is expressed as k_m=k_0+$m\Delta k$, where Δk is the scanning interval of k_m. If B_m and z_D are denoted by B_m=1 and z_D=z–z_0, Eq. (3-7) is reduced to

$$\begin{aligned} U_R(z) &= \exp\{j[-k_0 + \frac{(M-1)}{2}\Delta k]Sz_D\} \frac{\sin(\frac{M}{2}\Delta k z_D S)}{\sin(\frac{1}{2}\Delta k z_D S)} \\ &= A_R \exp(j\phi_R) \end{aligned} \tag{3-8}$$

Therefore the amplitude A_R of U_R is given by

$$A_R = \frac{\sin(\frac{B_k}{2} z_D S)}{\sin(\frac{\Delta k}{2} z_D S)} \tag{3-9}$$

where $B_k=M\Delta k$ is the scanning range. When z_D is close to zero, Eq. (3-9) can be approximated as $A_R=M\sin(MWz_D)/(MWz_D)$, where $W=\Delta kS/2$. The phase distribution ϕ_R of U_R is given by

$$\phi_R = [-k_0 + \frac{(M-1)}{2}\Delta k]Sz_D = -k_C S z_D \tag{3-10}$$

where $k_C=k_0-(M-1)\Delta k/2$ is the central wave number.

From Eqs. (3-9) and (3-10), the amplitude of A_R becomes maximum and its phase ϕ_R becomes zero at $z_D=0$ where z is equal to the coordinate z_0 of the point object Q. From this basic characteristic, the coordinate z_0 of the object point Q can be obtained.

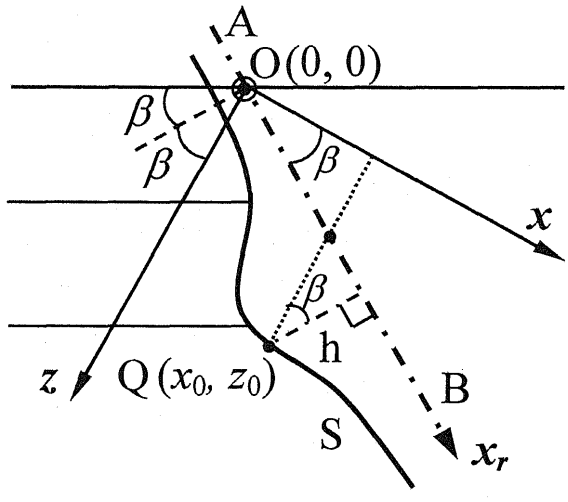

Fig 3-2 Height h from standard plane AB in measurement of surface profile S.

Now measurement of surface profile S of an object is considered as shown in Fig.3-2. The coordinate z of each point on the surface of the object is calculated with the back-propagation method described above. In order to get the height distribution of the surface, a reference plane AB is defined as shown in Fig.3-2. The intersecting angle between the reference plane and the coordinate x is β so that the interference fringe reflected by the reference plane propagates in the direction of the z axis which is the optical axis of the imaging system. The coordinate x_r of the reference plane corresponding to the object point Q is expressed as

$$x_r = x_0 \cos\beta + z_0 \sin\beta \tag{3-11}$$

The height h normal to the reference plane on a point (x_r, y_r) is given by

$$h(x_r, y_r) = (z_0 - x_0 \tan\beta)\cos\beta. \tag{3-12}$$

3.3 Numerical analysis on back-propagation method

Characteristics of the back-propagation method are discussed in this section. The scanning interval of k_m is given by

$$\Delta k = \frac{2\pi}{M-1}\left(\frac{1}{P_0} - \frac{1}{P_{M-1}}\right) = \frac{(k_{M-1} - k_0)}{M-1}. \tag{3-13}$$

Since $U_m(z)$ is a discrete function with respect to k_m, $U_R(z)$ becomes a periodic function with respect to z. Considering Eqs. (3-4)-(3-7), the period of $U_R(z)$ or the measurement range of z is given by

$$z_{max} = \frac{2\pi}{\Delta k S}. \tag{3-14}$$

The phase ϕ_R changes linearly with respect to z, and its period which is called central period is given by Eq. (3-10)

$$P_C = \frac{2\pi}{k_C S} = \frac{2P_0 P_{M-1}}{(P_0 + P_{M-1})S}. \tag{3-15}$$

Figure 3-3 shows the simulation results of the back-propagation method. The scanning period of the fringe is from 200μm to 400μm with M=6, Δk=0.0031(rad/μm), β=45°, and z_{max}=2000μm. The value of z_0 is 1525μm. The amplitude B_m of the interference signal is a constant value of 1 for all P_m. Figure 3-3 indicates that the amplitude distribution A_R of U_R has a maximum value at z=z_A and its phase distribution ϕ_R has a zero value at z=z_ϕ with the period P_C of 266.7μm. When there is no error in the measurement, the values of z_A and z_ϕ are equal to the position z_0 of the point object.

It is assumed that the measured phase distribution α_m contains a measurement error which has a normal distribution function with the average value of zero and the standard deviation value of σ. The simulation results in the condition of σ=0.36rad are shown in Fig. 3-4. In this case, both values of z_A and z_ϕ are different from the real value of z_0, where z_A=1579μm and z_ϕ=1531μm. Therefore the position of z_ϕ is not greatly affected by the noise compared to the position of z_A. The accurate value of z_0 is obtained from the position of z_ϕ where the difference between z_A and z_0 is less than P_C/2.

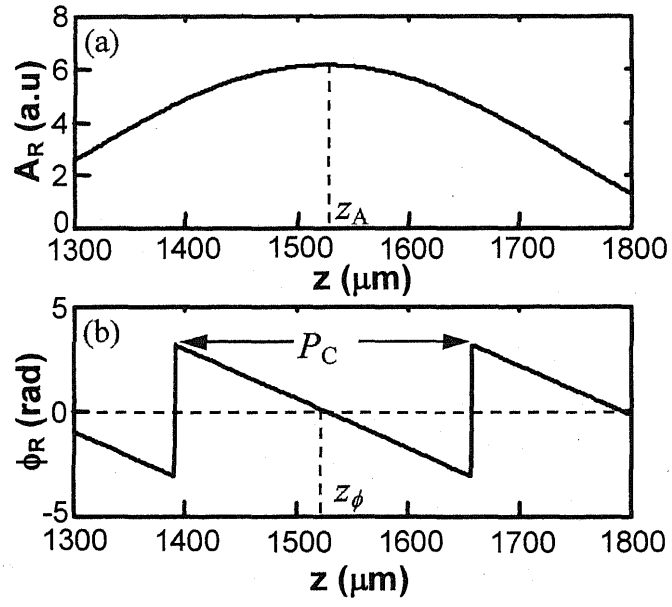

Fig. 3-3 Simulation results of the back-propagation method for one point object. (a) amplitude distribution, (b) phase distribution.

The phase gradient of the measured phase distribution α_{mz} is also used to get the position z_0 of the object. In the method using the phase gradient which is called phase gradient method hereafter, the phase distributions α_{mz} obtained from the interference signal are unwrapped with respect to different values of k_m as shown in Fig. 3-5. The values of α_{mz} shown in Fig. 3-5 are not on a linear line because of the noise with σ=0.36rad. A linear line is fitted for the values of α_{mz} with the least-squares method to obtain phase gradient q which is given by

$$q = \frac{\partial \alpha_{mz}}{\partial k_m} = z_0 \sin 2\beta. \tag{3-16}$$

The value of z_0 obtained from the value of q is denoted by z_g.

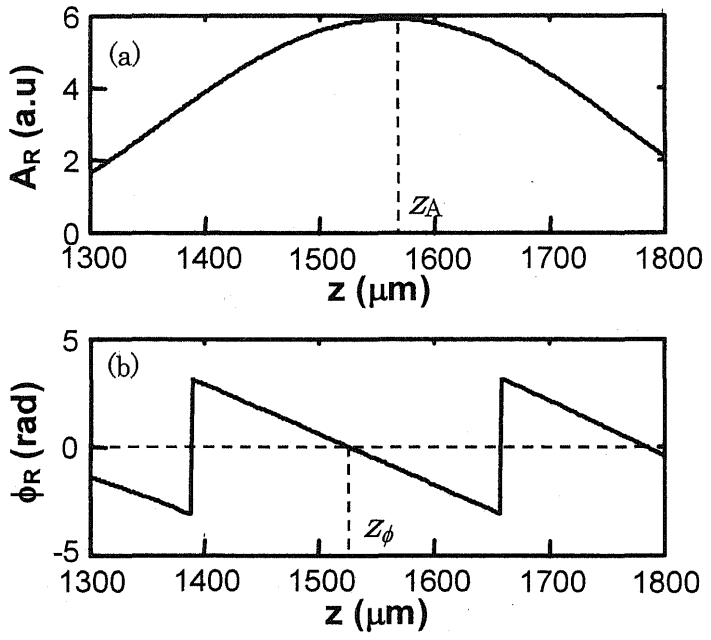

Fig. 3-4 Simulation results of the back-propagation method when the measured phase distribution contains a measurement error with standard deviation σ of 0.36rad. (a) amplitude distribution, (b) phase distribution.

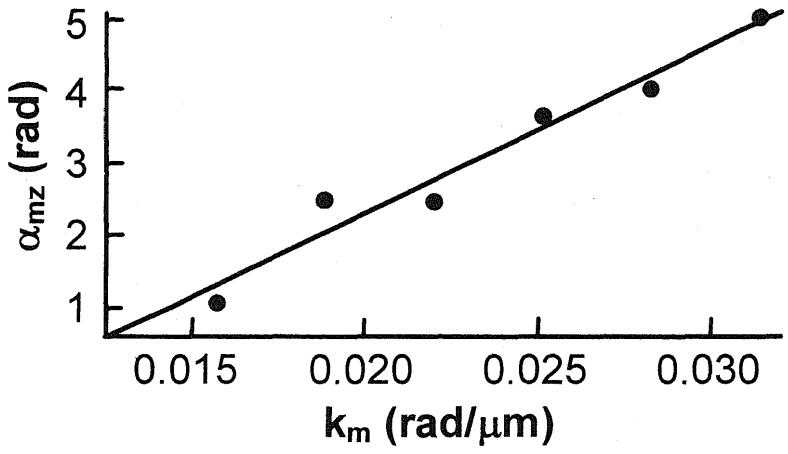

Fig. 3-5 Unwrapped result of measured phase distribution α_m which contains a measurement error with standard deviation σ of 0.36rad.

Table 3-1 Standard deviations of z_g, z_A and z_ϕ for different values of σ when z_0=1525μm.

σ(rad)	0.06	0.12	0.24	0.36
S{z_g} (μm)	4.7	8.6	18.1	32.8
S{z_A}(μm)	4.7	8.6	18.1	32.8
S{z_ϕ}(μm)	0.9	2.1	4.1	20.2

Comparing the phase gradient method and the back-propagation method, some simulations were done for the noises with the different values of σ. Two hundred trials at a fixed value of σ were carried out to obtain the average and standard deviation value of z_g, z_A and z_ϕ. The results about the standard deviations are shown in Table.3-1, where $S\{w\}$ means the standard deviation of w. It was made clear from the simulation that z_g and z_A have the same characteristics. The

differences between the average value of z_A and the value of z_0 are within a few tenths of microns. The differences between the average value of z_ϕ and the value of z_0 are within a few microns. At σ=0.36rad, the value of $S\{z_\phi\}$ becomes large because in some trials the difference between z_A and z_0 is larger than $P_C/2$ and the value of z_ϕ is shifted by one period P_C from a value of about z_0. The standard deviation value σ of the noise in the experiment described in the next section is estimated to be about 0.12rad. It is concluded that the value of z_ϕ obtained from the back-propagation method has a higher accuracy than the value of z_g.

3.4 Experiments

3.4.1 *Experiment setup*

The experimental setup is shown in Fig. 3-6. A 50mw laser diode is used as the light source. A laser beam collimated with a lens L_0 is divided into two beams by beam splitter BS1. The beams reflected from mirror M1 and mirror M2 produce the interference fringe. Piezoelectric transducer 1 (PZT1) changes the angle θ of mirror 1, which changes the periods P_m of the interference fringe. The piezoelectric transducer 2 (PZT2) vibrates with frequency f_c of 125*Hz* to produce the sinusoidal phase modulation in the interference fringe. The interference fringe is divided into two parts by beam splitter BS2. One part is incident on a photo diode (PD) which detects the interference signal at one point of x_f. Considering Eqs. (3-1) and (3-3), the detected interference signal is given by

$$I_m(t, x_f) = A_m + B_m \cos(a \cos \omega_c t + k_m x_f) \tag{3-17}$$

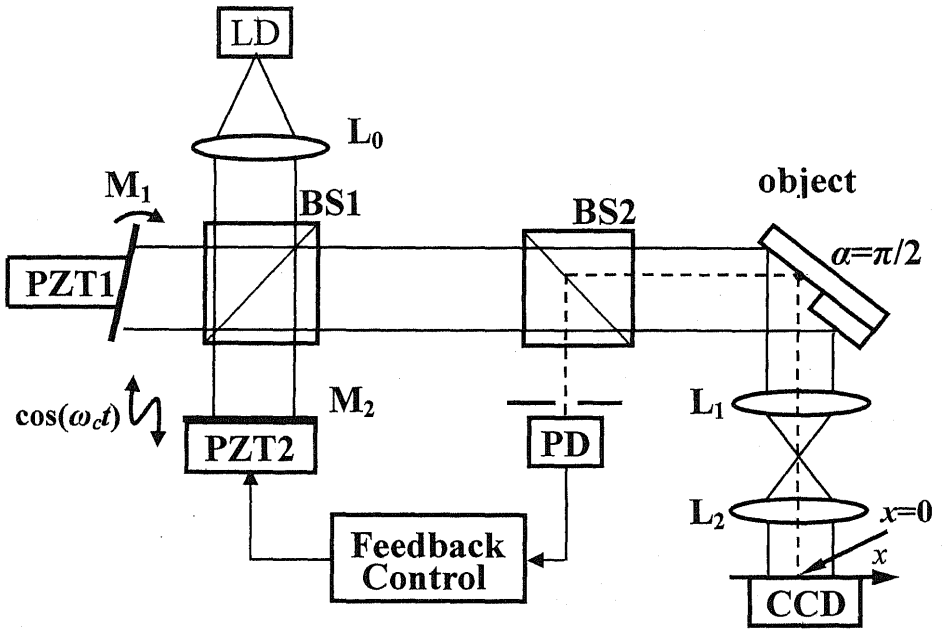

Fig. 3-6 Experiment setup of the multi-period fringe projection for surface profile measurement.

In the feedback control circuit, a feedback signal of $S_f=B_m\cos(k_m x_f)$ is produced by eliminating the DC component of A_m and sampling $I_m(t, x_f)$ when $\cos(\omega_c t)=0$. A feedback control signal made from the signal S_f is applied to the PZT2 so that S_f becomes zero by moving mirror M2. Thus the feedback control system makes the phase of the point x_f fixed at $\pi/2$ while the period P_m of the interference fringe is changed. The point x_f is defined as the origin point of the x_p axis or x axis, and the expression of Eq. (3-1) is realized. The phase distribution at the constant phase point is detected with the time interval of 3 minutes, and Fig. 3-7 shows the phase stability at the constant phase point where α_f is the phase distribution at the constant phase point. From Fig.3-7, the phase fluctuation at the constant phase point is less than $2\pi/100$.

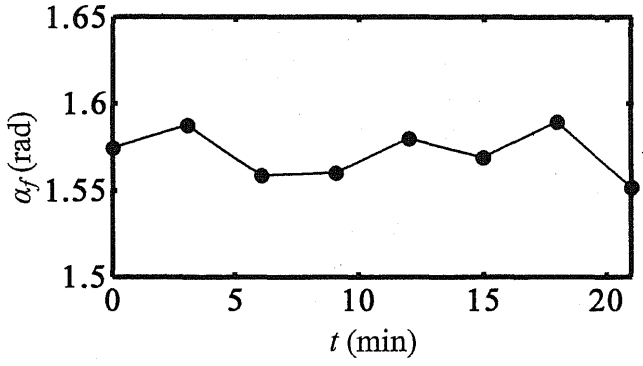

Fig. 3-7 Phase stability of constant phase point

The other part of the interference fringe is projected on the surface of the object. The image of the object's surface is formed with the afocal imaging system whose magnification is $M_{12}=f_2 / f_1$, where f_1 and f_2 are the focal length of L_1 and L_2, respectively. A high-speed CCD camera with the frame period of 1ms is used to detect the sinusoidally phase-modulated interference fringe. The period of the fringe is determined by the phase distribution of on line at the central of the detection plane. Figure 3-8 is the detected fringe pattern at the CCD camera when the object is a mirror. The calculated periods at different part of the fringe pattern is shown in Tab. 3-2. From Tab. 3-2, the change of the period of the fringe pattern is less than 0.1μm which is satisfied for the experiment.

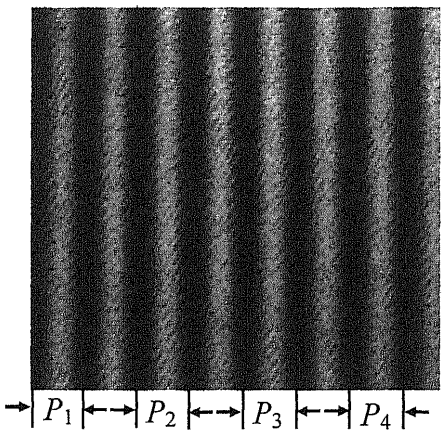

Fig. 3-8 Detected fringe pattern when object is a mirror

Table 3-2 Calculated periods at different position of the fringe pattern.

Measured area	P_1	P_2	P_3	P_4	average
Period (μm)	249.8	249.9	250.0	249.7	249.8

3.4.2 *Experiment results*

First an optical surface with a step profile made by two gauge blocks was used as an object. Height H of the step profile was 1000μm. The parameters used in the experiment were as follows: P_1=249.8μm, P_2=285.2μm, P_3=332.6μm, P_4=400.3μm, Δk=0.0031rad/μm, β=45°, z_{max}=2000μm, P_C=266.7μm, f_1=100mm, and f_2=50mm. The image size on the x-y plane of the CCD image sensor were 256×240 pixels with the pixel size of 7.4μm, and the measuring region on the object was about 3.8×3.6mm^2 with M_{12}=1/2. Figure 3-9 shows the amplitude A_R and phase ϕ_R for one measuring point of x=1.45mm and y=1.79mm on the object surface. From these results, the measured value of z_0 or z_ϕ was 2862μm. The measured value of h calculated with Eq. (3-9) was 998μm at the point of x=1.45mm and y=1.79mm. Figures 3-10 and 3-11 show the measured height

distribution h over the reference plane and along one line of y=1.79mm, respectively, where the notation of x_r is the x axis of the reference plane. Because of the shadow of the step profile, there is no interference signal reflected from x_r=0.98mm to x_r=1.95mm. The average value of the height difference H on the line of y=1.79mm was 998μm. The measurements were repeated at intervals of a few minutes. The measurement repeatability of about 2.5μm was obtained from the rms value of the differences of the measurement results.

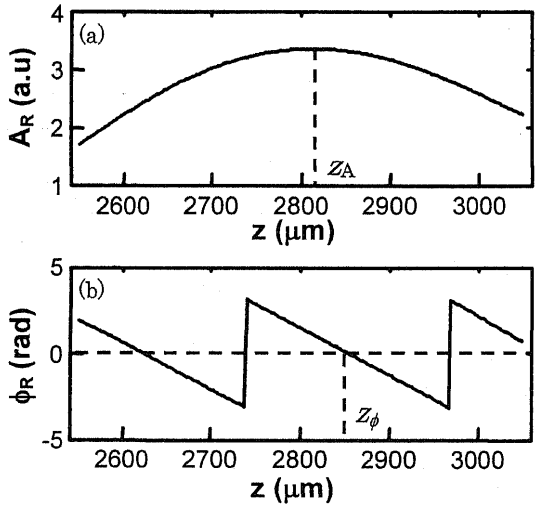

Fig. 3-9 Back-propagation results for one point of x_0=1.45mm, y=1.79mm on the object surface. (a) amplitude distribution, (b) phase distribution.

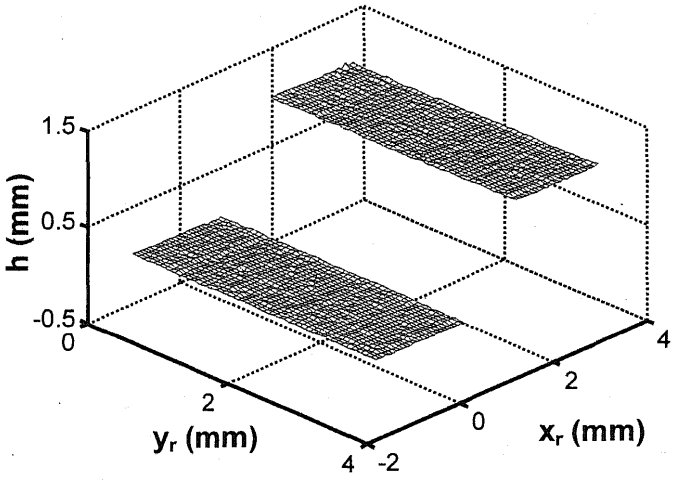

Fig. 3-10 Measured height distribution of the step profile made by two gauge blocks.

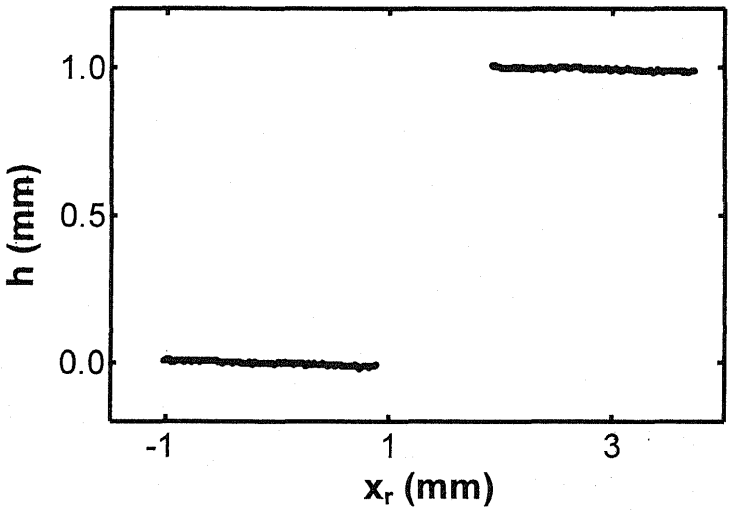

Fig. 3-11 Cross section of the measured height distribution of Fig.8 at y=1.79 mm.

Next a rough surface of aluminum with a step profile was used as the object. Since the average height of the step profile was about 2mm, the measurement range z_{max} was set at 2521μm in the condition that the value of β was 16° and the scanning interval Δk was 0.0046rad/μm. When β was 16°, the size of the shadow on the lower surface of the object caused by the edge point of the step profile became small. In order to decrease the random noise in the measurement of rough surface, the following six periods of the interference fringe were used: P_1=177.9μm, P_2=205.8μm, P_3=243.3μm, P_4=297.1μm, P_5=376.2μm, and P_6=501.0μm where P_C=484.6μm. The measuring region was about 7.6×7.2mm^2 with f_1=100mm, f_2=25mm, and M_{12}=1/4. Figure 3-12 shows the height distribution of the step profile, where the height distributions of the upper and lower surfaces forming the step-profile are drawn with the separated axis of h. The measured value of the height H between the central point on the two measuring surface of the step profile was 2070μm. The measurement repeatability of 7.5μm was obtained by repeating the measurement 3 times at intervals of a few minutes. This repeatability was larger than that in the measurement of the optical surfaces of gauge blocks because the measurement error in the phase α became larger for the rough surface.

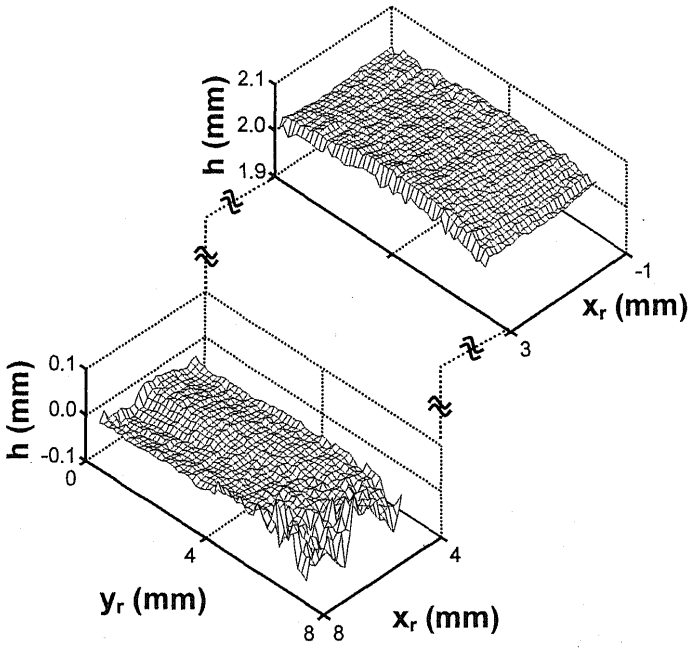

Fig 3-12 Measured height distributions of two rough surfaces forming the step-profile.

3.5 Summary

A multi-period fringe projection interferometry by using the back-propagation method was presented. The feedback technology was incorporated to keep the phase on one point of the object surface at $\pi/2$ during the scanning of the fringe period. In the back-propagation method the optical fields with different fringe periods were back-propagated to the stationary point of the phase. The position of the object surface was obtained from the distance of the back-propagation on which the amplitude of the sum of the back-propagated optical fields became maximum and its phase became zero. The simulation made it clear that the back-propagation method had a measurement accuracy higher than the phase gradient method. The measurement repeatability was 2.5μm for the optical

surface profile with a step height of 1mm made by the gauge blocks, and it was 7.5μm for the rough surface profile with a step height of about 2mm made by the aluminum plates.

Chapter 4

Measurement of two surface profiles by using back-propagation method

4.1 Introduction

It is important to measure positions of the surfaces of a transparent object in three dimensions. To achieve the three-dimensional measurement of thickness and surface profiles of a transparent object, white light interferometers[20] and wavelength-scanning interferometers[21] have been developed. In white light interferometers, thickness of a film is measured by finding a position where the amplitude of the interference signal is maximum by scanning the optical path difference (OPD). In wavelength-scanning interferometers, thickness of a film is measured by detecting a phase of the interference signal which varies according to the scanning of the wavelength instead of the scanning of the OPD. In the case of linear wavelength-scanning, the positions of the reflecting surfaces are determined by the peaks of the frequency spectrum of the interference signal.

On the other hand, the fringe projection method and multi-period fringe project method have been used to measure the surface of object successfully. But it is very difficult for these methods to measure a transparent object. A fringe projection interferometry using Fourier transform method is used to the thickness of a thin film[22]. A thin film is put on the reference plate, and it is considered as a discontinuity on the surface of reference plate. The thickness of the thin film is obtained from the surface profile of the reference plate. This method can only give the thickness of the thin film, but the two surface profiles can't be obtained.

In this paper, a multi-period fringe projection interferometry using back-propagation method is applied for measuring the two surface profiles of a object. In the back-propagation method which was proposed in Refs.15 and 16, the optical fields on each point of the object surface are back-propagated to the constant phase point. When the back-propagated fields reach to the constant phase point, the amplitude of the sum of the back-propagated fields with the different fringe periods becomes maximum and its phase becomes zero. For the measurement of surfaces of transparent object, the amplitude distribution gives two maximum peaks which related to the points of font surface and rear surface. At the same time, the phase distribution corresponding to the two peaks of amplitude distribution becomes zero. The back-propagation distance from the each point of the object to the constant phase point provides the positions of the two surfaces of the object. In experiments, a glass plate with two parallel surfaces is measured. It is confirmed in the experiments that a transparent object of several millimeters can be measured with a high accuracy of several micros by using the back-propagation method in the multi-period fringe projection. An acrylic plate has also been measured and the measurement result is compared with the result measured by a confocal microscope.

4.2 Interference signal for two surfaces

A schematic configuration for the multi-period fringe projection is shown in Fig. 4-1. Two plane waves of wavelength λ propagate in different directions which produce a parallel interference fringe in the space. The two plane waves U_1 and U_2 are written as

$$U_1 = a_0 \exp\{ik[x_p \sin(-\theta_m) + z_p \cos\theta_m]\} \tag{4-1}$$

$$U_2 = a_0 \exp\{ik[x_p \sin\theta_m + z_p \cos\theta_m]\} \tag{4-2}$$

The coordinate system (x_p, y_p, z_p) is involved with the fringe pattern as shown in Fig. 4-1. The intersecting angles between the two waves and the z_p axis are $\pm\theta_m$,

respectively. The interference signal of the two plane waves in the coordinate system (x_p, y_p, z_p) is written as

$$I_{12} = 2a_0^2 \cos(\frac{2\pi}{\lambda} 2x_p \sin\theta_m) = 2a_0^2 \cos(\frac{2\pi}{P_m} x_p) \tag{4-3}$$

The period of the fringe pattern is expressed by $P_m=\lambda/2\theta_m$ since $\sin\theta_m \approx \theta_m$ when θ_m is small. Changing the intersecting angles θ_m as θ_0, θ_1..., and θ_{M-1}, the periods of the fringe pattern P_m are scanned as P_0, P_1..., and P_{M-1} accordingly. The phase of the interference fringe at $x_p=0$ is kept at $\pi/2$ during the period scanning by using feedback controlling. The original point O is the constant phase point of the coordinate system where the phase of the fringe pattern does not change while the period of the fringe pattern is scanned.

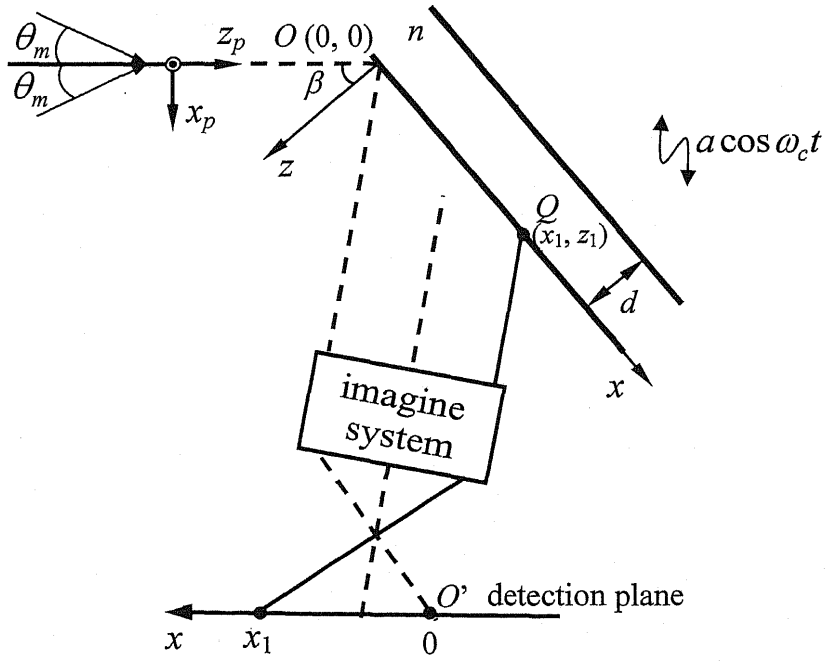

Fig. 4-1 Schematic configuration for multi-period fringe projection and detection of the fringe patterns by sinusoidal phase-modulating interferometry.

It is assumed that there is a glass plate whose two surfaces are parallel. The refractive index of the glass plate is n. An image of the point object is formed on a detection plane with an imaging system. The intersection angle between the optical axis and the z_p axis is 2β. Another coordinate system (x, y, z) is defined. The original point O of the coordinate system (x, y, z) is the same as that of the coordinate system (x_p, y_p, z_p). The z axis is the bisector of the intersection angle between the z_p axis and the optical axis. The magnification of the imaging system is assumed to be unit for the sake of simplicity. The position of x=0 on the detection plane corresponds to the original point O. In the coordinate system (x, y, z), the two plane waves are written as

$$U_1 = a_0 \exp\{ik[x\sin(\beta+\theta_m) - z\cos(\beta+\theta_m)] + \pi/2\} \tag{4-4}$$

$$U_1 = a_0 \exp\{ik[x\sin(\beta+\theta_m) - z\cos(\beta+\theta_m)] + \pi/2\} \tag{4-5}$$

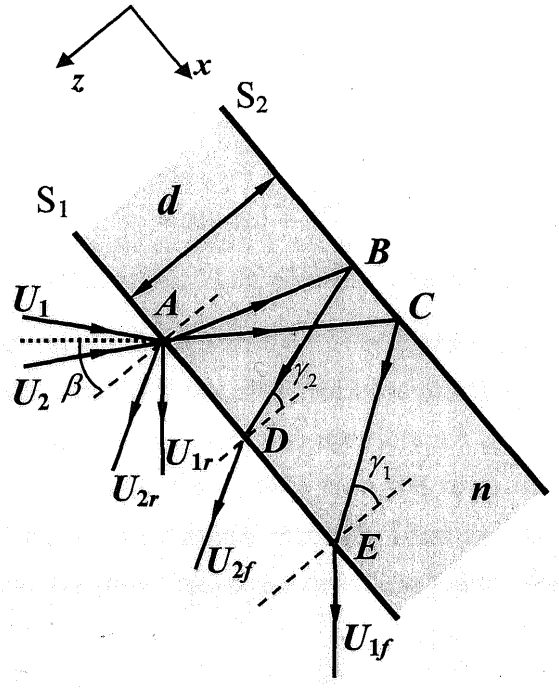

Fig. 4-2 Propagation of the two plane wave in the glass plate

The plane waves U_1 and U_2 are divided in two parts which are shown in Fig. 4-2. One is reflected by surface S_1 and is denoted as U_{1r} and U_{2r}, respectively, the other is refracted and reflected by surfaces S_1 and S_2, and then refracted by surface S_1 which is denoted as U_{1f} and U_{2f}, respectively. U_{1r}, U_{2r}, U_{1f} and U_{2f} are written as

$$U_{1r} = r_1 a_0 \exp\{ik[x\sin(\beta+\theta_m) + z\cos(\beta+\theta_m)] + \pi/2\} \tag{4-6}$$

$$U_{2r} = r_1 a_0 \exp\{ik[x\sin(\beta-\theta_m) + z\cos(\beta-\theta_m)]\} \tag{4-7}$$

$$U_{1f} = r_2 a_0 \exp\{ik[(x+2d\tan\gamma_1)\sin(\beta+\theta_m) + z\cos(\beta+\theta_m)] + \pi/2\} \tag{4-8}$$

$$U_{2f} = r_2 a_0 \exp\{ik[(x+2d\tan\gamma_2)\sin(\beta-\theta_m) + z\cos(\beta-\theta_m)]\} \tag{4-9}$$

where r_1, r_2 is the proportional coefficient corresponding to the reflection and refraction, γ_1 and γ_2 are the refraction angles of $\beta + \theta_m$ and $\beta - \theta_m$, which is given

by

$$\gamma_1 = \arcsin[\frac{\sin(\beta+\theta_m)}{n}] \tag{4-10}$$

$$\gamma_2 = \arcsin[\frac{\sin(\beta-\theta_m)}{n}] \tag{4-11}$$

Q is a point object on the front surface of the glass plate. The position of the point objects Q is expressed by $x=x_1$, $z=z_1$, and the image of the point object Q is formed at $x=x_1$ on the detection plane. The interference fringe intensity oscillates sinusoidally in the direction of the x_p axis with the form of $a\cos\omega_c t$ in order to apply the sinusoidal phase modulation method. Then the following interference signal of point object Q is detected on the detection plane which is shown in Fig. 4-3:

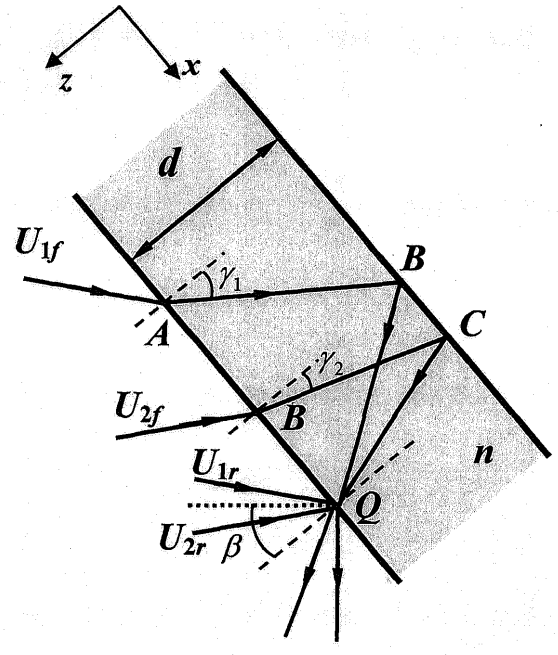

Fig. 4-3 Interference signal of point object Q

(1) The interference signals made up of U_{1r} and U_{2r}, U_{1f} and U_{2f} are denoted as I_1 and I_2, which are given as

$$I_1 = 2r_1^2 a_0^2 \cos[z_c \cos\omega_c t + \frac{2\pi}{P_m}(x_1 \cos\beta + z_1 \sin\beta) + \pi/2] \tag{4-12}$$

$$\begin{aligned} I_2 = 2r_2^2 a_0^2 \cos\{&z_c \cos\omega_c t + \frac{2\pi}{P_m}(x_1 \cos\beta + z_1 \sin\beta) \\ &- 2dk[\tan\gamma_1 \sin(\beta+\theta_m) - \tan\gamma_2 \sin(\beta-\theta_m)] + \pi/2\} \end{aligned} \tag{4-13}$$

since $\theta_m << 1$, $\cos\theta_m \approx 1$ and $\tan\gamma_1 - \tan\gamma_2 \approx 0$, I_2 is approximately written as

$$\begin{aligned} I_2 = 2r_2^2 a_0^2 \cos[&z_c \cos\omega_c t + \frac{2\pi}{P_m}(x_1 \cos\beta + z_1 \sin\beta) \\ &- \frac{2\pi}{P_m} d(\tan\gamma_1 + \tan\gamma_2)\cos\beta + \pi/2] \end{aligned} \tag{4-14}$$

(2) The interference signals made up of U_{1r} and U_{2f}, U_{1f} and U_{2r} are denoted as I_3 and I_4, which is given as

$$\begin{aligned} I_3 = 2r_1 r_2 a_0^2 \cos[&z_c \cos\omega_c t + \frac{2\pi}{P_m}(x_1 \cos\beta + z_1 \sin\beta) \\ &+ \frac{2\pi}{\lambda} 2d \tan\gamma_2 \sin(\beta-\theta_m) + \pi] \end{aligned} \tag{4-15}$$

$$\begin{aligned} I_4 = 2r_1 r_2 a_0^2 \cos[&z_c \cos\omega_c t + \frac{2\pi}{P_m}(x_1 \cos\beta + z_1 \sin\beta) \\ &- \frac{2\pi}{\lambda} 2d \tan\gamma_1 \sin(\beta+\theta_m) + \pi] \end{aligned} \tag{4-16}$$

(3) The interference signals made up of U_{1r} and U_{1f}, U_{2r} and U_{2f} are denoted as I_5 and I_6, which is given as

$$I_5 = 2a_0^2 \cos[k \tan\gamma_1 \sin(\beta+\theta)] \tag{4-17}$$

$$I_6 = 2a_0^2 \cos[k \tan\gamma_2 \sin(\beta - \theta)] \tag{4-18}$$

I_5 and I_6 is the shearing interference signal and don't changed with the sinusoidal phase modulation, so the interference signal detected from the sinusoidal phase modulation interferometry is written as

$$\begin{aligned} I_m(x,z,t) &= I_1 + I_2 + I_3 + I_4 \\ &= B_m \cos(z_c \cos\omega_c t + \Phi_m), \quad m = 0,\cdots,M-1. \end{aligned} \tag{4-19}$$

Since $\theta_m << 1$, $\cos\theta_m \approx 1$ and $\tan\gamma_1 - \tan\gamma_2 \approx 0$, the distance between point B and C at the rear surface is smaller than the size of one pixel, the interference signal from the rear surface can be look as being reflected from one point Q_1 at the rear surface, which is shown in Fig. 4-4.

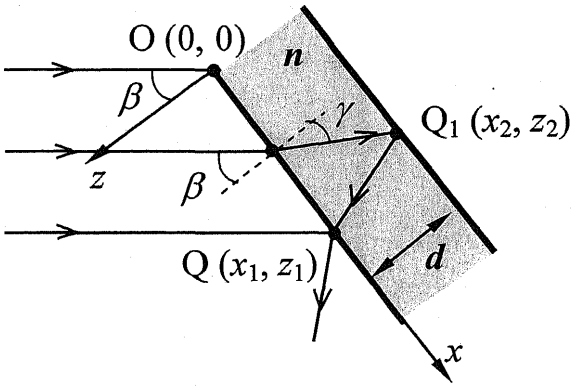

Fig. 4-4 Observed interference signal reflected from the two surfaces

4.3 Detection of surfaces by back-propagation method

The coordinate x of the object is provided by the position of the detection plane, the following phase Φ_{mz} is extracted from the phase Φ_m by subtracting the value of $k_m x_1 \cos\beta_1 + \pi/2$ from the calculated value of Φ_m:

$$\Phi_{mz}(z) = \Phi_m(x, z) - (k_m x_1 \cos\beta + \pi/2) \tag{4-20}$$

where $k_m = \frac{2\pi}{P_m}$, and it is called wave number of the fringe pattern.

Since the coordinate x_1 of the object point Q is known from the position of the detection plane, a method which is called the back-propagation method is used to get the coordinate z of the point object.

In the back-propagation method, the detected fields of the point objects Q regarding the variable z are defined as

$$D_m(x_1, z) = B_m \exp[j\Phi_{mz}(z)]. \tag{4-21}$$

When the detected field D_m is back-propagated to the position z, the back-propagated field of $U_m(z)$ is given by

$$U_m(z) = D_m \exp(-j\alpha_{mz}), \quad m = 0, \cdots, M-1. \tag{4-22}$$

where α_{mz} is denoted as

$$\alpha_{mz} = k_m z \sin\beta. \tag{4-23}$$

The sum of the back-propagated fields over all of k_m produces the following reconstruction field as a function of back-propagation variable z:

$$U_R(z) = \sum_{m=0}^{M-1} U_m(z) = A_R \exp(j\phi_R). \tag{4-24}$$

When all of the detected fields of the point objects Q are back-propagated to the position of the stationary point O, the amplitude of A_R becomes maximum, and its phase ϕ_R becomes zero. The back-propagation distance z is expressed as z_P and z_Q. From this basic characteristic, the coordinate z_1 of the object point Q, the coordinate (x_2, z_2) of the object Q_1 and the thickness d of the glass plate can be obtained and expressed as

$$z_1 = z_A \tag{4-25}$$

$$x_2 = x_1 - \frac{(z_P - z_Q)\tan\beta}{2} \tag{4-26}$$

$$z_2 = z_A - \frac{(z_P - z_Q)\tan\beta}{2\tan\gamma_1} \tag{4-27}$$

$$d = \frac{(z_P - z_Q)\tan\beta}{2\tan\gamma_1} \tag{4-28}$$

Figure 4-5 shows the simulation results of one point on the surface of the glass plate by using back-propagation method. The scanning period of the fringe is from 140μm to 800μm with M=18, Δk=0.0022(rad/μm), β=30°, n=1.5. The thickness of the plate is 2830μm, and the value of z_1 and z_Q are 0μm and -2000μm, respectively. The amplitude B_m of the interference signal is a constant value of 1 for all P_m. Figure 4-5 indicates that the amplitude distribution A_R of U_R has a maximum value at z=z_{AP} and z=z_{AQ}, at the same time its phase distribution ϕ_R has a zero value at z=$z_{\phi P}$ and z=$z_{\phi Q}$ with the period P_C of 476.6μm. The simulation result gives that z_{AP} = 5μm, z_{AQ} = -2010μm, $z_{\phi P}$ = 2μm and $z_{\phi Q}$ = -2004μm

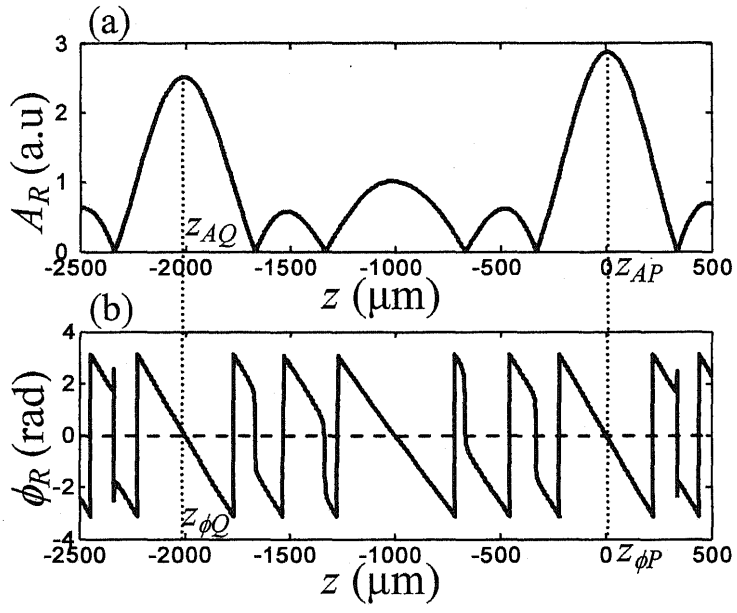

Fig. 4-5 Simulation results of the back-propagation method for one point object. (a) amplitude distribution, (b) phase distribution.

There are not any noises in this simulation, but there are errors in the simulation result. In order to find the reason of these errors, some simulations are done for the different values of z_1 and z_Q. The simulation results are shown in Tab. 4-1. From Tab. 4-1, we find that the errors of z_{AP}, z_{AQ}, $z_{\phi P}$ and $z_{\phi Q}$ increased with the distance between z_1 and z_Q decreased, and the errors of z_{AP} and z_{AQ} is larger than the errors of $z_{\phi P}$ and $z_{\phi Q}$. It can be drawn a conclusion from this simulation that the errors in the simulation with no noise is because of the extending of the two peaks in the A_R distribution which denote the position of two surfaces of the object.

Tab. 4-1 Simulation results and errors of the back-propagation method without noise

Simulation positions (μm)		Back-propagation result of A_R (μm)				Back-propagation result of ϕ_R (μm)			
z_P	z_Q	z_{AP}	errors of z_{AP}	z_{AQ}	errors of z_{AQ}	$z_{\phi P}$	errors of $z_{\phi P}$	$z_{\phi Q}$	errors of $z_{\phi Q}$
0	-500	14	14	-525	-25	8	8	-516	-16
0	-1000	8	8	-1018	-18	5	5	-1012	-12
0	-2000	5	5	-2010	-10	2	2	-2004	-4
0	-4000	2	2	-4005	-5	1	1	-4002	-2

In the simulation above, the amplitude B_m of the interference signal is assumed to be a constant value of 1 for all P_m, which caused the distribution of A_R to be like a Sinc function. The extending of two peaks in the Sinc function affects each other, which caused the errors in the back-propagation method. In order to decrease this effect, we make B_m has a Gauss distribution which is given as

$$B_m = \exp[\frac{(m-m_0)^2}{2\sigma^2}], \quad m = 1, 2, \cdots, M. \tag{4-29}$$

where m_0 is the middle value of m. The distribution of B_m is shown in Fig. 4-6. The simulation result of object with one surface is shown in Fig. 4-7, and the simulation result of object with two surfaces is shown in Fig. 4-8. From Figs. 4-7 and 4-8, we find that the distribution of A_R is not like a Sinc function, the distribution of the two peaks is extending like a Gauss function. The simulation result of object with two surfaces gives that z_{AP} = 2μm, z_{AQ} = -2002μm, $z_{\phi P}$ = 0μm and $z_{\phi Q}$ = -2001μm. The error of this simulation is smaller than the simulation when B_m is a constant value of 1 for all P_m. The same simulations for the different values of z_1 and z_Q also have been done, and the result is shown in Tab. 4-2. Comparing Tabs. 4-1 and 4-2, we find that the error caused by the extending of two peaks in A_R distribution decrease when B_m is a Gauss distribution.

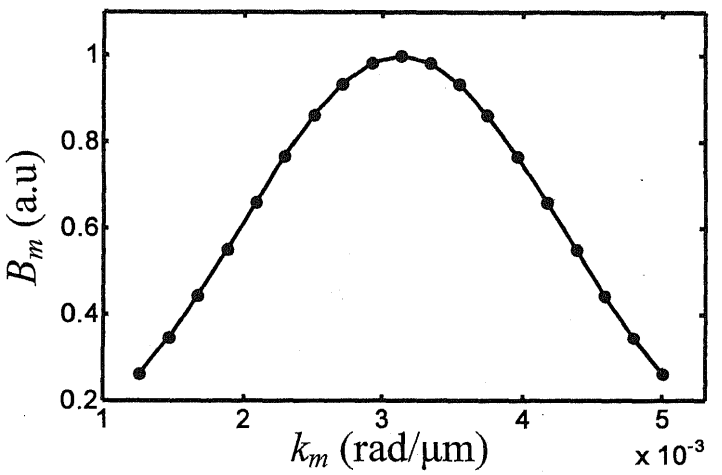

Fig. 4-6 Distribution of B_m

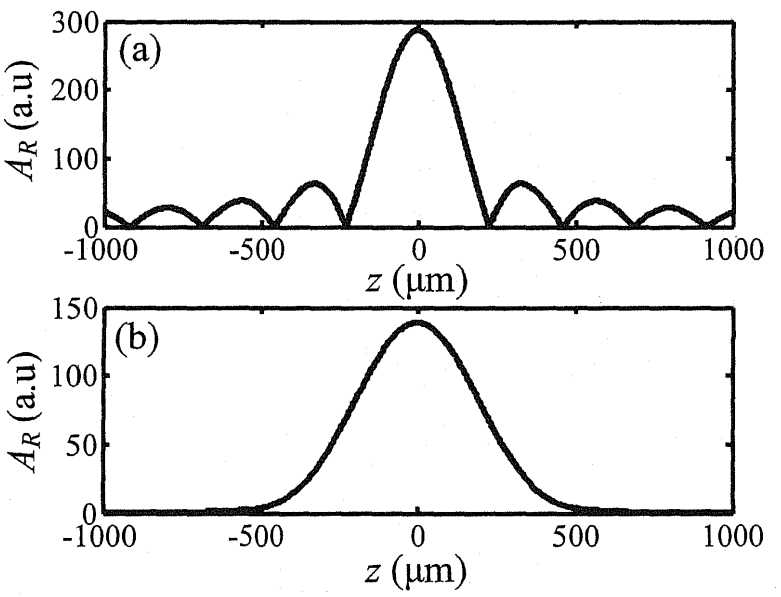

Fig. 4-7 Simulation results of object with one surface, (a) B_m is not Gauss distribution, (b) B_m is Gauss distribution.

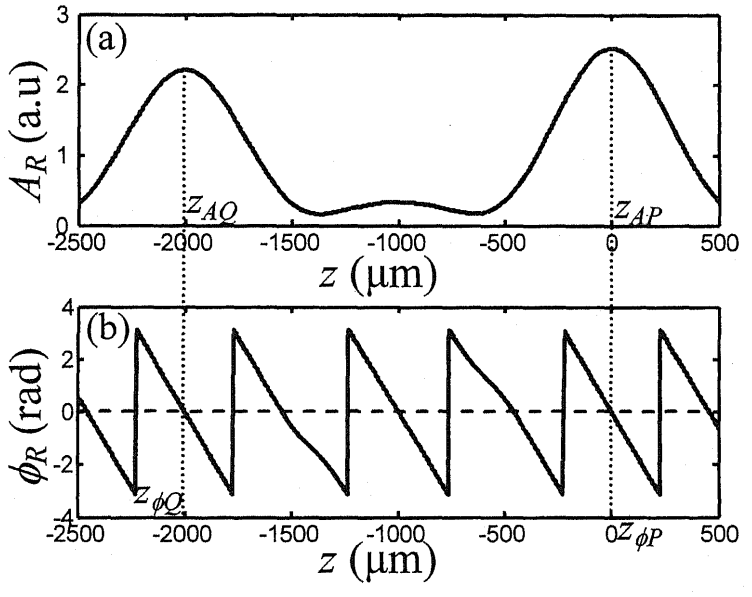

Fig. 4-8 Simulation results of the back-propagation method for one point object with B_m is Gauss distribution. (a) amplitude distribution, (b) phase distribution.

Tab. 4-2 Simulation results and errors of the back-propagation method when B_m is a Gauss distribution without noise

Simulation positions (μm)		Back-propagation result of A_R (μm)				Back-propagation result of ϕ_R (μm)			
z_P	z_Q	z_{AP}	errors of z_{AP}	z_{AQ}	errors of z_{AQ}	$z_{\phi P}$	errors of $z_{\phi P}$	$z_{\phi Q}$	errors of $z_{\phi Q}$
0	-500	7	7	-510	-10	4	4	-505	-5
0	-1000	3	3	-1007	-7	3	3	-1004	-4
0	-2000	2	2	-2003	-3	1	1	-2002	-2
0	-4000	1	1	-4002	-2	1	1	-4001	-1

By using the method we described above, the error in the measurement of 2mm

glass plate is decreased. Next, some simulations were done for the noises with the different values of σ. Two hundred trials at a fixed value of σ were carried out to obtain the average and standard deviation value of z_{AP}, z_{AQ} and $z_{\phi P}$, $z_{\phi Q}$. The results about the standard deviations are shown in Tab. 4-3, where $S\{w\}$ means the standard deviation of w. From Tab. 4-3, the differences between the average value of z_{AP}, z_{AQ} and the value of z_P, z_Q are within a few tenths of microns. The differences between the average value of $z_{\phi P}$, $z_{\phi Q}$ and the value of z_P, z_Q are within a few microns. The standard deviation value σ of the noise in the experiment described in the next section is estimated to be about 0.12rad. It is concluded that the value of $z_{\phi P}$, $z_{\phi Q}$ obtained from the back-propagation method has a higher accuracy than the value of z_{AP}, z_{AQ}.

Table 4-3 Standard deviations of z_{AP}, z_{AQ} and $z_{\phi P}$, $z_{\phi Q}$ for different values of σ when z_P=0μm, z_Q=-2000μm.

σ(rad)	0.06	0.12	0.24	0.36
$S\{z_{AP}\}$ (μm)	5.2	10.1	21.5	38.8
$S\{z_{AQ}\}$(μm)	5.5	10.5	22.0	39.2
$S\{z_{\phi P}\}$(μm)	1.5	3.0	5.2	24.6
$S\{z_{\phi Q}\}$(μm)	1.8	3.2	5.4	26.2

From Tab.4-2, the error in the measurement of 1mm glass plate is still large. We consider the back-propagation result of I_1, I_2 and I_3, I_4 separately. Figure 4-9 (a) and (b) show the back-propagation result when there is only I_1 and I_2 or only I_3 and I_4 in the detected signal when the thickness of object is 1mm. It is obviously that the back-propagation result of I_3 and I_4 is at the central of the two peaks which are given by I_1 and I_2. It will cause the measurement error in the back-propagation method, especially when the thickness of the object is thin. Since I_3 and I_4 are the interference signal made by the optical wave from front surface and rear surface, respectively, in the experiment, an optical path difference L is given according to the thickness of the object which has lower coherence. By using this method the error caused by I_3 and I_4 is decreased.

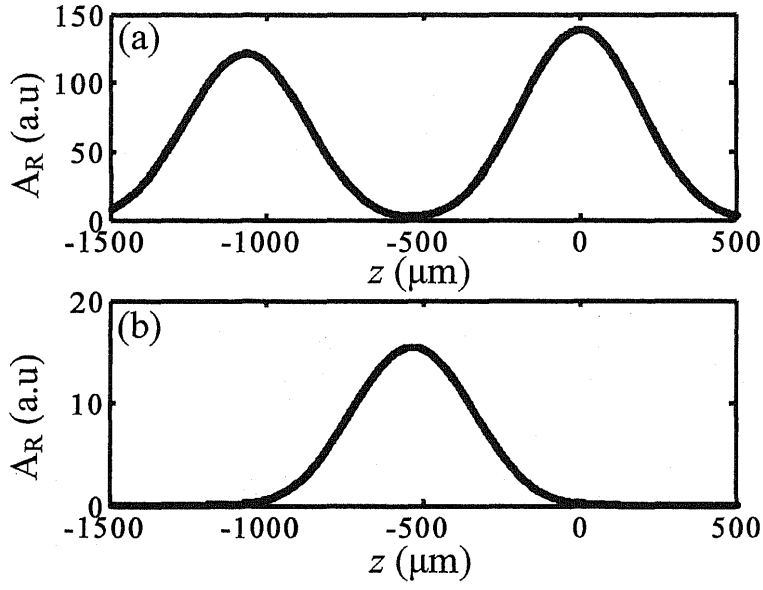

Fig. 4-9 Back-propagation result of object with two surface with thickness of 1mm, (a) I_1 and I_2, (b) I_3 and I_4

4.3 Experiments

4.4.1 *Experiment setup*

The experimental setup is shown in Fig. 4-10. A 50mw laser diode is used as the light source. A laser beam collimated with a lens L_0 is divided into two beams by beam splitter BS1. The beams reflected from mirror M1 and mirror M2 produce the interference fringe. Piezoelectric transducer 1 (PZT1) changes the angle θ of mirror 1, which changes the periods P_m of the interference fringe. The piezoelectric transducer 2 (PZT2) vibrates with frequency f_c of $125Hz$ to produce the sinusoidal phase modulation in the interference fringe. The interference fringe is divided into two parts by beam splitter BS2. One part is incident on a photo diode 1 (PD1) which detects the interference signal at one point of x_f. The detected interference signal is given by

$$I_m(t, x_f) = A_m + B_m \cos(a \cos \omega_c t + k_m x_f) \tag{4-30}$$

In the feedback control circuit, a feedback signal of $S_f = B_m\cos(k_m x_f)$ is produced by eliminating the DC component of A_m and sampling $I_m(t, x_f)$ when $\cos(\omega_c t) = 0$. A feedback control signal made from the signal S_f is applied to the PZT2 so that S_f becomes zero by moving mirror M2. Thus the feedback control system makes the phase of the point x_f fixed at $\pi/2$ while the period P_m of the interference fringe is changed. The point x_f is defined as the origin point of the x_p axis or x axis, and the expression of Eq. (4-4) is realized. The phase distribution at the constant phase point is detected with the time interval of 3 minutes, and Fig. 4-11 shows the phase stability at the constant phase point where α_f is the phase distribution at the constant phase point when P=205μm and 878μm. From Fig.3-7, it is found that the phase fluctuation at the constant phase point of small period is larger than that of larger period, but the fluctuation is less than $2\pi/100$ which can be accepted in the experiment.

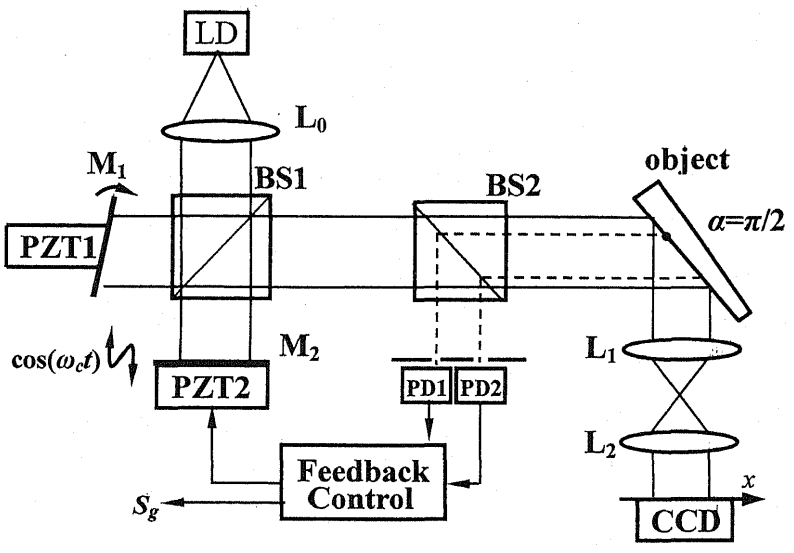

Fig. 4-10 Experiment setup of the multi-period fringe projection for surface profile measurement.

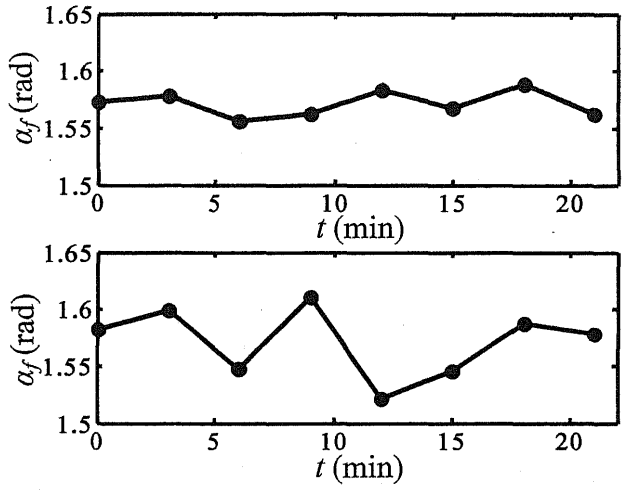

Fig. 4-11 Phase stability of constant phase point,
(a) P=878μm, (b) P=205μm

The other part of the interference fringe is projected on the surface of the object. The image of the object's surface is formed with the afocal imaging system whose magnification is $M_{12} = f_2 / f_1$, where f_1 and f_2 are the focal length of L_1 and L_2, respectively. A high-speed CCD camera with the frame period of 1ms is used to detect the sinusoidally phase-modulated interference fringe.

Another photo diode (PD2) is fixed adjacent to PD1 which detects the interference signal at one point of x_g. The detected interference signal is $I_m(t, x_g)$. A signal of $S_g = B_m\cos(k_m x_g)$ is produced by feedback control circuit as we do to $I_m(t, x_f)$. The relation between P_m and S_g is measured for two times which is shown in Fig.4-12, and by using this relation we can adjust the period of fringe pattern accurately. The period used in the experiment is shown in Tab. 4-4.

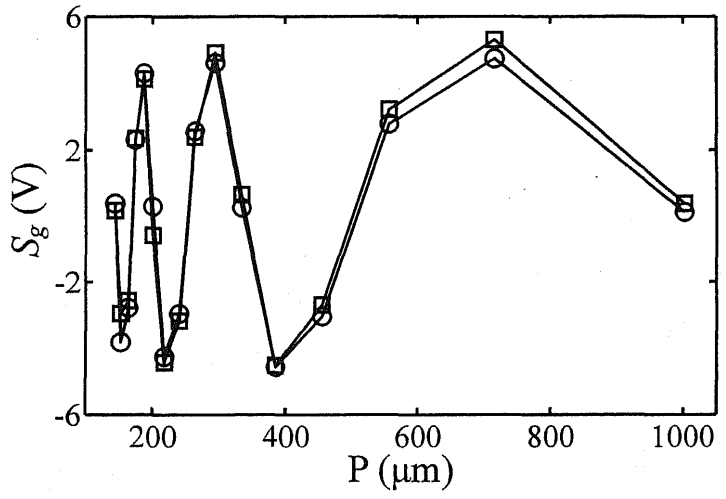

Fig. 4-12 Relation between P_m and S_g

Table 4-4 Periods used in the experiment

	First time (μm)	Second time (μm)
P_1	143.5	143.2
P_4	172.4	172.9
$P7$	217.8	217.3
P_{10}	294.1	295.1
P_{13}	454.8	455.9
P_{16}	1000.9	1002.9

4.4.2 *Experiment results*

A. Result of a glass plate with thickness of 2mm

First a glass plate was used as an object. The thickness d of the glass plate is 2mm.

The parameters used in the experiment were as follows: P_1=143.0μm, P_I=1002.4μm, M=16, Δk=0.0023rad/μm, z_{max}=3mm, β=45°, f_1=100mm, and f_1=25mm. The image size on the x-y plane of the CCD image sensor were 256×240 pixels with the pixel size of 7.4μm, and the measuring region on the object was about 7.4×7.2mm^2 with M_{12}=1/4. Figure 4-13 shows the amplitude A_R and phase ϕ_R for one measuring point of x=2.90mm and y=3.58mm on the front surface of the glass plate. Figure 4-9 indicates that the amplitude distribution A_R of U_R has two peaks at $z=z_{AP}$ and $z=z_{AQ}$. The phase distribution ϕ_R becomes zero at $z=z_{\phi P}$ and $z=z_{\phi Q}$ which is corresponding to the two peaks in the amplitude distribution. From these results, the measured values of $z_{\phi A}$ and $z_{\phi Q}$ were -2124μm and 14μm. The measured value of d was 2001μm at the point x=2.90mm and y=3.58mm. The measured values of z_{AP} and z_{AQ} were -2128μm and 16μm. The measured value of d was 2005μm. The other two points have also been checked, and the result is shown in Tab. 4-5. It is obvious that the measured values obtained from the phase distribution have higher accuracy than that obtained from the amplitude distribution. Figures 4-14 shows the measured position of the two surfaces of the glass plate where the axis of z is shown separated. The average value of the thickness d was 2001μm. The measurements were repeated 3 times at intervals of a few minutes. The repeatability in the thickness measurement was about 2.5μm which was the rms value of the differences between the average values of the thickness. Since the two surfaces of the glass plate are parallel, the profile shown in Fig. 4-14 can also be look as the measure error of the back-propagation method. From Fig. 4-14, the fluctuation of the surface is about 2.8μm, the measurement error of the back-propagation method is about 2.8μm.

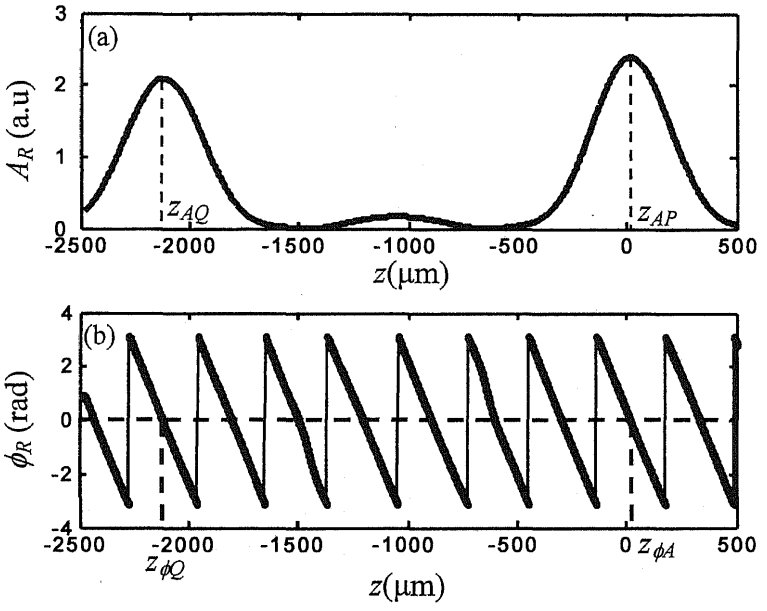

Fig. 4-13 Results of the back-propagation for one point of x_1 =2.90mm on the front surface and x_2 =3.30mm on the back surface of glass plate: (a) amplitude distribution A_R, (b) phase distribution ϕ_R.

Table 4-5 Comparison of measurement result of three points on the surface

	Back-propagation result of A_R (μm)			Back-propagation result of ϕ_R (μm)		
	z_{AP}	z_{AQ}	d	$z_{\phi P}$	$z_{\phi Q}$	d
Point 1	16	-2128	2005	14	-2114	2001
Point 2	17	-2132	2006	12	-2118	2002
Point 3	14	-2129	2005	13	-2115	2001

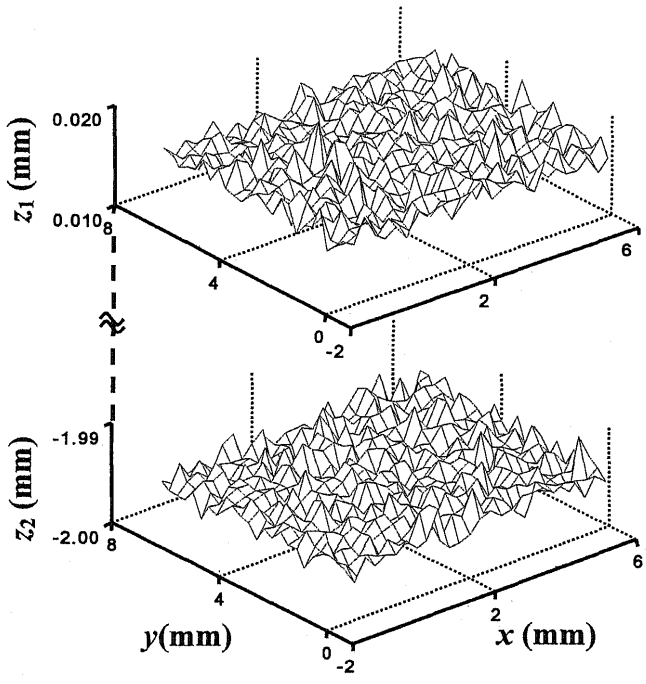

Fig. 4-14 Measured positions of the two surfaces of 2mm glass plate

B. Result of a glass plate with thickness of 1mm

At the same condition, a glass plate with the thickness of 1mm is measured. The back-propagation result of one point on the surface of the glass plate is show in Fig. 4-15. The measured value of d was 1008μm at this point. The other two points have also been checked, and the result is shown in Tab. 4-6.

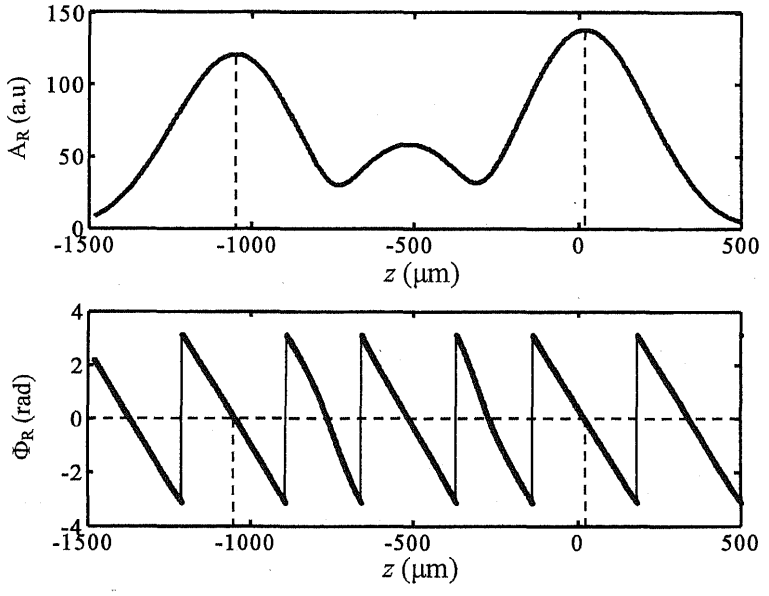

Fig. 4-15 Results of the back-propagation for one point on surface of 1mm glass plate: (a) amplitude distribution A_R, (b) phase distribution ϕ_R.

Table 4-6 Back-propagation result of three points on the surface of the glass plate

	Back-propagation result of A_R (μm)			Back-propagation result of ϕ_R (μm)		
	z_{AP}	z_{AQ}	d	$z_{\phi P}$	$z_{\phi Q}$	d
Point 1	10	-1080	1012	8	-1065	1008
Point 2	11	-1075	1010	10	-1068	1009
Point 3	8	-1086	1015	7	-1062	1006

It is obvious that there is measurement error caused by the peak value at the central of the amplitude distribution, which is made by I_3 and I_4. In order to

decrease this error, we check the coherent length distribution of the laser diode, which is shown in Fig. 4-16. L is the optical path difference (OPD) of M1 and M2 and V is the visibility of the fringe which is given as

$$V(x)=\frac{I_{\max}(x)-I_{\min}(x)}{I_{\max}(x)+I_{\min}(x)}. \tag{4-31}$$

Considering the visibility of fringe pattern, I_1, I_2, I_3 and I_4 are written as

$$I_1 = 2r_1^2 a_0^2 V \cos[\alpha_1(x_1, z_1)] \tag{4-32}$$

$$I_2 = 2r_2^2 a_0^2 \cos[\alpha_2(x_1, z_1)] \tag{4-33}$$

$$I_3 = 2r_1 r_2 a_0^2 \cos[\alpha_3(x_1, z_1)] \tag{4-34}$$

$$I_4 = 2r_1 r_2 a_0^2 \cos[\alpha_4(x_1, z_1)] \tag{4-35}$$

The amplitude distribution A_R is related to the visibility of fringe pattern. In the experiment, the OPD of M1 and M2 is adjusted almost to 0, which can be denoted as the point A in Fig. 4-16. Since the thickness of the glass plate is about 1mm, the OPD produced by the front surface and the rear surface is about 2mm, the fringe visibility of I_3 and I_4 is at point C. In Fig. 4-15, there is a peak at the central of amplitude distribution. We find that the visibility distribution at a minimum value at the point D, so we change the position of *M*1 to the point B. By doing this, the back-propagation result of one point is shown in Fig. 4-17, where the peak produced by I_3 and I_4 has been decreased. The measurement result of three points are checked which is shown in Tab. 4-7. Figures 4-18 shows the surface profile of the two surfaces of the glass plate where the axis of z is shown separated. The fluctuation of the surface is about 3.2μm, the measurement error of the back-propagation method is about 3.2μm.

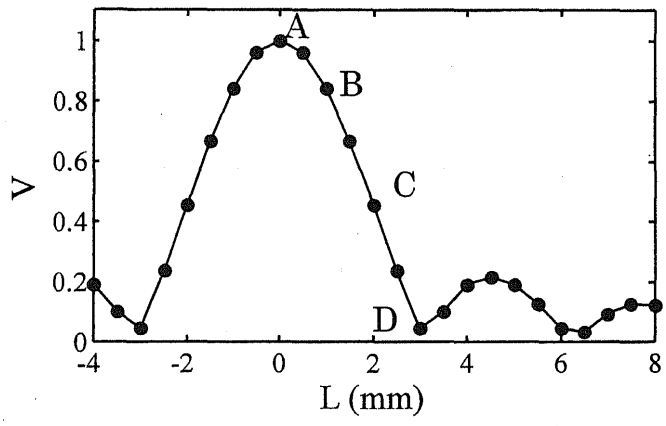

Fig. 4-16 Coherent length distribution of the laser diode

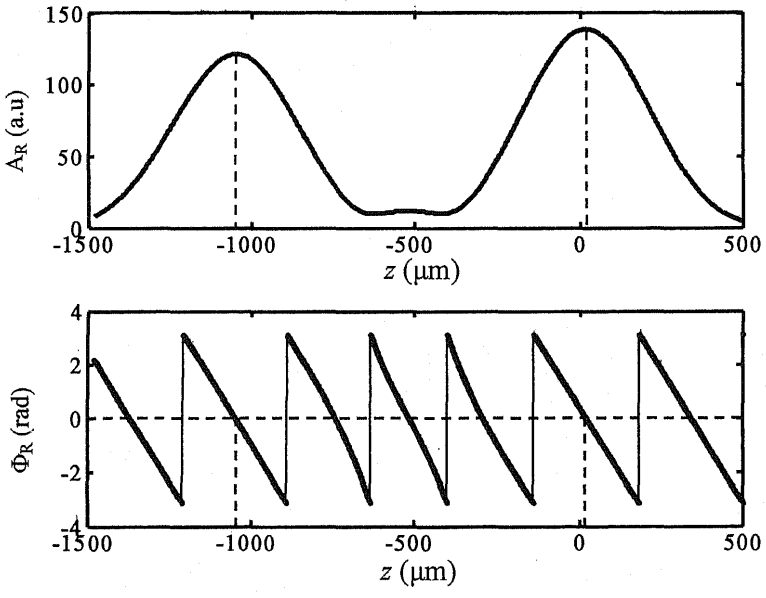

Fig. 4-17 Results of the back-propagation for one point on surface of 1mm glass plate after changing the position of M1: (a) amplitude distribution A_R, (b) phase distribution ϕ_R.

Table 4-7 Back-propagation result of three points on the surface of the glass plate after changing the position of M1

	Back-propagation result of A_R (μm)			Back-propagation result of ϕ_R (μm)		
	z_{AP}	z_{AQ}	d	$z_{\phi P}$	$z_{\phi Q}$	d
Point 1	8	-1065	1006	6	-1057	1003
Point 2	12	-1063	1007	5	-1059	1004
Point 3	6	-1064	1005	7	-1055	1003

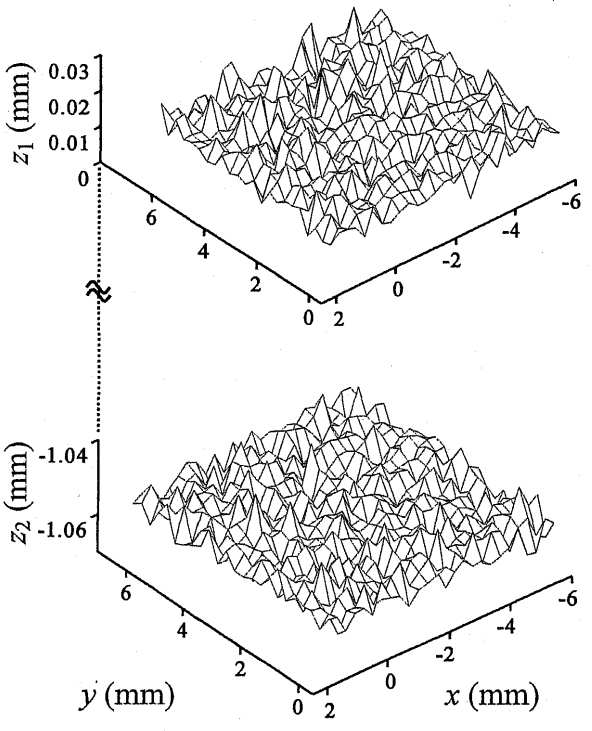

Fig. 4-18 Measured surface profile of the two surfaces of 1mm glass plate

C. Result of an acrylic plate

Last an acrylic plate was used as an object. The front surface of the acrylic plate is made up of a step profile and an inclined plane which is shown in Fig. 4-19.

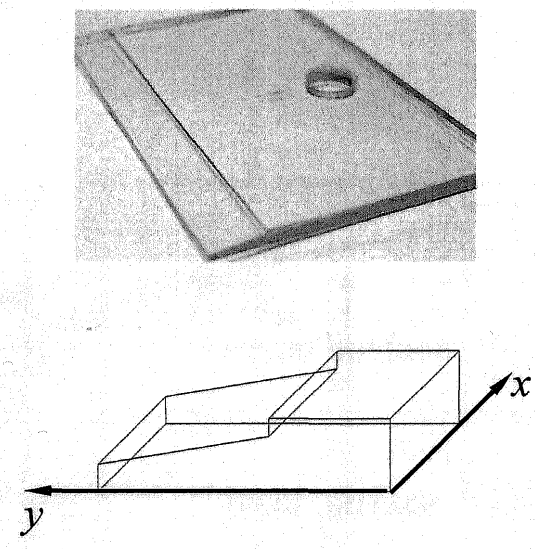

Fig. 4-19 Measured acrylic plate

The parameters used in the experiment were as follows: P_1=143.0μm, P_1=1002.4μm, M=16, Δk=0.0023rad/μm, β=30°, f_1=100mm, and f_1=25mm. The image size on the x-y plane of the CCD image sensor were 256×240 pixels with the pixel size of 7.4μm, and the measuring region on the object was about 7.4×7.2mm^2 with M_{12}=1/4.

First, the fringe pattern is projected along the x-axis direction. For the same coordinate y, the acrylic plate has the same thickness along the x direction. The theory of glass plate can be used directly. Figure 4-20 show the measured position z along one line of x=3.58mm. Because of the shadow of the step profile, there is no interference signal reflected from y_1=5.33mm to y_1=5.68mm. The upside and underside lines on Fig. 4-20 are the surface profile of front surface and rear surface along one line of x=3.58mm, respectively. The sample has also

been measured by a confocal microscope. The measurement results of two methods are compared, which is shown in Figs. 4-21 and 4-22. Figure 4-21 (a) shows the comparison of front surface. Figure 4-21 (b) shows the comparison of front surface when the slope angle of the incline plane is subtracted. Figure 4-22 (a) and (b) show the comparison of the rear surface. From Figs. 4-21 and 4-22, we find that the back-propagation method has the same measurement result as the confocal microscope.

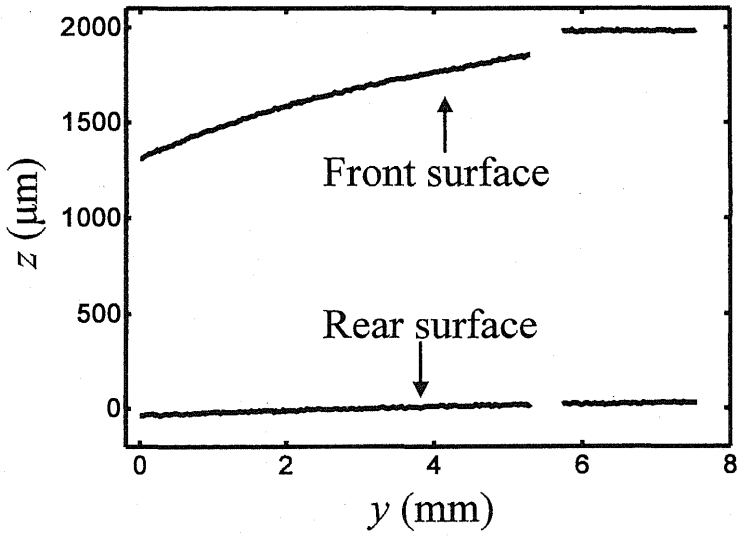

Fig. 4-20 Surface profile of front surface and rear surface along one line of x=3.58mm

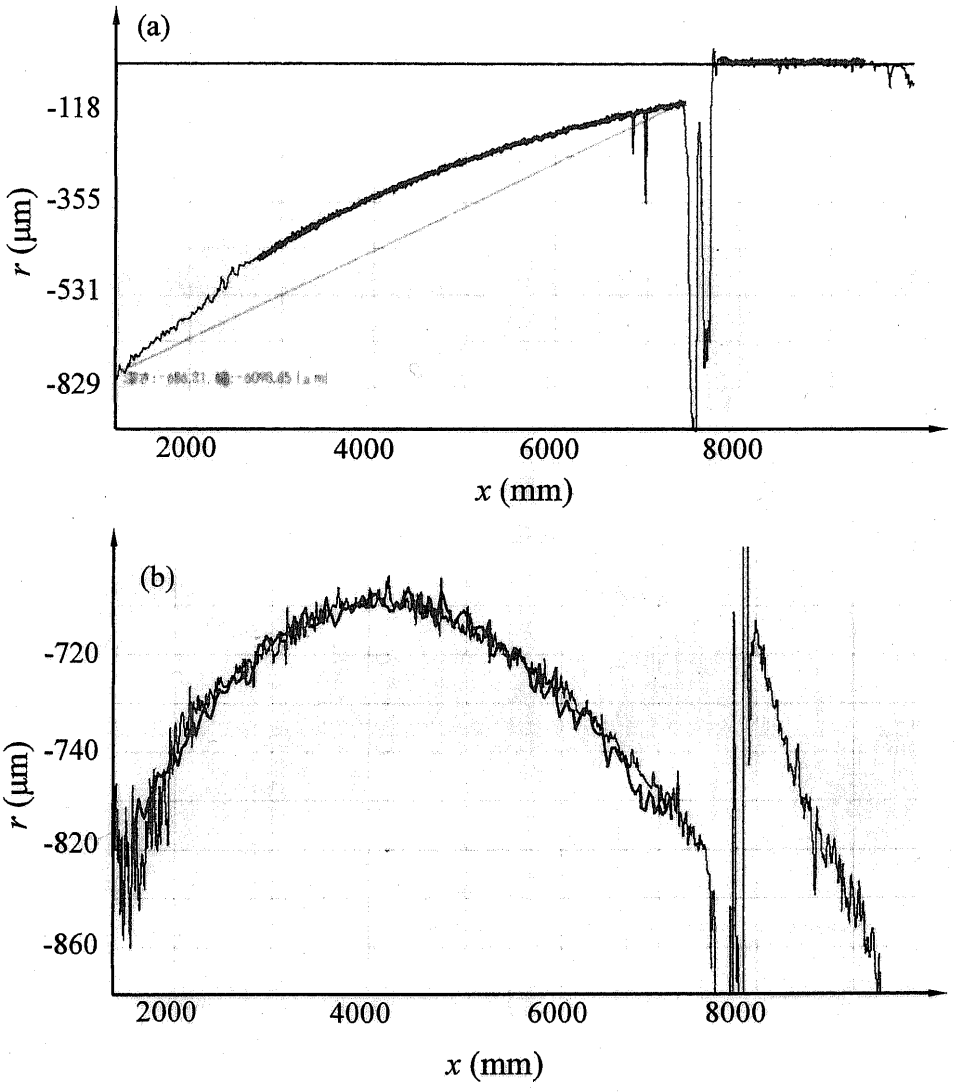

Fig. 4-21 Comparison of front surface profile measured by back-propagation method and confocal microscope, (a) comparison of front surface, (b) comparison of front surface when the slope angle of the incline plane is subtracted

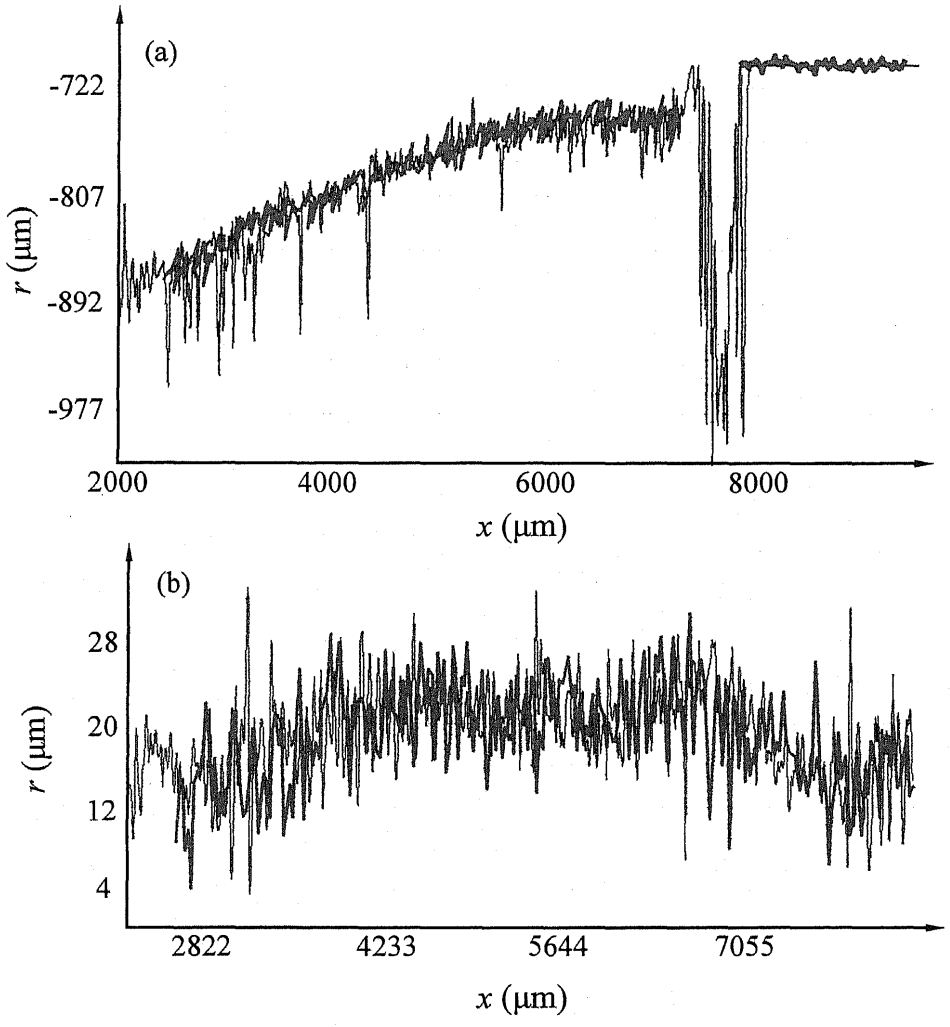

Fig. 4-22 Comparison of rear surface profile along one line measured by back-propagation method and confocal microscope, (a) comparison of rear surface, (b) comparison of rear surface when the slope angle of the incline plane is subtracted

Figures 4-23 shows the measured position of the two surfaces of the acrylic plate where the axis of z is shown separated. The measurements were repeated 3 times at intervals of a few minutes. The repeatability in the thickness measurement was about 3.5μm which was the rms value of the differences between the average values of the thickness.

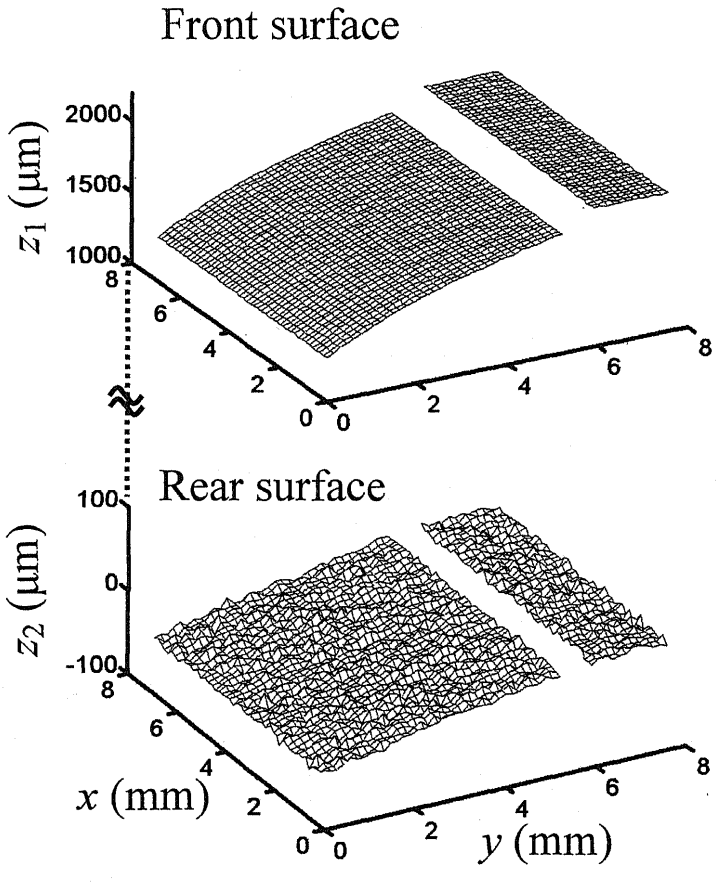

Fig. 4-23 Measured two surface profiles of the acrylic plate

Next, the fringe pattern is projected along the y-axis direction. For the same coordinate x, the thickness of the acrylic plate is different along the y direction. The theory of glass plate should be modified. Figure 4-24 shows the propagation of the fringe when the object has an incline surface. The interference signal detected from point Q (x_0, z_0) is propagated from point Q_1 (x, z). But in the theory, we assumed that the thickness between two surfaces is a constant value. In the back-propagation method, the measurement result gives the coordinate of point Q_2 (x_m, z_m). The coordinate of Q_1, and Q_2 is given as

$$x = x_0 - \Delta x$$
$$z = z_0 - \Delta z \tag{4-36}$$

$$x_m = x_0 - \Delta x_m$$
$$z_m = z_0 - \Delta z_m \tag{4-37}$$

where Δx, Δz and Δx_m can be expressed by Δz_m which is written as

$$\Delta x = \frac{2\tan\gamma\tan(\gamma+2\delta)}{\tan\gamma+\tan(\gamma+2\delta)}\Delta z_m \tag{4-38}$$

$$\Delta z = \frac{2\tan\gamma}{\tan\gamma+\tan(\gamma+2\delta)}\Delta z_m \tag{4-39}$$

$$\Delta x_m = \tan\gamma\Delta z_m \tag{4-40}$$

δx and δz is denoted as measurement error when the object has an incline surface. From Eqs. (4-38)-(4-40), δx and δz is obtained

$$\delta x = \frac{\tan\gamma\sin 2\delta}{\sin 2(\gamma+\delta)}\Delta z_m \tag{4-41}$$

$$\delta z = -\frac{\sin 2\delta}{\sin 2(\gamma+\delta)}\Delta z_m \tag{4-42}$$

From the measurement result of Δz_m, the measurement error at this condition is obtained. Figure 4-25 shows the distribution of δz, where Fig. 4-25 (a) is the result of simulation and Fig. 4-25 (b) is the result of experiment.

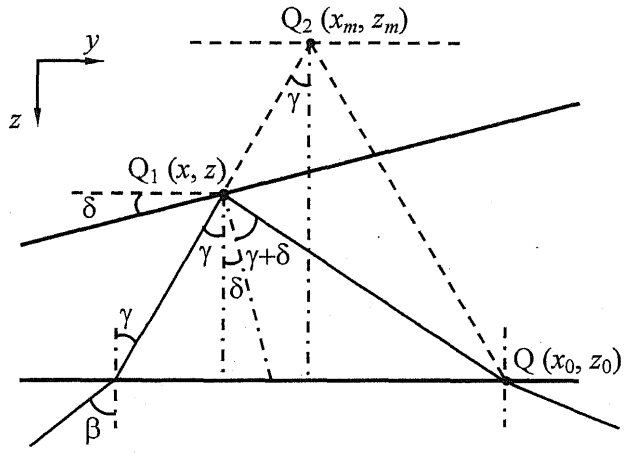

Fig. 4-24 Fringe propagation when the object has an incline surface

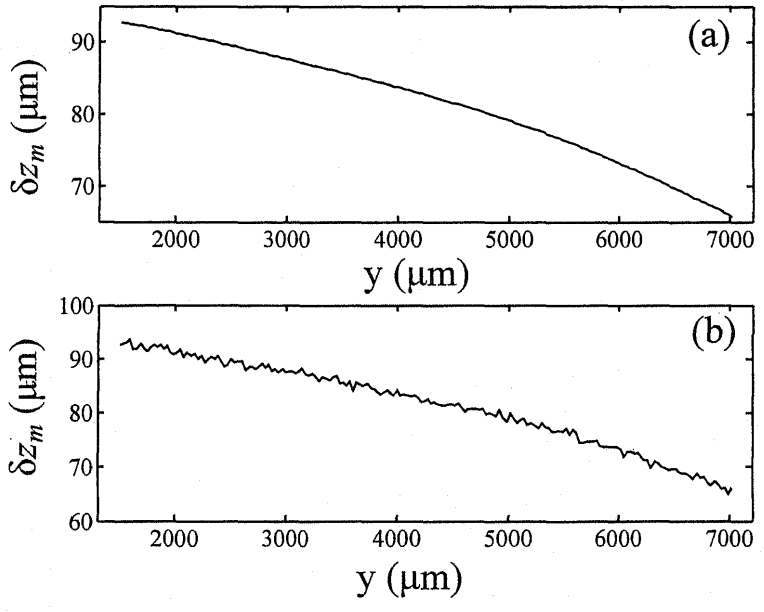

Fig. 4-25 Measurement error of the object with incline surface, (a) simulation result, (b) experiment result

4.4 Summary

A multi-period fringe projection interferometry by using the back-propagation method was used to measure two surface profiles of the object. The feedback technology was incorporated to keep the phase on one point of the object surface at $\pi/2$ during the scanning of the fringe period. The interference signal is made up of four waves from the front surface and the rear surface of the object. In the back-propagation method the optical fields with different fringe periods were back-propagated to the stationary point of the phase. The position of the object surface was obtained from the distance of the back-propagation on which the amplitude of the sum of the back-propagated optical fields became maximum and its phase became zero. The simulation made it clear that the extending of two peaks of A_R distribution will bring error to the measurement, and when the amplitude B_m of the interference signal is a Gauss distribution, this error decreased. The measurement of a glass plate gave the measurement precision of this method was 2.8μm and the repeatability of this method was 2.5μm. An acrylic plate had also been measured. The measured result was compared with that measured by the confocal microscope.

Chapter5

Measurement of surface profiles using continuous period-scanning for back-propagation method

5.1 Introduction

In Chapter 3 and 4, multi-period fringe projection interferometry with back-propagation method has been reported and has been used to measure surface profile of object. Comparing with other methods using multi-period fringe projection interferometry, the back-propagation method has a higher accuracy and it can be used to measure the front and rear surface profiles in one time successfully. But there is a shortcoming for not only the back-propagation method but also other methods using multi-period fringe projection interferometry, which is that the measurement time for these methods is long. Since the interference signals for all the periods are detected and processed discretely, it takes a large amount of time to process these data. For example, the experiment in Chapter 4 has used 16 periods of fringes in the measurement. For each period, the CCD capture time is 0.032s, and the captured data should be calculated in 20s without the data input and output time. The process time for all the 16 periods takes more than five minutes. It is important to find a method which can capture the interference signal and process the data in one time.

In this Chapter a continuous period-scanning of the fringe period is introduced into the multi-period fringe projection interferometry. The period of the fringe

patter is change continuously, and the interference signal is a time-varying signal. The frequency components of the interference signal are calculated by using Fourier transformation[23]. The phase distribution due to the scanning of the period is reflected into the frequency components of the interference signal. Amplitudes and phases of the continuous period-scanning fringe patterns are obtained by using inverse Fourier transformation. The method allows us to capture the interference signal and process the data in one time. The period of fringe is obtained from the phase distribution at different time. The back-propagation method is used to get the surface profile of the object. The back-propagation distance from the each point of the object to the constant phase point provides the position of the object surface. The capture time of this method is about 0.224s for 28 periods of fringes, and the computation time of this method is about 40s without the data input and output time. The process time for all the 28 periods takes less than one minute, which is much shorter than the discrete period-scanning method used in Chapter 4. In the experiment, an acrylic plate is measured. The repeatability in the thickness measurement was about 3.6μm. The measured result is almost the same as the discrete period-scanning method used in Chapter 4.

5.2 Detection of continuous optical fields

A schematic configuration for the continuous period-scanning fringe projection is shown in Fig. 5-1. The intersecting angles between the two waves and the z_p axis are $\pm\theta_m$, respectively. The interference signal of the two plane waves in the coordinate system (x_p, y_p, z_p) is written as

$$\begin{aligned} I_{12} &= 2a_0^2 \cos[\frac{2\pi}{\lambda} 2x_p \sin\theta(t)] \\ &= 2a_0^2 \cos[\frac{2\pi}{P(t)} x_p] \qquad t = 1, \cdots, s \end{aligned} \tag{5-1}$$

The period of the fringe pattern is expressed by $P(t)=\lambda/2\theta(t)$ since $\sin\theta(t)\approx\theta(t)$ when $\theta(t)$ is small. The intersecting angles $\theta(t)$ is continuously changed, which

make the periods of the fringe pattern $P(t)$ be scanned accordingly. The phase of the interference fringe at x_p=0 is kept at $\pi/2$ during the period scanning by using feedback controlling. The original point O is the constant phase point of the coordinate system where the phase of the fringe pattern does not change while the period of the fringe pattern is scanned.

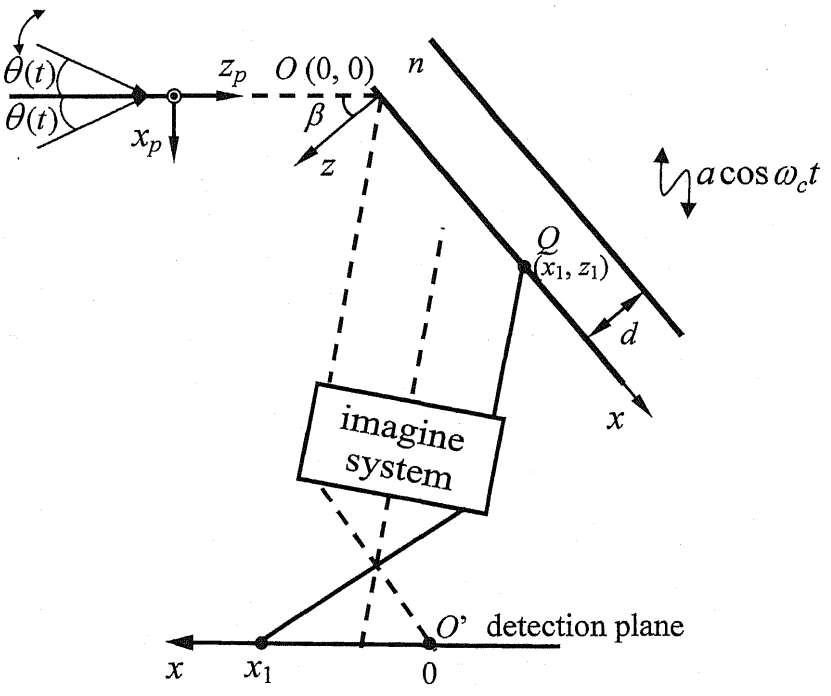

Fig. 5-1 Schematic configuration for continuous period-scanning fringe projection and detection of the fringe patterns by sinusoidal phase-modulating interferometry.

It is assumed that there is a glass plate whose two surfaces are parallel. The refractive index of the glass plate is n. An image of the point object is formed on a detection plane with an imaging system. The intersection angle between the optical axis and the z_p axis is 2β. Another coordinate system (x, y, z) is defined. The original point O of the coordinate system (x, y, z) is the same as that of the coordinate system (x_p, y_p, z_p). The z axis is the bisector of the intersection angle

between the z_p axis and the optical axis. The magnification of the imaging system is assumed to be unit for the sake of simplicity. The position of x=0 on the detection plane corresponds to the original point O. In the coordinate system (x, y, z), the two plane waves are written as

$$U_1 = a_0 \exp\{ik\{x\sin[\beta+\theta(t)]-z\cos[\beta+\theta(t)]\}+\pi/2\} \tag{5-2}$$

$$U_2 = a_0 \exp\{ik\{x\sin[\beta-\theta(t)]-z\cos[\beta-\theta(t)]\}\} \tag{5-3}$$

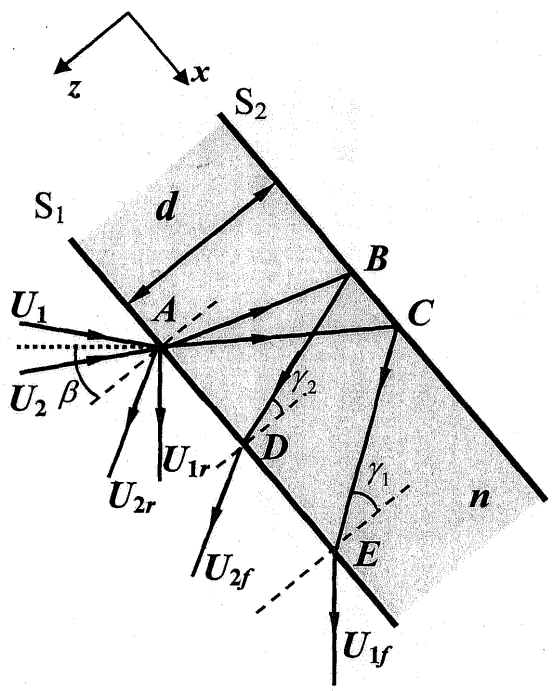

Fig. 5-2 Propagation of the two plane wave in the glass plate

The plane waves U_1 and U_2 are divided in two parts which are shown in Fig. 5-2. One is reflected by surface S_1 and is denoted as U_{1r} and U_{2r}, respectively, the other is refracted and reflected by surfaces S_1 and S_2, and then refracted by surface S_1 which is denoted as U_{1f} and U_{2f}, respectively. U_{1r}, U_{2r}, U_{1f} and U_{2f} are written as

$$U_{1r} = r_1 a_0 \exp\{ik\{x\sin[\beta+\theta(t)]+z\cos[\beta+\theta(t)]\}+\pi/2\} \quad (5\text{-}4)$$

$$U_{2r} = r_1 a_0 \exp\{ik\{x\sin[\beta-\theta(t)]+z\cos[\beta-\theta(t)]\}\} \quad (5\text{-}5)$$

$$U_{1f} = r_2 a_0 \exp\{ik\{(x+2d\tan\gamma_1)\sin[\beta+\theta(t)]+z\cos[\beta+\theta(t)]\}+\pi/2\} \quad (5\text{-}6)$$

$$U_{2f} = r_2 a_0 \exp\{ik\{(x+2d\tan\gamma_2)\sin[\beta-\theta(t)]+z\cos[\beta-\theta(t)]\}\} \quad (5\text{-}7)$$

where r_1, r_2 is the proportional coefficient corresponding to the reflection and refraction, γ_1 and γ_2 are the refraction angles of $\beta + \theta(t)$ and $\beta - \theta(t)$, which is given by

$$\gamma_1 = \arcsin\{\frac{\sin[\beta+\theta(t)]}{n}\} \quad (5\text{-}8)$$

$$\gamma_2 = \arcsin\{\frac{\sin[\beta-\theta(t)]}{n}\} \quad (5\text{-}9)$$

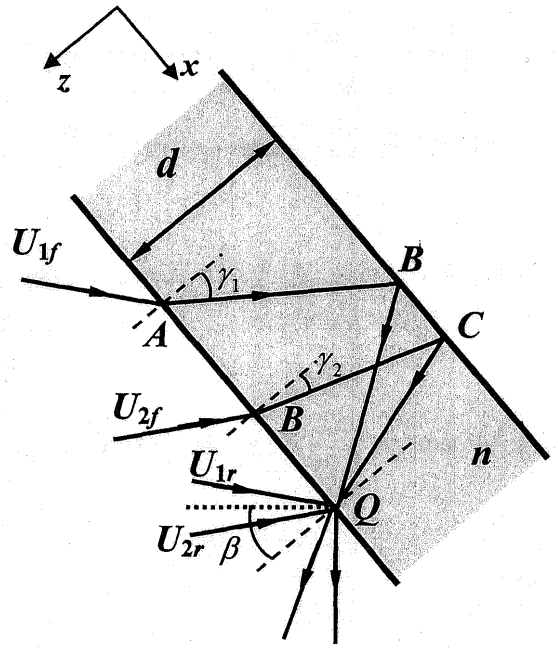

Fig. 5-3 Interference signal of point object Q

Q is a point object on the front surface of the glass plate. The position of the point objects Q is expressed by $x=x_1$, $z=z_1$, and the image of the point object Q is formed at $x=x_1$ on the detection plane. The interference fringe intensity oscillates sinusoidally in the direction of the x_p axis with the form of $a\cos\omega_c t$ in order to apply the sinusoidal phase modulation method. Then the following interference signal of point object Q is detected on the detection plane which is shown in Fig. 5-3:

(1) The interference signals made up of U_{1r} and U_{2r}, U_{1f} and U_{2f} are denoted as I_1 and I_2, which are given as

$$I_1 = 2r_1^2 a_0^2 \cos[z_c \cos\omega_c t + \frac{2\pi}{P(t)}(x_1 \cos\beta + z_1 \sin\beta) + \pi/2] \tag{5-10}$$

$$\begin{aligned} I_2 = 2r_2^2 a_0^2 \cos\{&z_c \cos\omega_c t + \frac{2\pi}{P(t)}(x_1 \cos\beta + z_1 \sin\beta) \\ &- 2dk\{\tan\gamma_1 \sin[\beta + \theta(t)] - \tan\gamma_2 \sin[\beta - \theta(t)]\} + \pi/2\} \end{aligned} \tag{5-11}$$

since $\theta_m << 1$, $\cos\theta_m \approx 1$ and $\tan\gamma_1 - \tan\gamma_2 \approx 0$, I_2 is approximately written as

$$\begin{aligned} I_2 = 2r_2^2 a_0^2 \cos[&z_c \cos\omega_c t + \frac{2\pi}{P(t)}(x_1 \cos\beta + z_1 \sin\beta) \\ &- \frac{2\pi}{P(t)} d(\tan\gamma_1 + \tan\gamma_2)\cos\beta + \pi/2] \end{aligned} \tag{5-12}$$

(2) The interference signals made up of U_{1r} and U_{2f}, U_{1f} and U_{2r} are denoted as I_3 and I_4, which is given as

$$\begin{aligned} I_3 = 2r_1 r_2 a_0^2 \cos\{&z_c \cos\omega_c t + \frac{2\pi}{P(t)}(x_1 \cos\beta + z_1 \sin\beta) \\ &+ \frac{2\pi}{\lambda} 2d \tan\gamma_2 \sin[\beta - \theta(t)] + \pi\} \end{aligned} \tag{5-13}$$

$$I_4 = 2r_1 r_2 a_0^2 \cos[z_c \cos\omega_c t + \frac{2\pi}{P(t)}(x_1 \cos\beta + z_1 \sin\beta) - \frac{2\pi}{\lambda} 2d \tan\gamma_1 \sin[\beta + \theta(t)] + \pi\} \tag{5-14}$$

so the interference signal detected from the sinusoidal phase modulation interferometry is written as

$$\begin{aligned} I(x,z,t) &= I_1 + I_2 + I_3 + I_4 \\ &= B\cos(z_c \cos\omega_c t + \Phi(x,z,t)).\ t = 1,\cdots,s \end{aligned} \tag{5-15}$$

Since $\theta(t)<<1$, $\cos\theta(t) \approx 1$ and $\tan\gamma_1 - \tan\gamma_2 \approx 0$, the distance between point B and C at the rear surface is smaller than the size of one pixel, the interference signal from the rear surface can be look as being reflected from one point Q_1 at the rear surface, which is shown in Fig. 5-4.

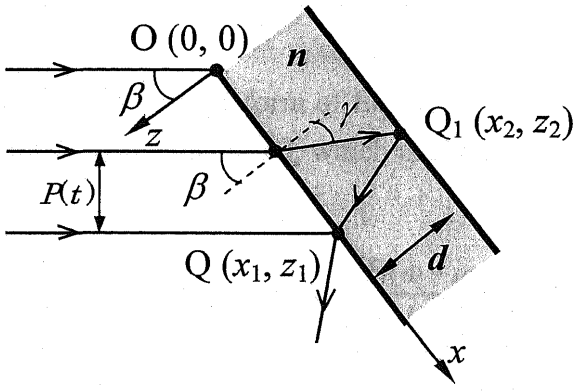

Fig. 5-4 Observed interference signal reflected from the two surfaces

The fast Fourier transform of $I(t)$ is given by

$$F(\omega)=\Im\{B\cos[\Phi(t)]\}\otimes[\sum_{m=-\infty}^{\infty}(-1)^m A_{2m}\delta(\omega-2m\omega_c)] \\ +\Im\{B\sin[\Phi(t)]\}\otimes\{\sum_{m=-\infty}^{\infty}(-1)^m A_{2m-1}\delta[\omega-(2m-1)\omega_c]\} \tag{5-16}$$

where $A_m=J_{|m|}(Z_c)\exp(jm\theta)$, $J_{|m|}$ is *m-th* Bessel function, $\delta(\omega)$ is the delta function, $\Im\{y\}$ is a Fourier transform of y, and the symbol $\otimes$ represents convolution.

In the conditions

$$\Im\{B\cos[\Phi(t)]\}=0 \quad |\omega|\geq\omega_c/2 \tag{5-17}$$

$$\Im\{B\sin[\Phi(t)]\}=0 \quad |\omega|\geq\omega_c/2 \tag{5-18}$$

we designate the frequency components existing in the ranges of $\omega_c/2<\omega<3\omega_c/2$ and $3\omega_c/2<\omega<5\omega_c/2$ by $F_1(\omega)$ and $F_2(\omega)$, respectively. Then we have

$$F_1(\omega-\omega_c)=-2BJ_1(z_c)\Im\{\sin[\Phi(t)]\}, \quad |\omega|<\omega_c/2 \tag{5-19}$$

$$F_2(\omega-2\omega_c)=-2BJ_2(z_c)\Im\{\cos[\Phi(t)]\} \quad |\omega|<\omega_c/2 \tag{5-20}$$

By taking the inverse Fourier transform of Eqs. (5-19) and (5-20), we can obtain the functions of $\sin[\Phi(t)]$ and $\cos[\Phi(t)]$, which is given by

$$2B\sin[\Phi(t)]=\Im^{-1}\left[\frac{F_1(\omega-\omega_c)}{-J_1(Z_c)}\right], \tag{5-21}$$

$$2B\cos[\Phi(t)]=\Im^{-1}\left[\frac{F_2(\omega-2\omega_c)}{-J_2(Z_c)}\right]. \tag{5-22}$$

where $\Im^{1}\{y\}$ is a inverse Fourier transform of y. The phase distribution of $\Phi(t)$ is given by

$$\begin{aligned}\Phi(t) &= \tan^{-1}\left[\frac{2B\sin[\Phi(t)]}{2B\cos[\Phi(t)]}\right] \\ &= \tan^{-1}\left[\frac{\Im^{-1}[F_1(\omega-\omega_c)/J_1(Z_c)]}{\Im^{-1}[F_2(\omega-2\omega_c)/J_2(Z_c)]}\right]\end{aligned} \tag{5-23}$$

$P(t)$ is obtained from the distribution of $\Phi(t)$. The coordinate x of the object is provided by the position of the detection plane, the following phase Φ_{tz} is extracted from the phase $\Phi(t)$ by subtracting the value of $k(t)x_1\cos\beta_1+\pi/2$ from the calculated value of $\Phi(t)$:

$$\Phi_{tz}(z,t)=\Phi(x,z,t)-[k(t)x_1\cos\beta+\pi/2] \tag{5-24}$$

where $k(t)=\dfrac{2\pi}{P(t)}$, and it is called wave number of the fringe pattern.

Since the coordinate x_1 of the object point Q is known from the position of the detection plane, a method which is called the back-propagation method is used to get the coordinate z of the point object.

In the back-propagation method, the detected fields of the point objects Q regarding the variable z are defined as

$$D(x_1,z,t)=B\exp[j\Phi_{tz}(z,t)]. \tag{5-25}$$

When the detected field D_m is back-propagated to the position z, the back-propagated field of $U_m(z)$ is given by

$$U(z,t)=D(x_1,z,t)\exp(-j\alpha_{tz}),\quad t=1,\cdots,s. \tag{5-26}$$

where α_{tz} is denoted as

$$\alpha_{tz}=k(t)z\sin\beta. \tag{5-27}$$

The sum of the back-propagated fields over all of $k(t)$ produces the following

reconstruction field as a function of back-propagation variable z:

$$U_R(z) = \sum_{t=1}^{s} U(z,t) = A_R \exp(j\phi_R). \tag{5-28}$$

When all of the detected fields of the point objects Q are back-propagated to the position of the stationary point O, the amplitude of A_R becomes maximum, and its phase ϕ_R becomes zero. The back-propagation distance z is expressed as z_P and z_Q. From this basic characteristic, the coordinate z_1 of the object point Q, the coordinate (x_2, z_2) of the object Q_1 and the thickness d of the glass plate can be obtained and expressed as

$$z_1 = z_A \tag{5-29}$$

$$x_2 = x_1 - \frac{(z_P - z_Q)\tan\beta}{2} \tag{5-30}$$

$$z_2 = z_A - \frac{(z_P - z_Q)\tan\beta}{2\tan\gamma_1} \tag{5-31}$$

$$d = \frac{(z_P - z_Q)\tan\beta}{2\tan\gamma_1} \tag{5-32}$$

5.3 Experiments

5.3.1 *Experiment setup*

The experimental setup is shown in Fig. 5-5. A 50mw laser diode is used as the light source. A laser beam collimated with a lens L_0 is divided into two beams by beam splitter BS1. The beams reflected from mirror M1 and mirror M2 produce the interference fringe. Piezoelectric transducer 1 (PZT1) is controlled by a function generator which is synchronized with the CCD camera. PZT1 changes the angle θ of mirror 1 continuously, which changes the periods $P(t)$ of the interference fringe continuously. The piezoelectric transducer 2 (PZT2) vibrates with frequency f_c of $125Hz$ to produce the sinusoidal phase modulation in the interference fringe. The interference fringe is divided into two parts by beam

splitter BS2. One part is incident on a photo diode (PD) which detects the interference signal at one point of x_f. The detected interference signal is given by

$$I(t, x_f) = A + B\cos(a\cos\omega_c t + k(t)x_f) \tag{5-33}$$

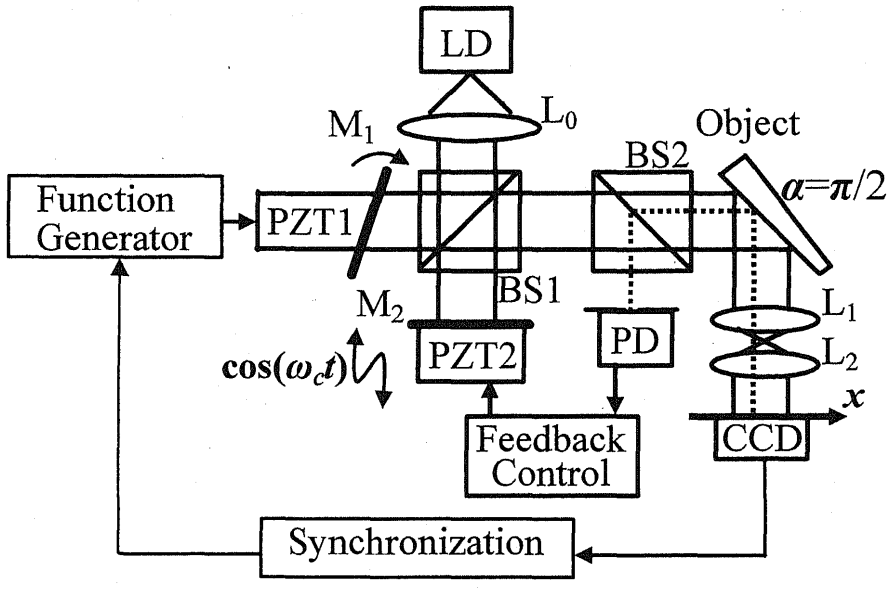

Fig. 5-5 Experiment setup of the continuous period-scanning fringe projection for surface profile measurement.

In the feedback control circuit, a feedback signal of $S_f = B\cos[k(t)x_f]$ is produced by eliminating the DC component of A and sampling $I(t, x_f)$ when $\cos(\omega_c t) = 0$. A feedback control signal made from the signal S_f is applied to the PZT2 so that S_f becomes zero by moving mirror M2. Thus the feedback control system makes the phase of the point x_f fixed at $\pi/2$ while the period $P(t)$ of the interference fringe is changed. The point x_f is defined as the origin point of the x_p axis or x axis. The other part of the interference fringe is projected on the surface of the object. The image of the object's surface is formed with the afocal imaging system whose magnification is $M_{12} = f_2 / f_1$, where f_1 and f_2 are the focal length

of L_1 and L_2, respectively. A high-speed CCD camera with the frame period of 1ms is used to detect the sinusoidally phase-modulated interference fringe.

5.3.2 *Experiment results*

A triangle wave with the frequency of 1.95Hz is produced by the function generator and applied to PZT1. The time-varying interference signal is detected by CCD camera and processed by the sinusoidal phase-modulation interferometer. The spectrum distribution of one point x=2.90μm, y=6.51μm on the surface of the object is shown in Fig. 5-6

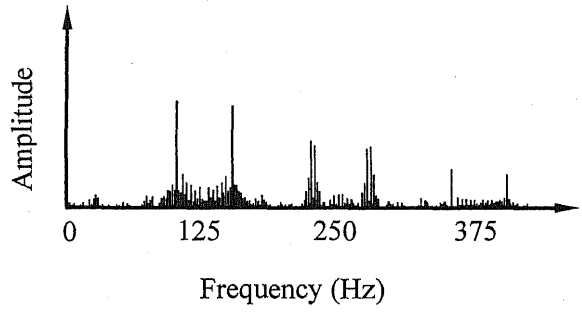

Fig. 5-6 Spectrum distribution of one point x=2.90μm, y=6.51μm on the surface of the object

The phase distribution $\Phi(t)$ of this point is shown in Fig. 5-7

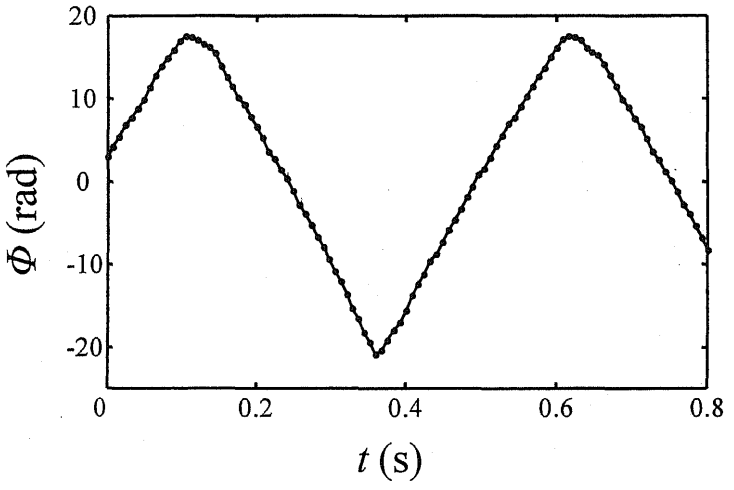

Fig. 5-7 Time-varying phase distribution $\Phi(t)$ of one point on the surface.

The phase distribution $\Phi(t)$ when time is from t=0.12s to t=0.344s is used for the back-propagation method. The capture time of this experiment is about 0.224s for 28 periods of fringe, which is much shorter than the capture time 0.512s in the experiment we have explained in Chapter 4, while there are only 16 periods of fringe used for the back-propagation method. The computation time of this method is about 30s, while the discrete period-scanning method used in Chapter 4 takes more than 5 minutes.

First a mirror is used as an object in order to determine the period of fringe pattern. The stability of the constant point is shown in Fig.5-8. The fluctuation of the phase distribution is less than $2\pi/100$. The periods of fringe pattern is obtained from the phase gradient of the line made by several adjacent points in one time. Keeping the control voltage of the function generator, the periods of the fringe pattern will be kept. The periods used in the experiment is shown in Tab. 5-1.

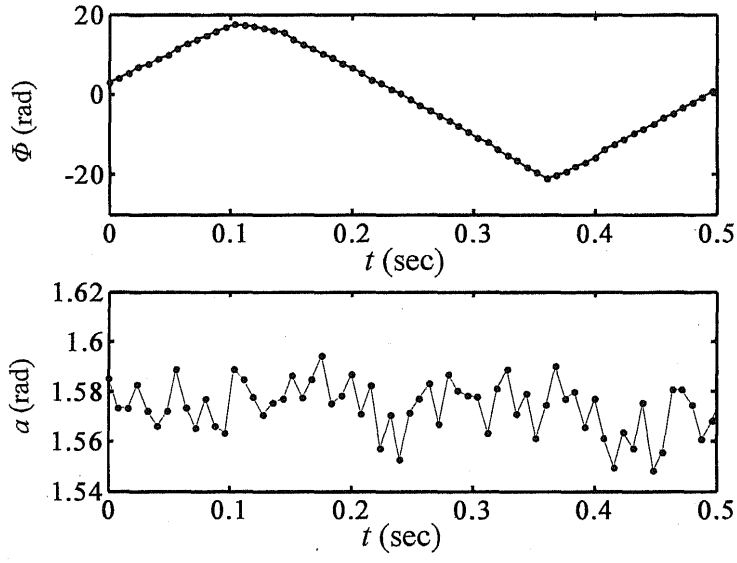

Fig. 5-8 Stability of the constant point of the continuous period scanning method

Table 5-1 Periods used in the experiment

	First time (μm)	Second time (μm)
P_1	168.5	167.9
P_4	185.4	185.8
$P7$	206.7	206.1
P_{10}	233.0	233.6
P_{13}	267.8	268.7
P_{16}	314.9	315.6
P_{19}	381.6	382.7
P_{22}	485.3	484.9
P_{25}	664.9	663.8
P_{28}	1053.7	1054.7

An acrylic plate which is used in Chapter 4 is used as an object. The front surface of the acrylic plate is made up of a step profile and an inclined plane. The parameters used in the experiment were as follows: P_1=168.0μm, P_{28}=1054.2μm, M=28, Δk=0.00112rad/μm, β=20°, f_1=100mm, and f_1=25mm. The image size on the x-y plane of the CCD image sensor were 256×240 pixels with the pixel size of 7.4μm, and the measuring region on the object was about 7.4×7.2mm^2 with M_{12}=1/4. Figures 5-9 show the measured position z along one line of x=3.58mm. Because of the shadow of the step profile, there is no interference signal reflected from y_1=5.33mm to y_1=5.68mm. The upside and underside lines on Fig. 5-9 are the surface profile of front surface and rear surface along one line of x=3.58mm, respectively. The measurement result is almost the same as in Chapter 4, but the measurement time 0.224s is much smaller than 0.512s in Chapter 4. The sample has also been measured by a confocal microscope. The measurement results of two methods are compared, which is shown in Figs. 5-10 and 5-11. Figure 5-10 (a) shows the comparison of front surface. Figure 5-10 (b) shows the comparison of front surface when the slope angle of the incline plane is subtracted. Figure 5-11 (a) and (b) show the comparison of the rear surface. From Figs. 5-10 and 5-11, we find that the continuous period-scanning for back-propagation method has almost the same measurement result as the confocal microscope.

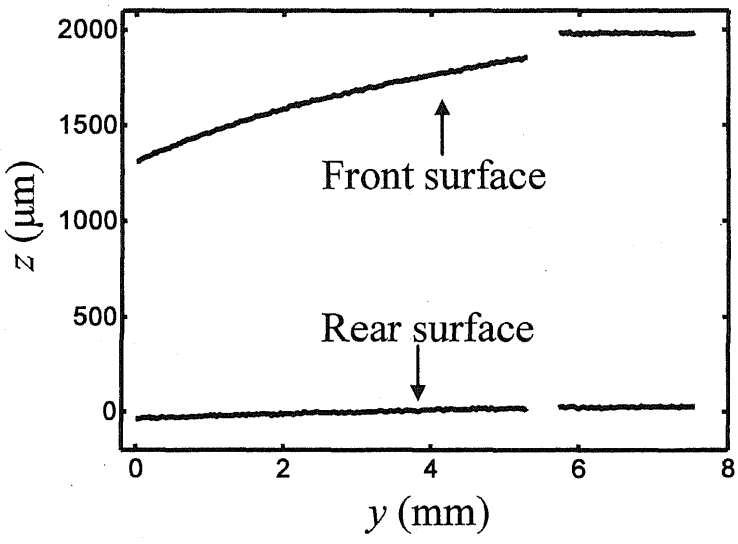

Fig. 5-9 Surface profile of front surface and rear surface along one line of x=3.58mm

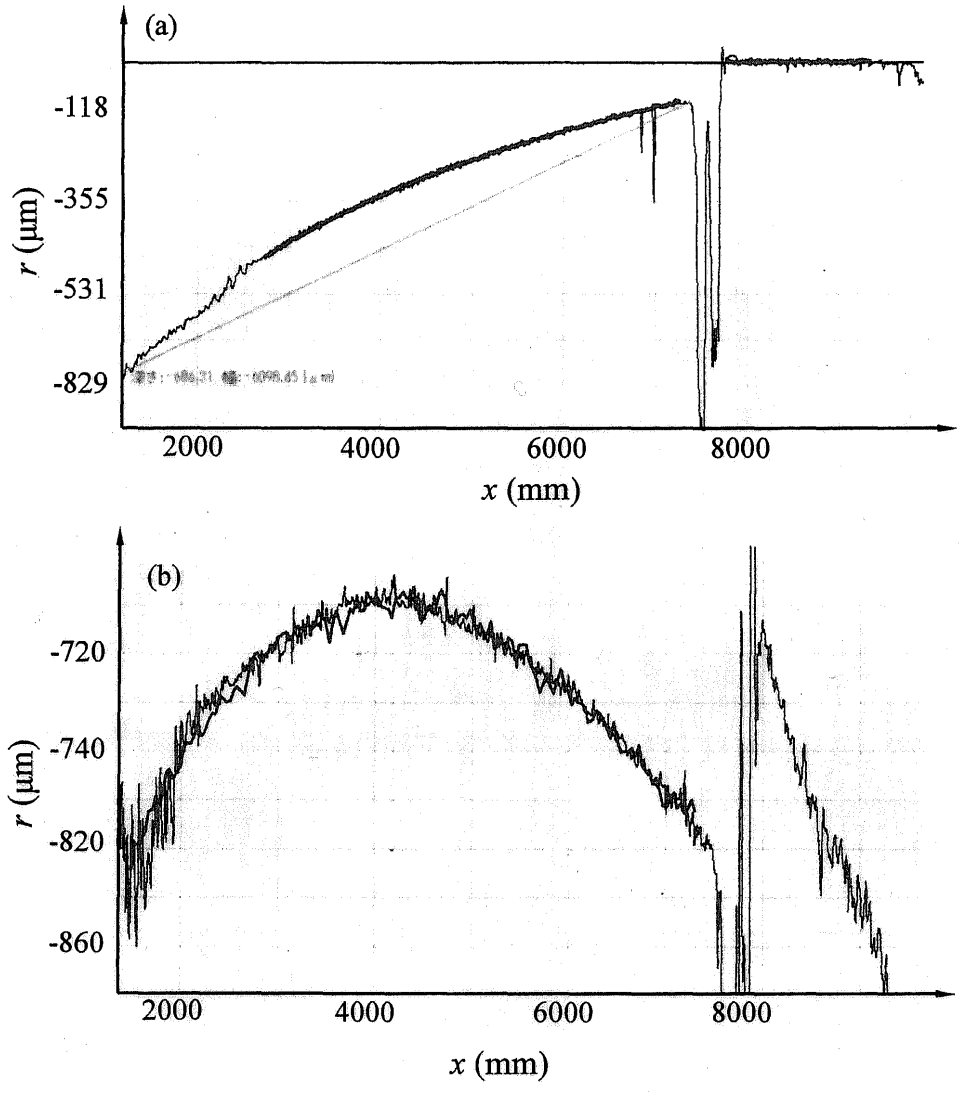

Fig. 5-10 Comparison of front surface profile measured by continuous period-scanning back-propagation method and confocal microscope, (a) comparison of front surface, (b) comparison of front surface when the slope angle of the incline plane is subtracted

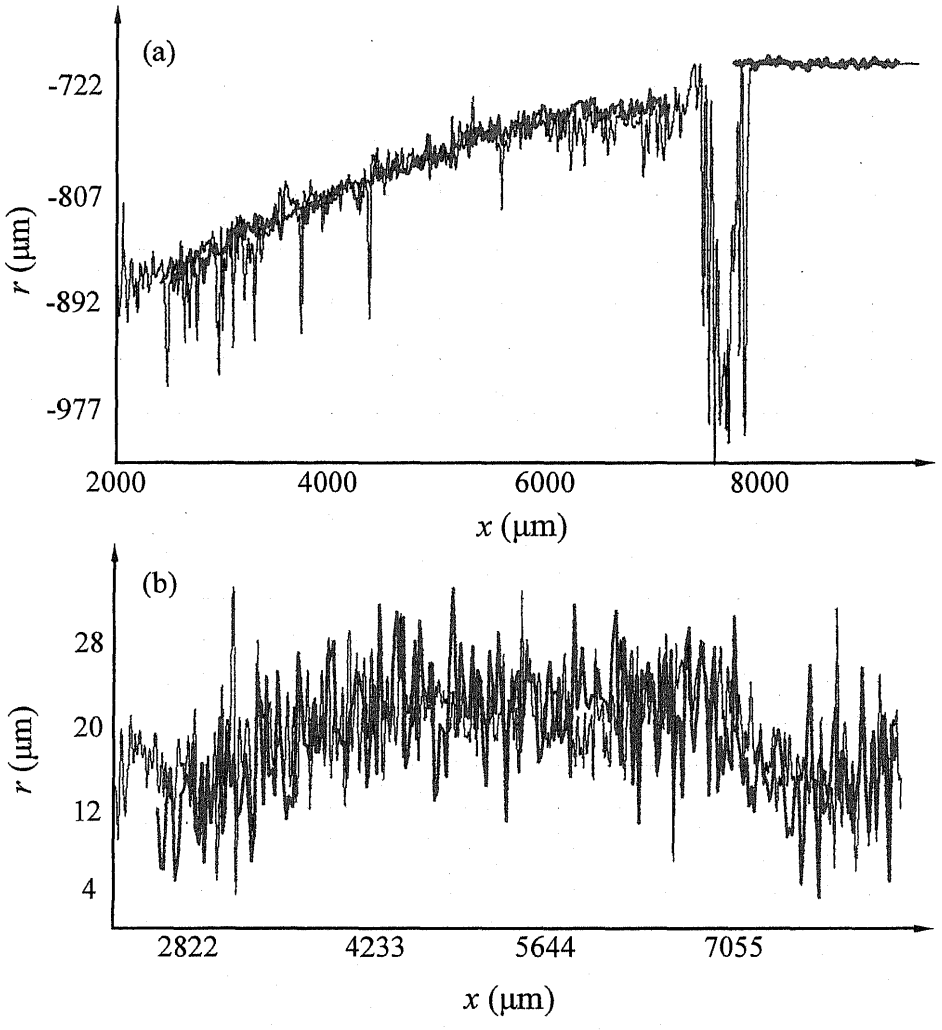

Fig. 5-11 Comparison of rear surface profile along one line measured by continuous period-scanning back-propagation method and confocal microscope, (a) comparison of rear surface, (b) comparison of rear surface when the slope angle of the incline plane is subtracted

Figures 5-12 shows the measured position of the two surfaces of the acrylic plate where the axis of z is shown separated. The measurements were repeated 3 times at intervals of a few minutes. The repeatability in the thickness measurement was about 3.6μm which is nearly to the result in Chapter 4.

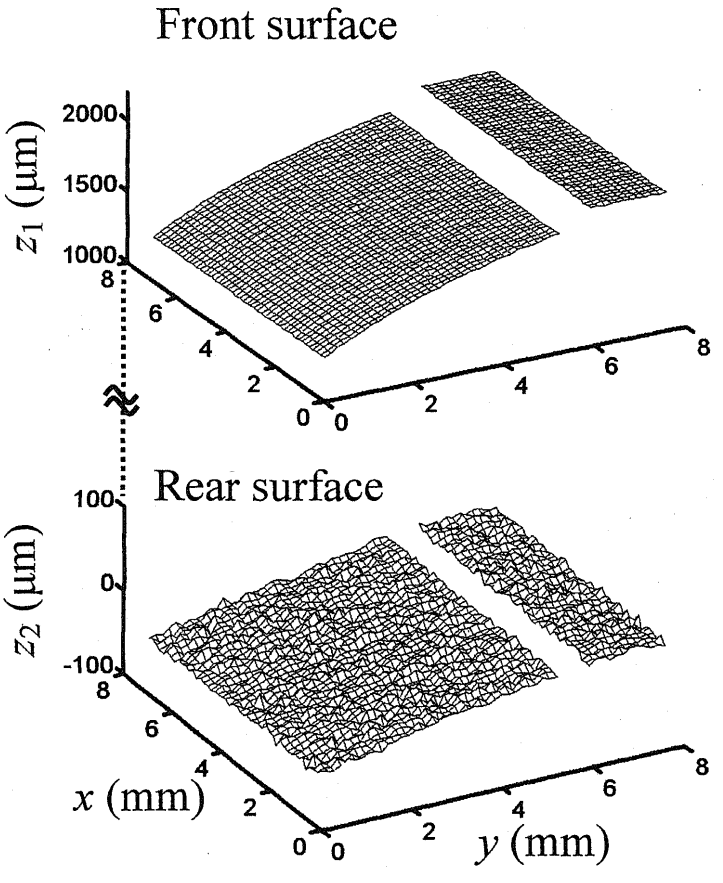

Fig. 5-12 Measured two surface profiles of the acrylic plate by continuous period-scanning back-propagation method.

5.4 Summary

A continuous period-scanning fringe projection interferometry by using the back-propagation method was used to measure two surface profiles of the object. The period of the fringe was scanning continuously by using a function generator. The time-varying phase distribution due to the scanning of the period was

extracted from Fourier transform of the sinusoidally phase-modulated interference signal. The back-propagation method was used to find the position of the object surface. This method could save measurement time distinctly. An acrylic plate had been measured. The repeatability in the thickness measurement was about 3.6μm.The measured result was almost the same as in Chapter 4, but the measurement time is much shorter than that in Chapter 4.

Chapter6

Conclusions

In this dissertation, we presented a multi-period fringe projection interferometry by using back-propagation method, and researched how to measure one surface or two surfaces profile by using the back-propagation method.

The multi-period fringe projection interferometry is compared with the single-wavelength interferometry and the fringe projection interferometry. The multi-period fringe projection method is suitable for measuring objects with large change of surface profile or surface profiles with discontinuities. There are three unwrapping method in the multi-period fringe interferometry, the spatiotemporal phase unwrapping method (SP method), temporal phase-unwrapping method (TP method) and back-propagation method (BP). The advantage of the BP method is presented.

The principle of sinusoidal phase modulation method (SPM) was presented. It also had been discussed how to detect the time-varying phase in SPM. The fundamental characteristics of two-dimensional Charge Couple Device (CCD), and the phase-lock system were described.

The measurement of one surface profile by using back-propagation method is presented. A multi-period fringe-projection is executed with a Twyman-Green interferometer. The phase-lock technique enables us to produce exactly the constant phase point of the fringe pattern. Amplitudes and phases of the fringe patterns with different periods on the object surface are detected by using sinusoidal phase-modulating interferometry. Optical fields of the different fringe periods on the object surface are made from the detected amplitudes and phases. The optical fields on each point of the object surface are back-propagated to the

constant phase point. When the back-propagated fields reach to the constant phase point, the amplitude of the sum of the back-propagated fields with the different fringe periods becomes maximum and its phase becomes zero. The back-propagation distance from the each point of the object to the constant phase point provides the position of the object surface. Simulations make it clear that measurement results by the back-propagation method are not sensitive to noises contained in the measured phase. This method achieves a measurement accuracy higher than the other methods in the multi-period fringe projection. A step profile made by gauge blocks and a step profile made by aluminum plates are measured. It is confirmed in the experiments that a distance of several millimeters can be measured with a high accuracy of several micros by using the back-propagation method in the multi-period fringe projection.

On the basis of Chapter 2 and Chapter 3, back-propagation method was used to measure two surface profiles of the object. The interference signal is made up of four waves from the front surface and the rear surface of the object. In the back-propagation method the optical fields with different fringe periods were back-propagated to the stationary point of the phase. The position of the object surface was obtained from the distance of the back-propagation on which the amplitude of the sum of the back-propagated optical fields became maximum and its phase became zero. The simulation made it clear that the extending of two peaks of A_R distribution will bring error to the measurement, and when the amplitude B_{m} of the interference signal is a Gauss distribution, this error decreased. The measurement of a glass plate gave the measurement precision of this method was 2.8μm and the repeatability of this method was 2.5μm. An acrylic plate had also been measured. The measured result was compared with that measured by the confocal microscope.

The back-propagation method used in Chapter 3 and Chapter 4 has a shortcoming which is that the measurement time for these methods is long, because of the discretely period-scanning. A continuous period-scanning fringe projection interferometry was proposed in Chapter 5 and was used to measure two surface profiles of the object. The period of the fringe was scanning continuously by using a function generator. The time-varying phase distribution due to the scanning of the period was extracted from Fourier transform of the

sinusoidally phase-modulated interference signal. The back-propagation method was used to find the position of the object surface. The measurement time of this method was much shorter than the back-propagation method using discrete period-scanning. An acrylic plate had been measured. The measured result was almost the same as in Chapter 4.

Reference

1. D. Malacara, "Twymann-Green Interferometer," in *Optical Shop Testing*, 2nd ed., D. Malacara, ed., (Wiley, New York 1992), pp. 51-94.
2. J. E. Greivenkamp and J. H. Bruning, "Phase Shifting Interferometers," in *Optical Shop Testing*, 2nd ed. D. Malacara, ed, (Wiley, New York 1992), pp. 653-686.
3. M. Takeda, H. Ina, and S. Kobayashi, "Fourier-transform method of fringe-pattern analysis for computer-based topography and interferometry," J. Opt. Soc. Am. **72**, 156-160(1982).
4. O. Sasaki and H. Okazaki, "Sinusoidal phase modulating interferometry for surface profile measurement," Appl. Opt. **25**(18), 3137-3140(1986).
5. K. Creath and J. C. Wyant, "Moire and Fringe Projection Techniques," in *Optical Shop Testing*, D. Malacara, ed, (Wiley, New York 1992), pp. 653-686.
6. S. Kuwamura and I. Yamaguchi, "Wavelength scanning profilometry for real-time surface shape measurement," Appl. Opt. **36**(19), 4473-4482 (1997).
7. C. Wagner, W. Osten and S. Seebacher, "Direct shape measurement by digital wavefront reconstruction and multiwavelength contouring," Opt. Eng. **39**(1), 79-85 (2000)
8. H. J. Tiziani, B. Franze and P. Haible, "Wavelength-shift speckle interferometry for absolute profilometry using a mode-hop free external cavity diode laser," J. Modern. Opt. **44**(8), 1485-1496 (1997).
9. H. Zhao, W. Chen and Y. Tan, "Phase-unwrapping algorithm for the measurement of three-dimensional object shapes," Appl. Opt. **33**(20), 4497-4500 (1994).
10. H. Zhang, M. J. Lalor and D. R. Burton, "Spatiotemporal phase unwrapping for the measurement of discontinuous objects in dynamic fringe-projection phase-shifting profilometry," Appl. Opt. **38**(16), 3534-3541 (1999).

11. J. M. Huntley and H. Saldner, "Temporal phase-unwrapping algorithm for automated interferogram analysis," Appl. Opt. **32**(17), 3047-3052 (1993).
12. H. O. Saldner and J. M. Huntley, "Temporal phase unwrapping application to surface profiling of discontinuous objects," Appl. Opt. **36**(13), 2770-2775 (1997).
13. J. M. Huntley and H. O. Saldner, "Error-reduction methods for shape measurement by temporal phase unwrapping," J. Opt. Soc. Am. A **14**(12), 3188-3196 (1997).
14. J. M. Huntley and H. O. Saldner, "Shape measurement by temporal phase unwrapping: comparison of unwrapping algorithms," Meas. Sci. Technol. **8**, 986-992 (1997).
15. H. Huan, O. Sasaki, and T. Suzuki, "Multiperiod fringe projection interferometry using a backpropagation method for surface profile measurement," Appl. Opt. **46**, 7268-7274 (2007)
16. O. Sasaki, H. Tai, and T. Suzuki, "Step-profile measurement by backpropagation of multiple-wavelength optical fields," Opt. Lett. **32**, 2683-2685 (2007)
17. H. Huan, O. Sasaki, and T. Suzuki, "Multi-period fringe projection interferometry using back-propagation method for shape measurement of glass plate," Proceedings of SPIE Vol. 6829, 68290C (2007).
18. L. H. Jin, Y. Otani and T. Yoshizawa, "Shadow moiré profilometry by frequency sweeping," Opt. Eng. **40**(7), 1383-1386 (2001).
19. O. Sasaki, T. Suzuki, and K.Takahashi, "Sinusoidal phase modulating laser diode interferometer with feedback control system to eliminate external disturbance," Opt. Eng. **29**(12), 1511-1515 (1990).
20. H. Maruyama, S. Inoue, T. Mitsuyama, M Ohmi and M Haruna, "Low-coherence interferometer system for the simultaneous measurement of refractive index and thickness," Appl. Opt. 41, 1315-1322 (2002).
21. T. Funaba, N. Tanno and H. Ito, "Multimode-laser reflectometer with a multichannel wavelength detector and its application," Appl. Opt. 36, 8919-8928 (1997).
22. C. Karaalioglu, Y. Slarlatos, "Fourier transform method for measurement of thin film thickness by speckle interferometry," Opt. Eng. 42(6),

1694-1698(2003).
23. H. Huan, O. Sasaki, T. Suzuki, "Movement measurement with a grating interferometer using sinusoidal phase-modulation", Optics Communications, Vol. **267**, No.2, 341-346

Publications

- 学会誌発表論文

1. Hai Huan, Osami Sasaki, and Takamasa Suzuki
   Multiperiod fringe projection interferometry using a backpropagation method for surface profile measurement,
   Appl. Opt. **46**, 7268-7274 (2007)
2. Hai Huan, Osami Sasaki, and Takamasa Suzuki
   Movement measurement with a grating interferometer using sinusoidal phase-modulation
   Optics Communications, Vol. **267**, No.2, 341-346

- 国際会議発表論文

1. Hai Huan, Osami Sasaki, and Takamasa Suzuki
   Multi-period fringe projection interferometry using back-propagation method for shape measurement of glass plate
   SPIE/COS Photonics Asia 2007, Jiuhua Grand Convention and Exhibition Center, Beijing, China, November. 2007
   Proceedings of SPIE Vol. 6829, 68290C (2007)

- 学会報告

1. 宦海, 佐々木修己, 鈴木孝昌,
   多周期縞投影干渉逆伝搬法による表面形状計測
   日本光学会年次学術講演会 （OPJ2006）一橋記念講堂, 東京, 2006
2. 宦海, 佐々木修己, 鈴木孝昌,
   多周期縞投影干渉逆伝搬法による表面形状計測
   2007 年(平成 19 年)春季第 54 回応用物理学会学術講演会, 青山学院大学, 横浜, 2007

Acknowledgments

I would like to express my sincerely appreciation to Professor Osami SASAKI for his strict guidance and help. He is very erudite in the field of optics and is also very diligent. Owing to his almost severe requirement, I learnt a lot of professional knowledge about the optical test and sinusoidal phase modulating interferometry, and observed many optical phenomenon. The knowledge will lay a good foundation in my future work and will be of great benefit to me.

I also would like to give my appreciation for the members of my doctor committee, Professor Hisakazu KIKUCHI, Professor Takashi SATO, Professor Masasi OOKAWA, Professor Takamasa SUZUKI. Thanks for them to spend much time to read my paper and give a lot of suggestion for my research.

I would also like to thank Professor Takamasa Suzuki for his many help.

I would like to thank Haruo Iwano, who is a technical official of Lab. All the tools and materials I need in my experiments were provided by him.

I would also like to thank Dr. Zhao Xuefeng for their enthusiastic encouragement, help and support. I am also indebted to my classmates in this laboratory for their good friendship and help.

Finally, I am deeply grateful to my parents, for their moral encouragement, understanding, and supports during the period of my PhD study.